STRUCTURAL AND FUNCTIONAL STUDIES ON

VACCINIA VIRUS E3 PROTEIN

By

SIKTA PATNAIK

Bachelor of Science in Agriculture
Acharya N. G. Ranga Agriculture University
Hyderabad, Andhra Pradesh, India
2007

Master of Science in Biotechnology
Stephen F. Austin State University
Nacogdoches, Texas
2010

Submitted to the Faculty of the
Graduate College of the
Oklahoma State University
in partial fulfillment of
the requirements for
the Degree of
DOCTOR OF PHILOSOPHY
May, 2019

STRUCTURAL AND FUNCTIONAL STUDIES ON

VACCINIA VIRUS E3 PROTEIN

Dissertation Approved:

Dr. Junpeng Deng

Dissertation Adviser

Dr. Robert Matts

Dr. Steve Hartson

Dr. Haobo Jiang

Outside Committee Member

Name: SIKTA PATNAIK

Date of Degree: MAY, 2019

Title of Study: STRUCTURAL AND FUNCTIONAL STUDIES ON VACCINIA VIRUS E3 PROTEIN

Major Field: BIOCHEMISTRY AND MOLECULAR BIOLOGY

Abstract: E3 protein from vaccinia virus is a key host-range protein, which suppresses the innate antiviral immune response of the infected cells. In response to the viral infection, Protein Kinase R (PKR) of the host cell initiates the immune response via a cascade of reactions. E3 attacks PKR to suppress the immune response, but the mechanism of PKR inhibition by E3 is unknown. In this study, it was found that the kinase domain of PKR had a physical interaction with E3 that has biochemical relevance. E3 follows two different pathways when inhibiting inactivated and activated PKR-KD. E3 binds to monomeric PKR-KD inhibiting its phosphorylation by forming an inactive heterodimer, which eventually leads to disruption of immune response via PKR in host cells. The mechanism of E3 inhibition of dimeric PKR-KD is unknown but the data suggests a weak interaction between the proteins leading to disruption of PKR activity. The study also detailed the importance of both N and C terminals of E3 for PKR inhibition. Further analysis of the interaction revealed that the inhibition of PKR-KD activation by E3 protein does not correlate with the dsRNA binding ability of PKR or E3.

ACKNOWLEDGEMENTS

This work was made possible with the help and support of many individuals. First and foremost, I would like to thank my advisor, Dr. Junpeng Deng for his guidance, support and mentoring. It was my pleasure to work with a stalwart like him in the field of crystallography for my PhD research. Dr. Deng taught me to be always inquisitive, connect seemingly unconnected aspects, keep questioning my results and always look for possible improvements. His philosophy and passion for research and finickiness about consistency in results will always be remembered and followed. His immense knowledge in the field of protein crystallography continues to amaze me every day as I interact with him. I am greatly indebted to have such a mentor.

I would also like to acknowledge my committee members Dr. Robert Matts, Dr. Steve Hartson and Dr. Haobo Jiang for serving on my thesis committee and offering valuable suggestions for making this thesis better. All the radioactive experiments were conducted in Dr. Matts's lab and gels were scanned at the core facility. These experiments were successful because of the expert guidance of Dr. Matts and Dr. Hartson. Dr. Matts expertise in PKR helped a lot during this thesis work.

Any of this wouldn't have been possible without the support of my friends and lab mates

Prabhat Kumar Pathak, Juhi Chaturvedi, Dr. Shuxia Peng, Jeff Woodruff, Olivia Davis, Jennifer Yang, Katherine Woosley, David Schwebs, Mansi Gulati, Shoukath Sultana, Nootan Pandey, Pallavi Biswas and Puspha Itagi. I would specially like to thank Prabhat for all his guidance and expertise in protein purification and also his well-timed humor which kept a lively atmosphere in the lab and Juhi for always encouraging me through the ups and downs of this journey.

Finally, I would like to thank my father who is my greatest inspiration, my mother, my sisters Smaraki, Smaranika and Mahadeepa, my father and mother-in-law who mentally and emotionally supported me a lot. Nothing would have been possible if not for the endless love, encouragement and sacrifice of two most important people of my life, my spouse Mahaprasad Kar and my pet Khushi.

TABLE OF CONTENTS

Chapter Page

ABBREVIATIONS

VACV: Vaccinia virus
PKR: Protein Kinase R
DRBD: Double Stranded RNA Binding Domain
IFN: Interferon
MEF: Mouse Embryonic Fibroblasts
PAMPs: Pathogen Associated Molecular Patterns
NMR: Nuclear Magnetic Resonance
HRI: Heme Regulated Inhibitor
PERK: PKR-like Endoplasmic Reticulum Kinase
GCN2: General Control Nonderepressible 2
eIF2α: Eukaryotic Initiation Factor 2 alpha subunit
KD: Kinase Domain
PCR: Polymerase Chain Reaction
LB: Luria-Bertani medium
MBP: Maltose Binding Protein
TEV: Tobacco Etch Virus
IPTG: Isopropyl β-D-1-thiogalactopyranoside
Ni-NTA: Nickel-Nitrilotriacetic Acid
DLS: Dynamic Light Scattering
SEC: Size Exclusion Chromatography
RT-PCR: Real Time-Polymerase Chain Reaction
TAE: Tris base, acetic acid and EDTA
GST: Glutathione *S*-transferases
SDS-PAGE: sodium dodecyl sulfate polyacrylamide gel electrophoresis
PSSpred: Protein Secondary Structure Prediction
HTH: Helix Turn Helix
His tag: Histidine tag
Tm: Melting temperature
OD_{600nm}: Optical Density at 600 nm wavelength

LIST OF TABLES

LIST OF FIGURES

Figure Page

Figure Page

Figure Page

Figure Page

CHAPTER I

INTRODUCTION

1.1. Introduction

Traditionally, vaccinia virus (VACV) has been used as vaccination against small pox. VACV is a large DNA virus that has the ability to replicate in the cytoplasm of the infected cells unlike other viruses [1]. It was used as a vaccine to eradicate small pox successfully. Although the vaccination for small pox has been discontinued for general public, certain military organization in the United States continue to vaccinate owing to the threat of small pox used as a bioterrorism agent [2]. Immune-challenged individuals, newborns, pregnant women and older people who come in contact with VACV viruses might develop complications, that are in some cases fatal [2]. Hence, there has been a greater need to study recombinant vaccinia viruses that would have familiar advantages of smallpox vaccine i.e. heat stability, low cost and ease of administration [3]. Not only for smallpox, but VACV has also been actively researched for development of recombinant vector viruses for immunization against other infectious diseases. The wide host range of VACV allows the development of recombinant vectors that could be used against infectious agents in a variety of experimental animals from rodents to primates [3]. An example of VACV developed for treating other diseases is the development of an AIDS vaccine that have led to the human testing of a first-generation recombinant VACV expressing the HIV-1 envelope gene [4, 5].

VACV encodes a number of host range genes and among them the most studied is the E3L gene that produces E3 protein. E3 protein is composed of 190 amino acids and comprises of two domains. The N-terminal contains a Z-DNA binding domain (ZBD) that binds to Z-form DNA. The C-terminal domain contains a dsRNA binding domain (DRBD) and binds to dsRNA produced during viral infection [6, 7]. The best characterized biological functions of the E3 protein includes its host range function, suppression of cytokine expression, and inhibition of interferon (IFN)-induced antiviral activity [8-10]. E3 protein suppresses the antiviral immune response of the host cells by blocking multiple immune response pathways. Of the number of ways, Protein Kinase R (PKR) is the most notable immune response protein that are affected by E3 (Fig. 1-1). Mammalian PKR is a double-stranded RNA dependent protein kinase that is transcriptionally induced by interferon and becomes activated in virus-infected cells by dsRNAs produced during the virus life cycle [11, 12]. There are two contradictory models that have been put forward regarding the biochemical capacity of E3 proteins to bind to dsRNA and their ability to suppress the innate immune response via PKR response pathway. It has been shown that E3 inhibits PKR by a novel mechanism in which the inhibitory E3 N-terminal domain is tethered to and inhibit the kinase domain of PKR, in association with the dsRNA binding motifs (DRBMs) of the two proteins mediated through dsRNA binding [13]. But an opposing model suggests that the dsRNA binding capability of E3 protein is not essential for its activity of inhibiting PKR [14].

Understanding the mechanism of E3 inhibition of PKR activity could be the key to developing recombinant vaccinia vectors that could treat numerous infectious diseases

including smallpox. The global immunity to smallpox has declined significantly due to the cessation of mass vaccination in the 1970s. Since there is no treatment for smallpox other than vaccination in the form of attenuated live vaccines, development of other forms of treatments are of the greatest importance.

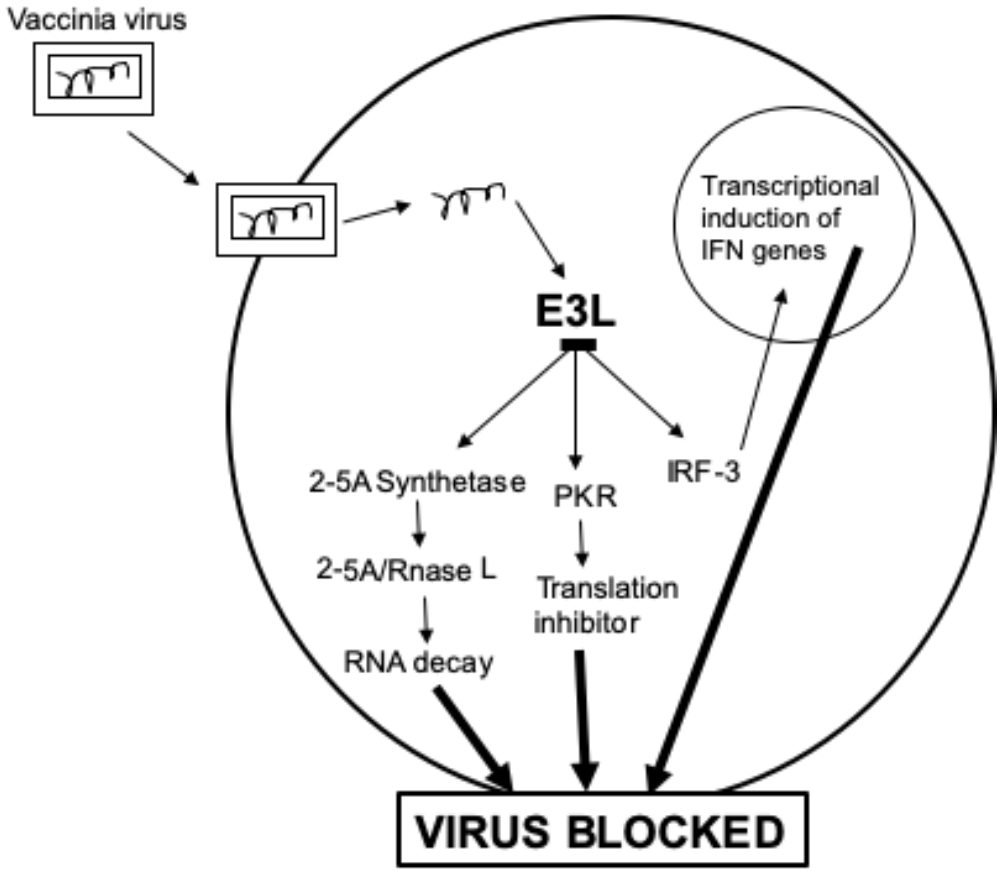

Figure 1.1. E3 suppression of host immune system.

E3L of VACV evades the IFN system by blocking IFN induction through IRF3 and IFN action through the 2-5A/RNase L pathway and protein kinase PKR. Figure adapted from reference [15].

1.2. Research Goals and Overview

My doctoral research has primarily focused on the mechanistic studies of vaccinia E3 protein and its inhibitory effect on the activity of mammalian PKR. Structural and functional approaches were directed to achieve this aim (Fig. 1.2). Efforts were made to attain stable and homogenous E3 protein which were used for understanding structure of the protein by x-ray crystallography. Functional studies were conducted to understand the protein-protein interactions between E3 and PKR.

A major gap in the knowledge of E3 is the absence of structure of E3 protein. E3 remains in an aggregated state in cytoplasm of host cells. A study reported that wildtype E3 proteins expressed in bacterial systems and purified in buffer containing 1M NaCl existed in a dimeric form. Although, the E3 protein remained as a dimer at a high ionic strength buffer, it was suggested that oligomerization of E3 also depended on concentration of protein [16]. The idea of using protein engineering to alleviate aggregation towards structural studies is enlightened from a recent success on a non-related difficult protein project conducted by a group in Baylor College of Medicine, Texas [17]. NS1 protein from H5N1 influenza virus suppresses antiviral interferon (IFN) induction in the host cells but how the protein antagonizes the IFN response was unknown [18]. NS1 protein remains in an aggregated form in the cytoplasm of the host cell similar to E3. Aiming to solve the atomic structure of NS1 by crystallography, the group performed a series of single point mutations where they determined two single mutations that completely removed aggregation. The approach allowed them to crystallize the NS1 protein and perform structural analysis of the crystal [17]. In this study, it was predicted that single/double point mutations of E3 proteins might

mitigate the problem of aggregation and thus help in the structural studies of this protein through x-ray crystallography.

This study also aimed at defining the physical and functional characteristics of protein-protein interactions between E3 and PKR. It is well known that E3 suppresses the activation of PKR by physically interacting with the full length PKR both in vivo and in vitro. Based on a recent study, it was found that the binding of E3 to PKR does not require dsRNA binding capacity to the dsRNA as suggested in a previous model [14]. In this study, we predicted that E3 and the kinase domain of PKR would physically interact to form an inactive complex that leads to the inhibition of PKR activity. It was also predicted that the dsRNA binding abilities was dispensable for the interaction between these proteins.

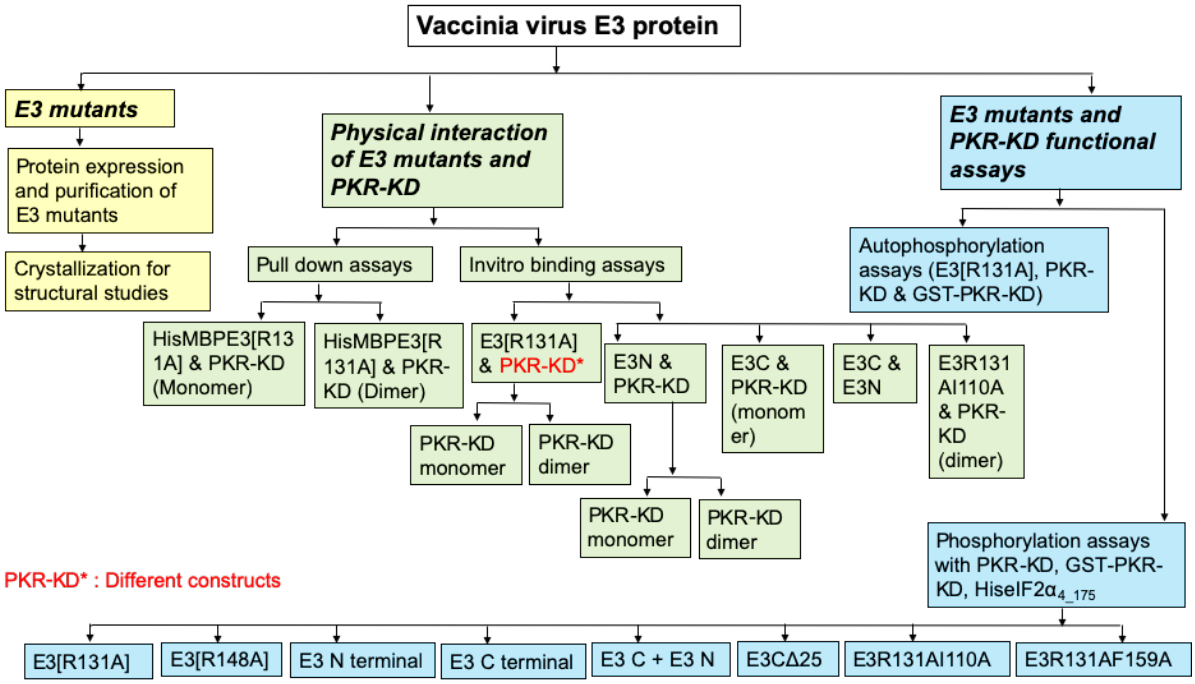

Figure 1.2. Various approaches were followed for conducting mechanistic studies on E3 protein.

CHAPTER II

REVIEW OF LITERATURE

2.1. ***Introduction***

Poxviruses comprise a large family of viruses that infect a wide variety of vertebrate and invertebrate hosts [19]. These viruses are a diverse family of double-stranded DNA viruses which replicate exclusively in the cytoplasm of infected cells and exhibit a varied host range [20]. Poxviruses include many important human and animal pathogens such a variola virus, the causative agent of smallpox. Another important member of this family is the VACV which was successfully used for the prevention and the eradication of smallpox [1].

Unlike variola virus that has a specific host, VACV displays a broad host range and encodes a number of immunomodulatory proteins such as host range proteins [21]. Of the 200 genes encoded by VACV, one-third are dedicated to host immune evasion [22]. Some examples of host range genes include SPI-1, K1L, C7L, p28/N1R, B5R, K3L, and E3L, the alteration or deletion of which restricts the virus replication in specific cell lines [8]. These host range genes encode for proteins that perform specific biological functions within the host cell in response to viral infections. This section of the chapter focuses on the E3 protein, its physical and chemical characteristics, functions and immune evasion property in regards to interaction with host cell proteins such as PKR.

*2.2. **VACV E3 protein***

E3 is an extensively studied vaccinia host range protein, which is expressed early in the viral replication cycle. It is a prototypic member of the orthopoxviruses and functions as an inhibitor of innate immune signaling and also essential for vaccinia virus replication in vivo in many human cell culture systems [23]. It is a highly conserved protein in VACV and E3 orthologues present in other poxviruses such as sheeppox virus, yaba monkey tumor virus, swinepox virus, myxoma virus, are relatively conserved but with comparatively less sequence conservation (Fig. 2.1). These E3 orthologues could partially complement important functions of E3, including suppression of PKR activation, cytokine expression and inhibition of the antiviral effects of IFN in vivo but, none of the E3 orthologues were able to restore pathogenicity in E3 protein deficient vaccinia virus [23].

Many studies over the past 15 years have clearly demonstrated E3 as a host range protein, required for VACV replication in many cell lines [8]. An E3 protein deleted VACV strain resulted in the inhibition of viral and cellular protein synthesis and reduced viral replication which was reverted by transient transfection of E3 [24]. In another study, E3 deleted VACV was unable to replicate productively (because of termination at the level of late gene expression) in a murine epidermis-derived dendritic cell line XS52 [25]. In the same study, it was observed that XS52 cell line that had infection with VACV lacking E3 resulted in activation of NF-κB and production of proinflammatory cytokines like TNF and IL-6 [25]. Many studies have focused on E3 in terms of defining the mechanism of evasion of host defenses such as in a study it was found that expression of E3 in cell lines interferes with several cellular pathways, resulting in promotion of cellular growth, resistance to

apoptosis, and impairment of antiviral activity [26]. It was observed that mouse NIH3T3 mammalian cells expressing E3 protein, inhibited eIF-2α phosphorylation and initiated IkBα degradation in response to dsRNA along with resistance to dsRNA-triggered apoptosis [26].

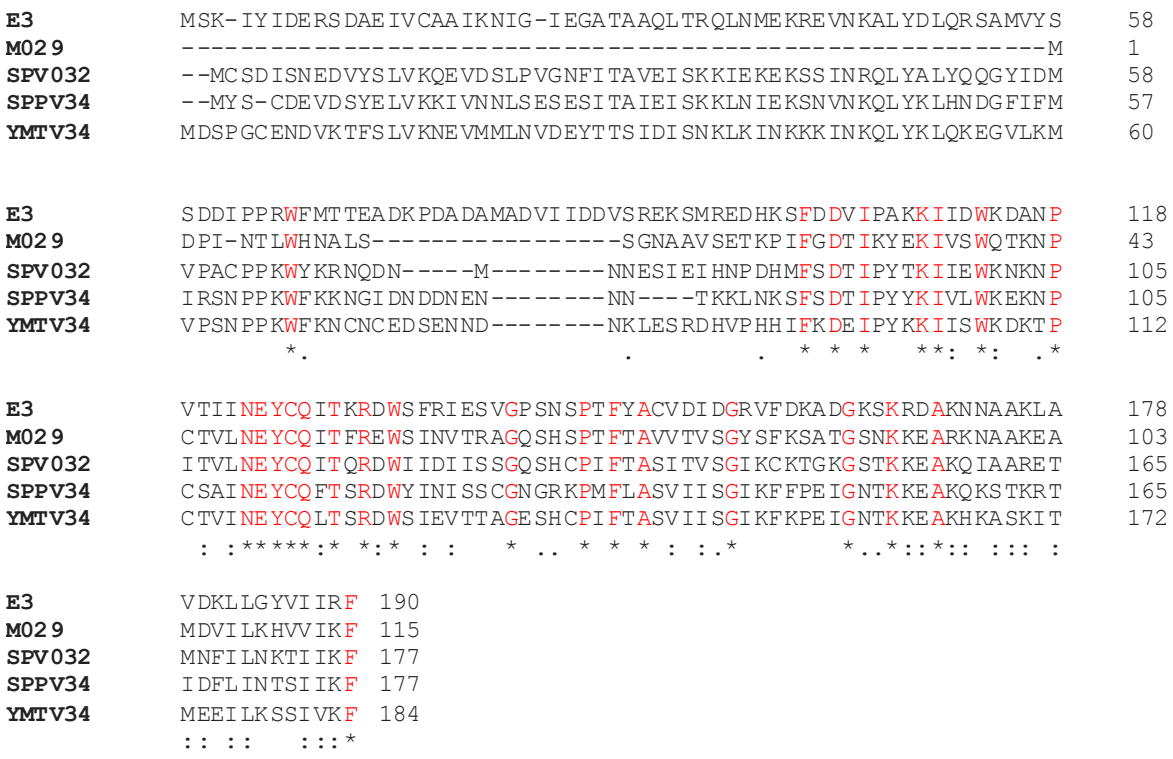

Figure 2.1. E3 and E3 orthologues sequence alignment.

E3 orthologues are early genes whose protein products display significant amino acid divergence. Protein sequence alignments were generated using the CLUSTALW OMEGA program. The "." symbol denotes semiconserved substitutions, the ":" symbol denotes conserved substitutions, and the "" symbol denotes complete conservation of the residue across all sequences. The amino acids highlighted in red indicate residues previously identified to contribute to E3 dsRNA binding. Figure adapted from reference [23].*

E3 protein consists of two conserved domains that are essential for pathogenesis [27]. Limited proteolysis of the E3 protein have shown the presence of two trypsin-resistant structural domains separated by a protease-sensitive interdomain bridge [16] (Fig. 2.2). The C-terminal double stranded RNA binding domain (DRBD) functions by sequestering dsRNA to avoid activation of IFN-inducible, dsRNA-dependent antiviral enzymes such as PKR [24, 27-29]. The N-terminal domain has a Z-DNA binding domain whose function is not well understood. It was found that the amino terminal domain was not necessary for viral replication but was required for pathogenicity in vivo [30]. The N-terminal contributed to neurovirulence of the virus [28]. It was observed in a study that pathogenesis in N-terminal mutants of VAVC E3 correlated with binding to Z-DNA in vitro and in vivo [31]. The N-terminus was found to be important for inhibiting PKR-dependent IFN in mouse embryonic fibroblasts (MEFs) [31]. Previous studies have revealed the Z-DNA binding activity of E3 is critical for viral pathogenesis but it was recently found that in variola virus E3 protein, its Z-DNA domain is required rather than its Z-DNA binding activity, for PKR inhibition [32].

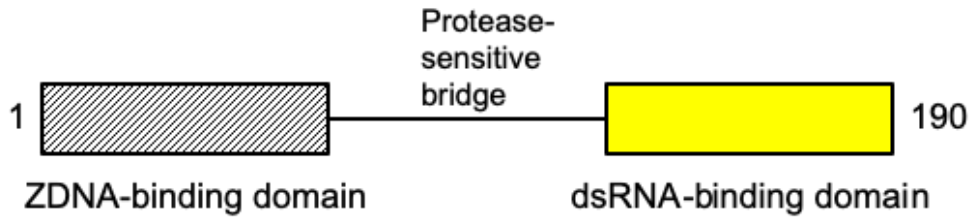

Figure 2.2. The domain structure of E3 protein with a N-terminal Z-DNA binding domain and a C-terminal dsRNA-binding domain separated by a protease-sensitive interdomain bridge.

E3 protein is an extensively studied protein but understanding its structure has been difficult. Scientists were successful in resolving the Z-DNA binding domain of one of the E3

orthologues. The crystal structure of the Z-DNA binding domain from the E3-like protein of Yaba-like disease virus, a Yatapoxvirus, in complex with Z-DNA was solved at 2.0 Å resolution (Fig. 2.3). The crystal structure of yabZαE3L has an α/β architecture, consisting of three β-strands and three α-strands. The three α helices (α1, α2, and α3) form a core domain, which is flanked by a β-sheet of three antiparallel strands (β1, β2, and β3). α2, and α3 form an helix-turn-helix motif and two antiparallel β-strands (β2 and β3) form a wing [33].

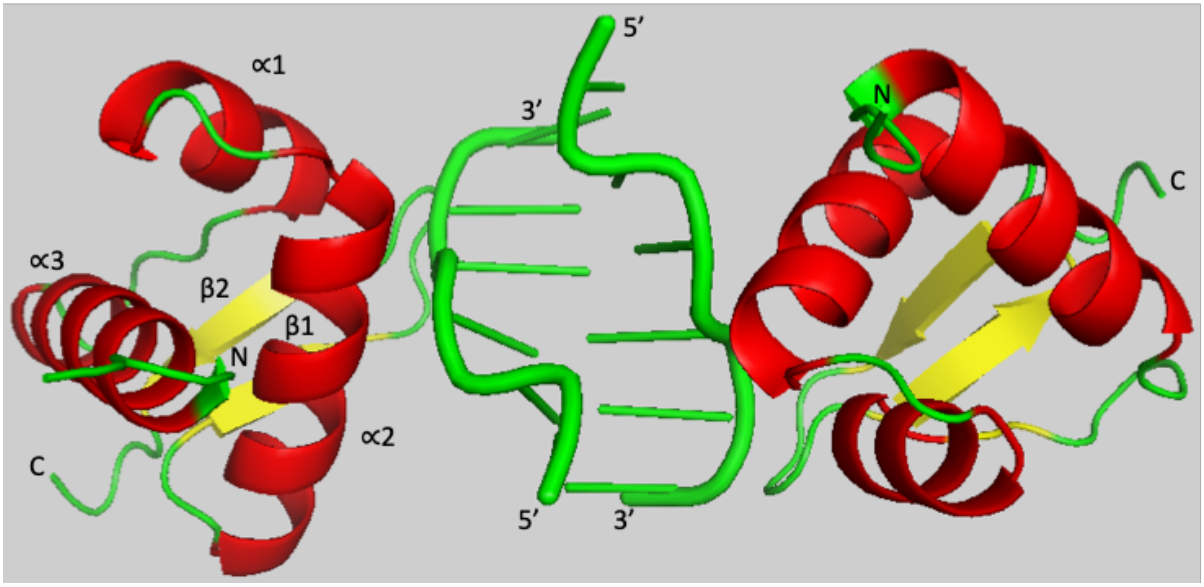

Figure 2.3. Crystal structure of Z-DNA binding domain of E3 orthologue.

The overall structure of the yabZαE3L:Z-DNA complex. The N and C terminus and secondary structure elements are labeled. Figure adapted from reference [33]. Figure generated by The PyMOL Molecular Graphics System, Version 2.0 Schrödinger, LLC.

The biological functions of VACV E3 protein such as host range function and inhibition of innate immune responses are known to be primarily mediated through the DRBD of E3 protein. It functions through sequestering virus-produced dsRNA in host cells [24, 34, 35]. E3 can inhibit stimulation of dsRNA-dependent PKR and activation of 2'-5'

oligoadenylate synthase [6, 27, 36]. In an E3 protein deleted VACV strain, an inhibition of viral and cellular protein synthesis and reduced viral replication was observed [24]. The viral replication was restored by transient transfection of E3 and was shown that the C-terminal domain of E3 was important for the rescue [24]. The nonessential nature of E3 N-terminal was detected for viral infection in cell cultures whereas the absolute requirement of both domains for full pathogenesis was observed in mice [28]. A recent study was conducted to better understand the biological relevance of dsRNA binding ability of E3. It was found that the dsRNA binding abilities of E3 was not essential for its biological functions [14]. This study involved a series of E3 mutants that were evaluated for dsRNA binding capacity and expression of host range functions (Table 2.1). It was also reported in this study that the domains of E3 required for biological functions overlap the domains critical for its biochemical capacity for dsRNA binding.

Table 2.1. Amino acids of E3 protein critical for dsRNA binding and host range

Mutant	Poly(I-C) binding[1]	Host range[2]
K109A	-	-
I110A	-	-
W113A	-	-
I122A	-	-
R131A	-	-
I154A	-	-
K167A	-	-
R168A	-	-
A174V	-	-
A175V	-	-
L182/183A	-	-
I105A	-	±
Y125A	-	±
F148A	-	±
F159A	-	±
K171A	-	±
E138A	±	+
L182A	±	+
L183A	±	+
I187/188A	±	+
D103A	+	±
E124A	+	±

1: −, no E3 mutant protein was detected from poly(I·C) bead pulldown, even after extended exposure of the Western blot films; ±, only a faint band of E3 mutant protein was detected by Western blotting following poly(I·C) bead pulldown.

2: −, the virus titer at 24 h postinfection is lower than the titer at 5 h postinfection; ±, the virus titer at 24 h postinfection is greater than the titer at 5 h postinfection, but the increase is not greater than 0.5 $\log_{10}$; +, the virus titer at 24 h postinfection is at least 0.5 $\log_{10}$ greater than the titer at 5 h postinfection.

Note: Table adapted from reference [14]

2.3. ***Protein Kinase R. (PKR)***

PKR belongs to the family of protein kinases, which include other kinases such as HRI, PERK, GCN2 and collectively constitute a functional family called the eIF2α protein kinases. PKR is a soluble protein rich in serine and threonine. It is constitutively expressed in most mammalian cell types. PKR is induced by type I interferons and plays an important role in the innate immunity defense mechanism of the cell against viral infections [37]. During

viral infections, pathogen associated molecular patterns (PAMPs) in the form of nucleic acids are produced in the host cell [38, 39]. These dsRNAs produced during viral infections lead to PKR activation. Activated PKR then leads to inhibition of protein synthesis and apoptosis [40]. PKR is also involved in stress responses, inflammation pathways, regulates cellular growth and proliferation, nutrient signaling and metabolism [41-43].

Human PKR is a 551 amino acid protein and consists of two distinct domains. The N-terminal (amino acids 1-170) has two DRBDs of approximately 65 amino acid residues each, separated by a 20 amino acid linker [44]. The structure of PKR N-terminal domain was solved using NMR and each DRBD consists of an α-β-β-β-α conformation (Fig. 2.4). The flexible 20 amino acid linker found between the two DRBDs in the N-terminal consists of random coil conformation and binds around the dsRNA helix for optimal interactions [40].

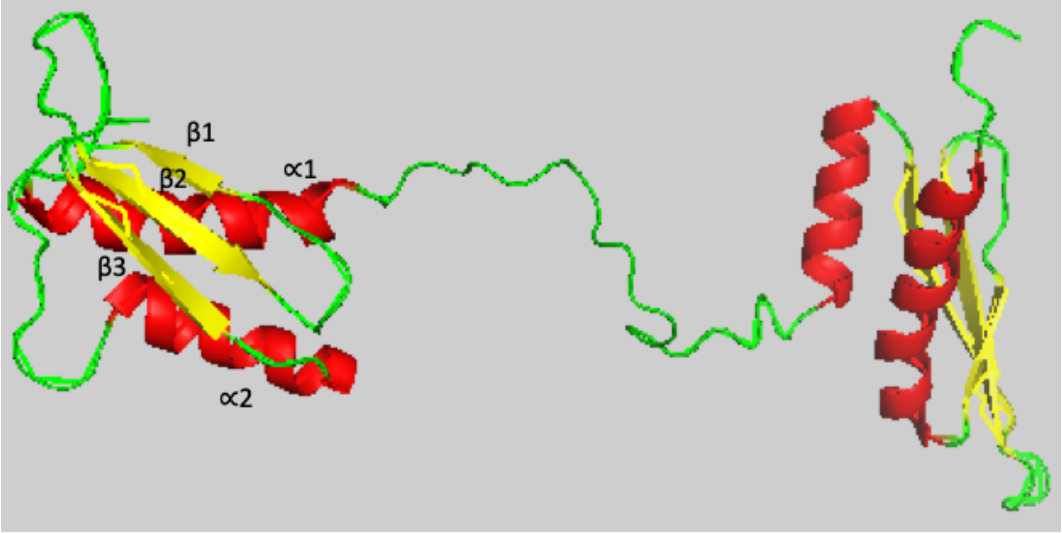

Figure 2.4. Structure analysis of N-terminal domain of PKR.

An NMR solution structure of the DRBD of human PKR, comprising two tandem-linked DRBDs both with an α-β-β-β-α fold separated by a flexible linker. Figure adapted from

reference [40]. Figure generated by The PyMOL Molecular Graphics System, Version 2.0 Schrödinger, LLC.

The C-terminal domain of PKR (amino acid 258-551) serves as the catalytic domain (also known as the kinase domain). It consists of a typical bilobal architecture of a smaller N-terminal lobe (N-lobe) and a larger C-terminal lobe (C-lobe) as in other protein kinases [45]. The structure of kinase domain of PKR was solved by x-ray crystallography in a complex form with its substrate eIF2α [45]. Amino acids 258-369 cover the smaller N-lobe of the kinase domain that consists of a twisted five-strand antiparallel β sheet (β1 to β5), a canonical helix αC laterally flanking one side of the β sheet, and a noncanonical helix α0 which integrates into the top groove of the β sheet. Amino acids 370-551 form the larger C-lobe of kinase domain and comprises two paired antiparallel β strands (β7-β8 and β6-β9) and eight α helices (αD to αJ) (Fig. 2.5). The active site of the PKR kinase domain occurs in a cleft between the N and C-lobes of the domain [45]. A sub-element of the activation site, termed as the P+1 loop, is notable for defining Serine/Threonine kinase specificity. This P+1 loop provides a docking site for the phosphoacceptor sequence of the substrate in the immediate vicinity of the active site [46]. The crystal structure solved detected the presence of threonine at position 451 of the P+1 loop, which best characterized function of PKR as a Serine/Threonine directed protein kinase [45]. The crystal structure shown in figure 2.5 is a complex of PKR kinase domain and its substrate eIF2α. The structure indicates a phosphorylated threonine 446 residue and adopts a fully structured winding conformation which is indicative of a catalytically active state [46, 47].

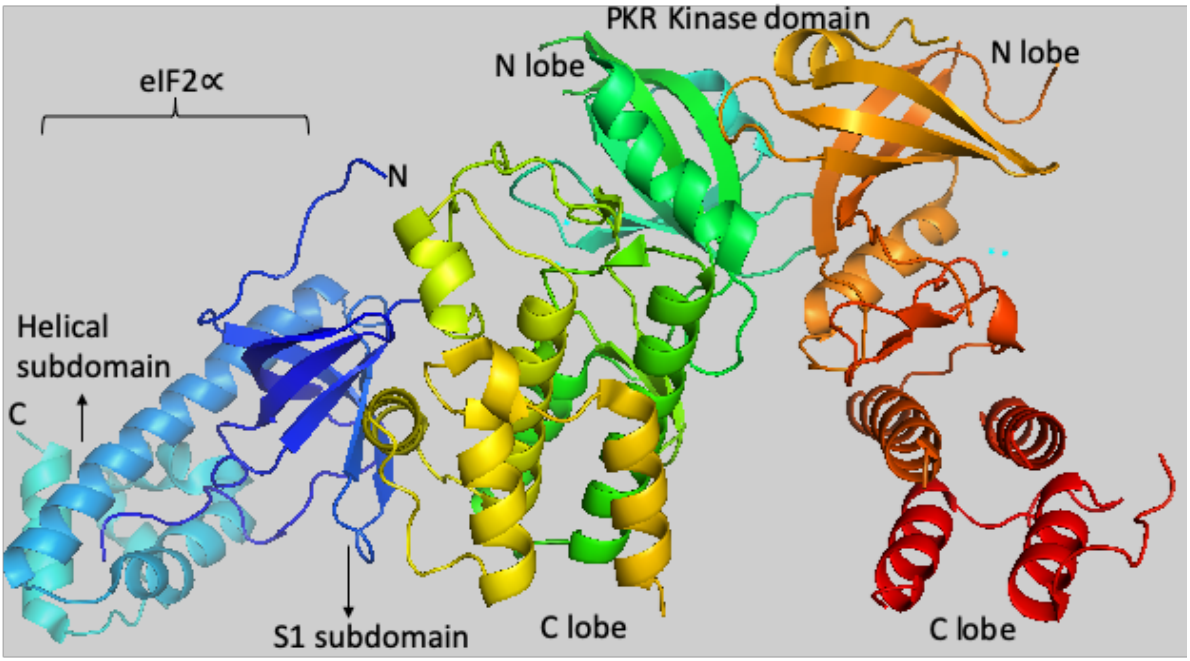

Figure 2.5. Structure of the PKR-eIF2α complex.

Cartoon representation of the PKR/eIF2α complex (P3221 crystal form) highlighting catalytic-domain dimerization mediated by the N lobe of PKR and eIF2α recognition mediated by the C lobe of PKR. Figure adapted from reference [45]. Figure generated by The PyMOL Molecular Graphics System, Version 2.0 Schrödinger, LLC.

2.4. ***Eukaryotic Translation Initiation Factor (eIF2α)***

Translation of an mRNA molecule by the ribosome occurs in three stages: initiation, elongation, and termination. Initiation starts when the small ribosomal subunit binds to the start of the mRNA sequence. A transfer RNA (tRNA) molecule carrying the amino acid methionine (Met-tRNA$_i$) binds to the start codon (AUG) of the mRNA sequence. This complex joins the 60S ribosomal subunit to form an 80S initiation complex. Each of these steps is stimulated by soluble protein factors known as eukaryotic initiation factors (eIFs). The primary role of eIF2 during the initiation process is to transfer Met-tRNA$_i$ to the 40S ribosomal units. The transfer is initiated by a ternary complex consisting of Met-tRNA$_i$,

eIF2 and GTP and is stimulated by other translation initiation factors such as eIF3, eIF1A, and possibly eIF5B [48, 49]. The resulting 43S preinitiation complex binds mRNA, forming the 48S complex, led by the mRNA-associated factors (eIF4E, eIF4G, eIF4A, eIF4B, and poly[A]-binding protein) and the eIF3 present in the 43S complex. The preinitiation complex scans the mRNA, pairs the anticodon of Met-tRNA$_i$ and the AUG start codon triggers hydrolysis of GTP by eIF2, dependent of the GTPase activating protein (GAP) eIF5. After release of eIF2–GDP and eIF3, the 60S subunit joins the assembly in a reaction stimulated by eIF5B and involves the hydrolysis of a second molecule of GTP [49, 50]. The eIF2-GDP complex does not bind to the Met-tRNA$_i$, and recycling of the GTP necessitates the guanine nucleotide exchange factor (GEF) eIF2B [51].

eIF2 is a multifunctional protein with three subunits: eIF2α, eIF2β and eIF2γ. Both the eIF2β and eIF2γ subunits are involved in the GTP binding during initiation of translation whereas the eIF2α subunit is a major site of control of the translation initiation process through the phosphorylation of a specific serine residue (Serine 51) [49, 52]. These subunits of eIF2 are well conserved in eukaryotes, homologues of these subunits are present in the archaea but not in bacteria [53]. eIF2α acts as a substrate to a number of protein kinases such as HRI (Heme regulated protein kinase), PKR (response to dsRNA in viral infected cells), GCN2 (response to amino acid starvation) and PERK (response to unfolded proteins in the endoplasmic reticulum) [54-58].

eIF2α is a protein with 303 amino acids and has an elongated two domain structure. The structure of N-terminal two-thirds of the human eIF2α was solved by x-ray crystallography [59]. The crystal structure revealed a two domain structure where the N-terminal (residues 1-89) form a five-stranded antiparallel β-barrel and the amino acid

residues 90-175 form a helical domain [53, 59] (Fig. 2.6). The connectivity of the strands within the β-barrel conforms to the OB (oligonucleotide-binding) fold [53, 60]. The structure of the same amino acid residues of yeast eIF2α was solved in a different study [53]. The structures of both human and yeast eIF2α were compared and was found to have extensive similarities but also some significant differences. The disulfide bridge between cysteine residue 69 and 97 found in human eIF2α is substituted with a hydrophobic interaction between valine residue 69 and cysteine 97 in case of the yeast protein. A four residue deletion between helices α1 and α2 of the helical domain and another four residue deletion between α3 and α4 helices in the yeast eIF2α are different in comparison to the human protein [53]. The other big difference in the crystal structure of yeast and human protein is the visibility of the surface loop consisting of residues 51-65 (connecting strands β3 and β4 of the N-terminal β-barrel domain) in the yeast eIF2α structure. This loop contains the residue serine 51, which is essential for phosphorylation by eIF2α specific kinases (Fig. 2.7).

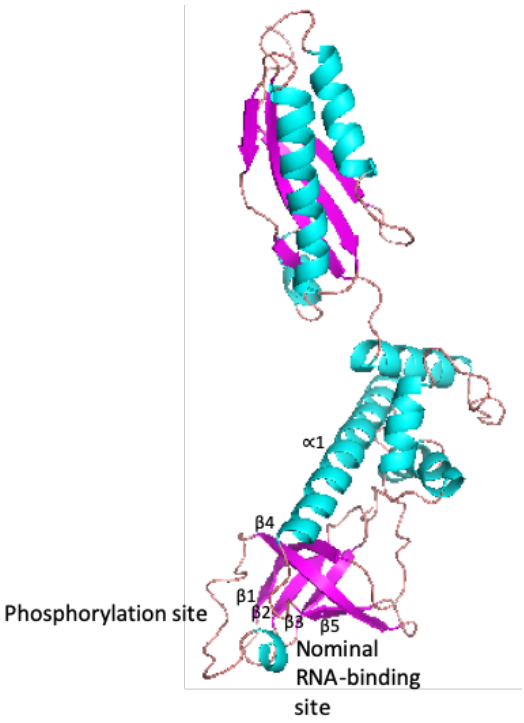

Figure 2.6. Overall structure of human eIF2α.

The phosphorylation site (Ser-51) is indicated. The RNA binding site is constituted by the β-sheets (purple). Figure adapted from reference [59]. Figure generated by The PyMOL Molecular Graphics System, Version 2.0 Schrödinger, LLC.

Another study on the structure of yeast eIF2α$_{1_175}$ was published where the eIF2α was in a complex with dimeric human PKR protein. It was found that except for the region surrounding the serine 51 phosphoacceptor site, the structure of the eIF2α-PKR complex was identical to the crystal structure reported earlier for the yeast eIF2α protein [45].

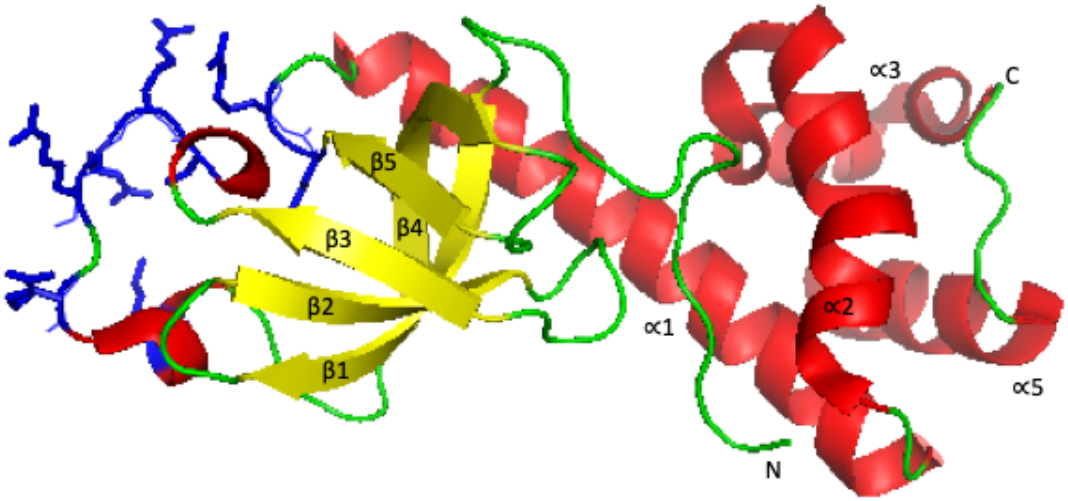

Figure 2.7. Crystal structure of the N-terminal of yeast eIF2α.

A diagram showing residues 1–175 of the yeast eIF2α structure, indicating the positions of some of the conserved side-chains in the vicinity of Ser51 (S51, R52, R53, R54, R56, K60, K86, R87). Figure adapted from reference [53]. Figure generated by The PyMOL Molecular Graphics System, Version 2.0 Schrödinger, LLC.

*2.5. **PKR phosphorylates eIF2α to inhibit protein synthesis***

There are three steps involved in PKR inhibition of protein synthesis that starts with PKR activation in which the kinase domain dimerization facilitates activation-segment autophosphorylation, which in turn promotes the specific recognition of eIF2α substrate. The phosphorylated eIF2α then leads to inhibition of protein synthesis.

In the event of viral infection, PKR initiates a cascade of reactions that initiate immune response against the virus. PKR exists as an inactive monomer in homeostasis but undergoes dimerization for its activation during viral infections. Multiple studies have proposed an autoinhibition model for PKR activation where dsRNA produced by viruses during infections bind to the DRBD of PKR, thus inducing a conformation change which

helps in dimerization of the protein [61-63]. Another study supported this autoinhibition model by proposing that PKR's second DRBD interacts with residues within the insert region (residues 328-335) to mask PKR's kinase domain [64]. Although it has been shown that dsRNA binding to DRBDs leads to PKR dimerization, evidence for a dsRNA independent mechanism also has been reported [65, 66]. A study conducted by Tan et al. found that PKR could dimerize in vivo and in vitro independently of the DRBDs and the dimerization in this case was mediated by amino acid residues 244 to 296 [67]. A model for PKR dimerization was predicted based on these findings suggested the interaction of dsRNA with the DRBDs of PKR functions in two ways. In the 1st method, dsRNA binding targets PKR to ribosomes that increases the effective intracellular PKR concentration leading to dimerization and subsequent functional activity. Whereas in the 2nd method, the dsRNA binding leads to a conformational change in PKR that exposes the amino acids 244-296 region to promote formation of a PKR homodimer of the kinase domain (Fig. 2.8) [67]. The importance of amino acids 244-296 for PKR dimerization was verified by Tan et al. where a cellular inhibitor P58^{IPK} binding to these residues altered the conformation of PKR kinase domain in such a way that even in the presence of DRBDs, PKR could no longer form a functional dimer [67]. Similarly, a study conducted by Romano et al. suggested that the N-terminal of VACV E3 protein interacted with the kinase domain of PKR and prevented dimerization via PKR residues 244-296, independent of dsRNA binding of E3 protein [13].

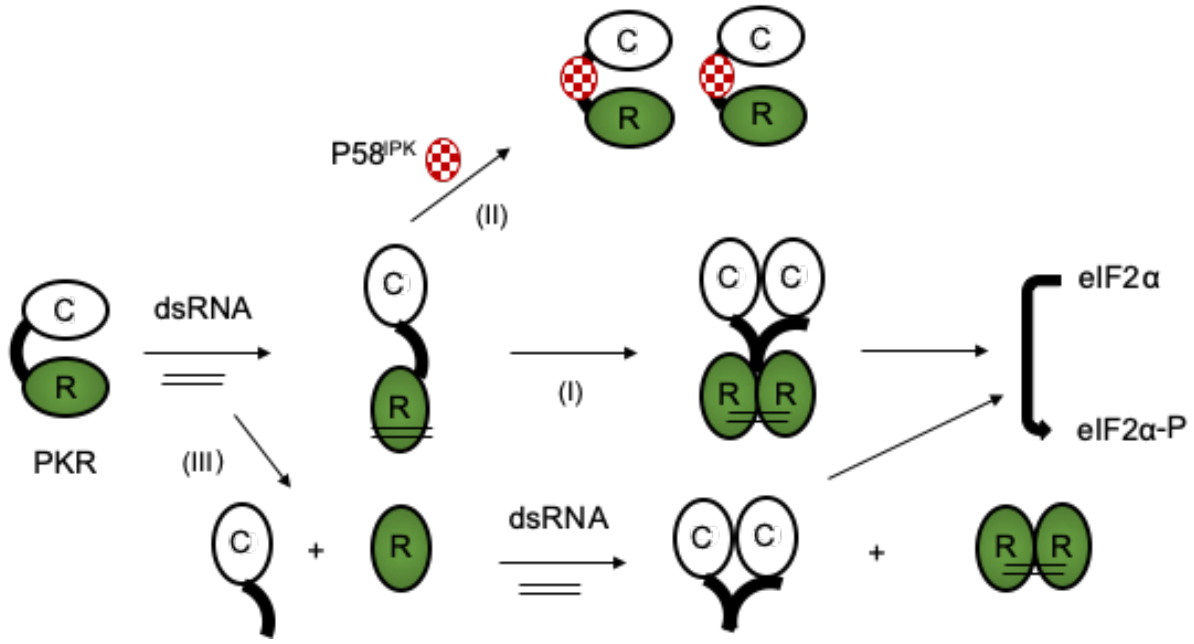

Figure 2.8. Proposed model for the modulation of PKR dimerization.

The catalytic domain (C) and the regulatory domain (R) containing DSRMs are shown. (I) dsRNA binding to the DSRMs bridges PKR molecules and induces a conformational change that unmasks the dimerization site with residues 244 to 296 (darkened region) to promote intermolecular association of PKR. (II) Binding of P58IPK to the aa 244-to-296 region leads to monomerization of PKR and presumably to inactivation of the kinase. (III) Deletion of the DSRM sequences results in a conformational alteration exposing this dimerization region, and thus the isolated catalytic domain is still capable of forming dimers via aa 244 to 296. Figure adapted from reference [67].

Based on the crystal structure of the dimeric kinase domain of PKR and eIF2α complex, it was observed that the residues on one face of N-lobe in the kinase domain are critical in forming the interface between monomers in active PKR dimers. This dimer interface orients the two kinase domains in a parallel, back-to-back manner with the PKR active sites facing outward [45]. Dimerization of PKR is followed by autophosphorylation and the back-to-back conformation of PKR kinase domain dimer makes transphosphorylation difficult. It was suggested that dimerization stimulates autokinase activity in cis-form or by

another dimer in close proximity [45]. Based on these findings another model for PKR activation was suggested and is shown in Figure 2.9.

The second step for PKR activation is autophosphorylation, which occurs simultaneously during dimerization. A study showed that a kinase dead PKR mutant K296R impaired PKR-KD dimerization, indicating that kinase domain dimerization promotes activation segment autophosphorylation of PKR, which in turn would stabilize dimerization [68]. Hence, it is considered that autophosphorylation and dimerization are mutually protected events. The activation segment which serves the phosphoregulatory function in PKR is located between helices αE and αEF in the lower catalytic lobe (residues 432-458) [46, 47]. Phosphorylation of certain residues within the activation segment is essential for PKR activity. Threonine 446 in the activation segment of PKR kinase domain undergoes phosphorylation and known to be critical for general activation of PKR catalytic efficiency, for stabilization of the PKR-KD dimer, and for eIF2α specific substrate recognition [13, 45, 68]. The 2nd threonine residue at 451 position in the activation segment also plays a major role in autophosphorylation of PKR-KD [45].

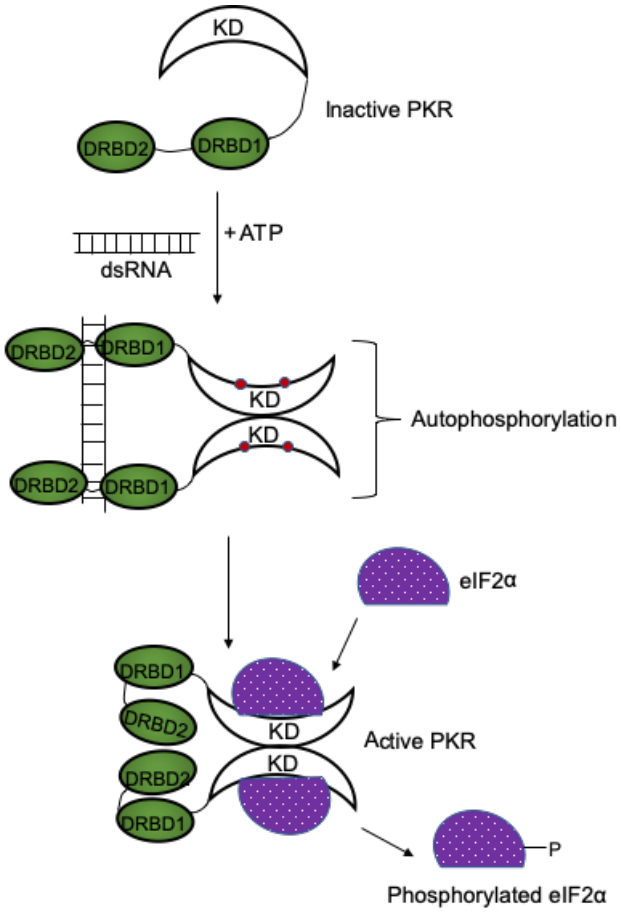

Figure 2.9. Model of PKR activation.

An inactive, unphosphorylated PKR monomer is activated by binding to dsRNA. Binding of activating ligands at the N-terminus of the kinase disrupts an autoinhibitory conformation to enable association between monomers and binding of ATP within the catalytic site of the kinase domain. Each monomer is autophosphorylated to form the fully active, dimeric enzyme. The autophosphorylated dimer dissociates from the activating ligand and binds to and phosphorylates protein substrates, exemplified by eIF2α. Figure adapted from reference [69].

The third step of PKR activation is the substrate phosphorylation of eIF2α. The phosphorylation of eIF2 by PKR kinase domain occurs at a specific residue, Serine 51. The crystal structure of PKR-KD and eIF2α complex indicates that eIF2α binds to the C-lobe of the PKR-KD at a region centered on the N-terminal end of helix αG. For binding with PKR-

KD, eIF2α utilizes the surface of its β barrel which involves all the five β-strands [45]. Comparison of the crystal structure of eIF2α with PKR-KD-eIF2α complex structure revealed that binding of PKR to eIF2 promoted the unfolding of helix insert of eIF2α which made the serine 51 site fully accessible to the phosphoacceptor binding site of PKR.

During the translation initiation process, prior to binding Met-tRNAi, the GDP bound to eIF2 must be exchanged for GTP. The exchange of GDP to GTP is mediated by eIF2B [70]. Phosphorylation of the conserved serine residue (Ser51) in eIF2α converts eIF2-GDP from a substrate to a competitive inhibitor of eIF2B [49]. Due to the increased affinity of eIF2 to its enzyme eIF-2B, a high sequestering interaction is formed between the two proteins, which inhibits the recycling of GTP to GDP. In order for the translation initiation process to start again eIF2α needs to form a complex with GTP which is impossible with the dead-end complex of eIF2 and eIF-2B thus blocking the initiation of translation and leading to reduction or inhibition of protein synthesis (Fig. 2.10) [49].

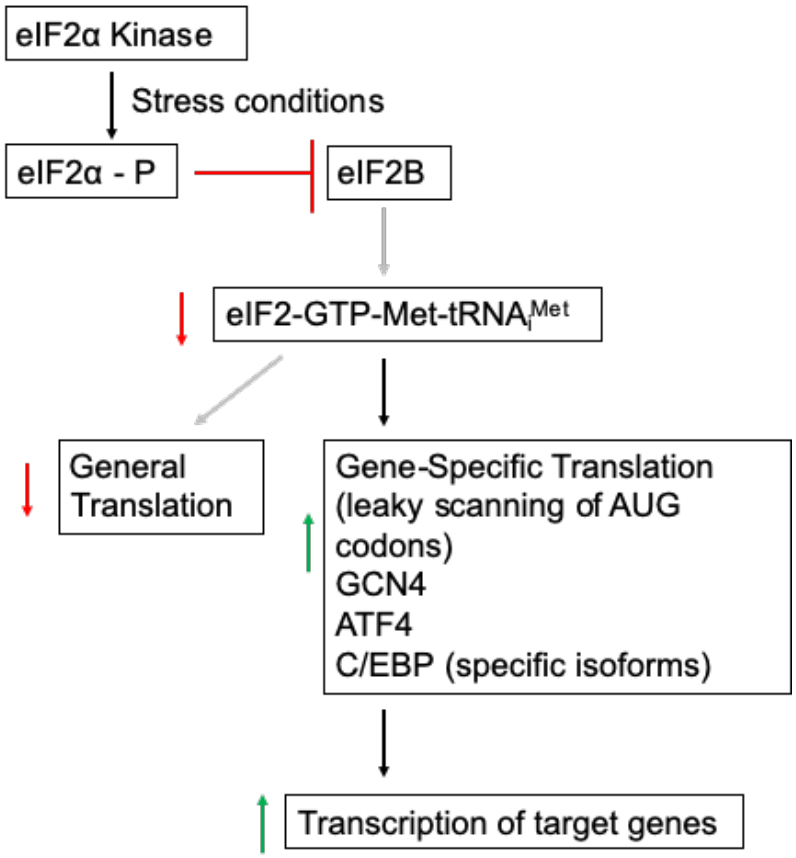

Figure 2.10. Stress response pathway for regulation of translation by eIF2α phosphorylation.

The eIF2α kinases phosphorylate eIF2α leading to inhibition of eIF2B (red bar). This results in low levels of ternary complex (grey arrow) resulting in reduced general translation (grey arrow) and increased translation of GCN4, ATF4, or certain isoforms of C/EBP (black arrow). Increased production of the transcription factors GCN4, ATF4, or C/EBP results in increased expression of their target genes (green arrow). Figure adapted from reference [71].

2.6. ***E3 inhibits the activation of PKR***

Activated PKR phosphorylates its substrate, eIF2α, and in turn the phosphorylated eIF2α inhibits protein synthesis during viral infections. These reactions are initiated by PKR activation as a host immune defense system against viruses. VACV E3 protein, produced early in the viral infection of host cells, downregulates PKR activity inhibiting the host

immune response [72]. E3 downregulated the host defense mechanisms which correlated with the accumulation of E3 early in VACV infection [29, 73]. An early study on vaccinia virus had reported an inhibitor of PKR autophosphorylation but it the involvement of E3 was not specified [74]. E3 is known to bind physically with PKR. Based on in vitro and in vivo binding assays in a study conducted by Sharp et al, two regions on PKR were known to interact with VACV E3 protein. One of the binding regions involved the DRBDs of PKR and the other overlaps the region of interaction with eIF2α and the pseudosubstrate VACV K3 protein [75]. This study demonstrated that E3 could directly interact with PKR and suggested that E3 downregulates PKR by forming nonfunctional heterodimers. These nonfunctional heterodimers could prove essential for controlling the activation of PKR through other cellular mechanisms such as heparin, which is a known activator of PKR and can substitute dsRNA for autophosphorylation of PKR kinase domain [76]. A model proposed by Sharp et al. explained the regulation of PKR activity by E3 (Fig. 2.11). PKR remains in a latent inactive state in homeostasis. In the advent of viral infection and a low concentration of dsRNA in the cell, activates PKR by undergoing dimerization. E3 protein produced early in the viral replication cycle binds to the catalytic domain of PKR for inhibiting its activation, in the absence of dsRNA. The interaction between E3 and PKR is different in the presence of higher concentration of dsRNA where E3 forms a nonfunctional heterodimer with the DRBDs of PKR thereby inhibiting the host immune response pathway [75].

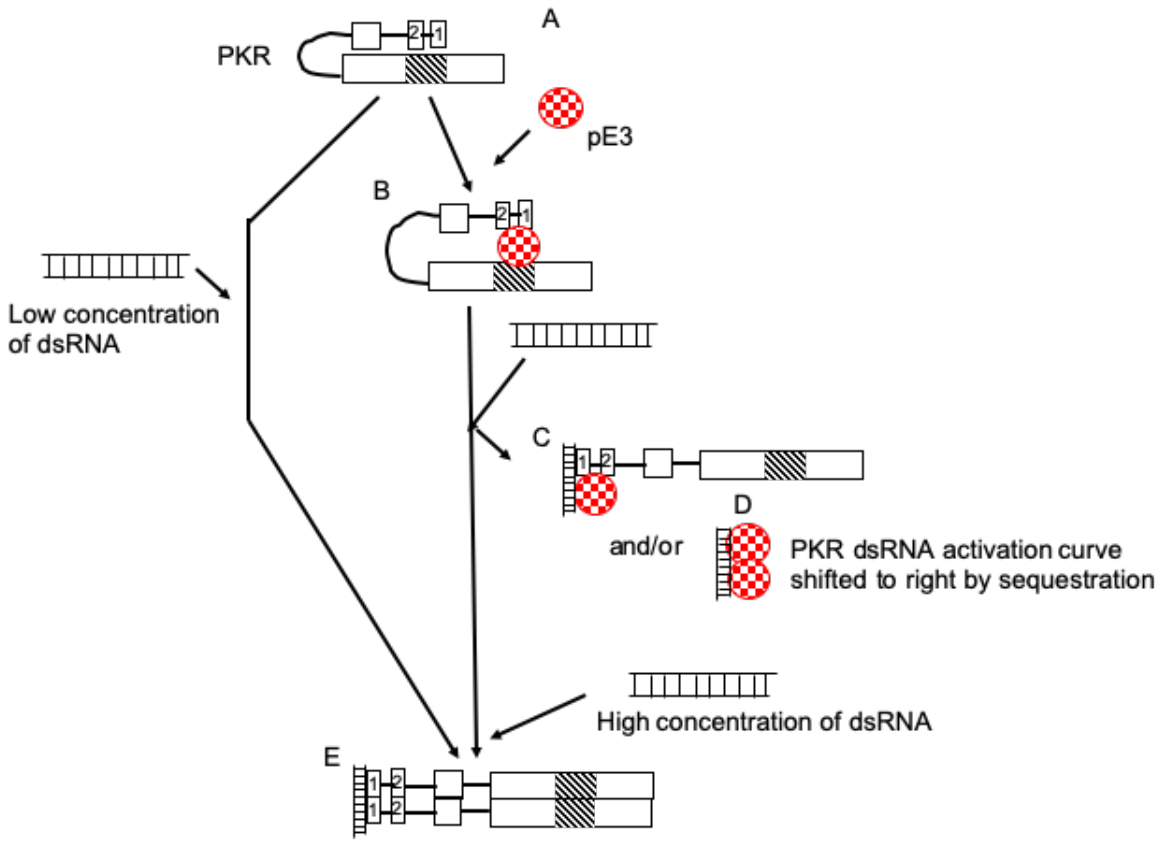

Figure 2.11. Model for the interaction of E3 with PKR and the dsRNA- dependent dimerization and activation of PKR.

The DRBDs of PKR are indicated by the number 1 or 2, for DRBD1 and DRBD2, respectively. The hatched box represents the substrate binding domain. The model begins with a depiction of PKR in its inactive state, showing the interaction of the regulatory domain masking the substrate binding domain (A). This is depicted as occurring via an intramolecular reaction but could just as well occur via an intermolecular reaction between two PKR molecules giving an inactive dimer. The model goes on to show that pE3 can prevent PKR activation by three different mechanisms: in the absence of dsRNA by interaction with the substrate binding domain (B) and by the formation of nonfunctional heterodimers formed by three different mechanisms (C): in the absence of dsRNA by interaction with the substrate binding domain (B); by the formation of nonfunctional heterodimers formed by interaction with dsRNA and the DRBDs of PKR (C); and by sequestration of dsRNA (D). The active form of PKR is depicted in E. Figure adapted from reference [75].

A second model for E3 and PKR interaction was proposed by Romano et al. (Fig. 2.12). It was suggested that a protein-protein contact occurred between the DRBD domains of PKR and E3 with a mutual binding to the same dsRNA that stabilized the complex of PKR-E3-dsRNA [13]. Coimmunoprecipitation in yeast extracts, suggested that a majority of the PKR molecules in yeast were physically associated with E3 in a manner dependent on the dsRNA binding activity of E3 [13]. The yeast two-hybrid and GST pull-down assays revealed complex formation between the C-terminal half of E3 and the N-terminal half of PKR. These segments contained their DRBDs and the interaction among them also depended on dsRNA binding by the E3 protein. Along with coimmunoprecipitation and GST pull-down assays, it was observed that binding between PKRΔ243-551 and EΔ37-86, K167A, R168A was rescued by high concentrations of dsRNA, indicating that complex formation is critically dependent on the DRBD containing segments of both proteins and dsRNA binding by E3 [13]. To summarize the model, an active homodimer of PKR in the presence of dsRNA is disrupted by the binding of E3 proteins, thus forming an inactive heterodimer. The N-terminal of E3 interacts with the C-terminal of PKR along with interactions between the DRBDs of both proteins. Interactions between E3 and PKR requires dsRNA. The inactive heterodimer of PKR-E3-dsRNA fails to initiate the immune response during viral infection.

The two different models predicted for E3 and PKR interaction emphasized on the fact that dsRNA binding ability is required for the E3 to inhibit PKR activity but a recent study revealed that for E3 to perform its biological functions, it does not require its biochemical capacity to bind to dsRNA [14].

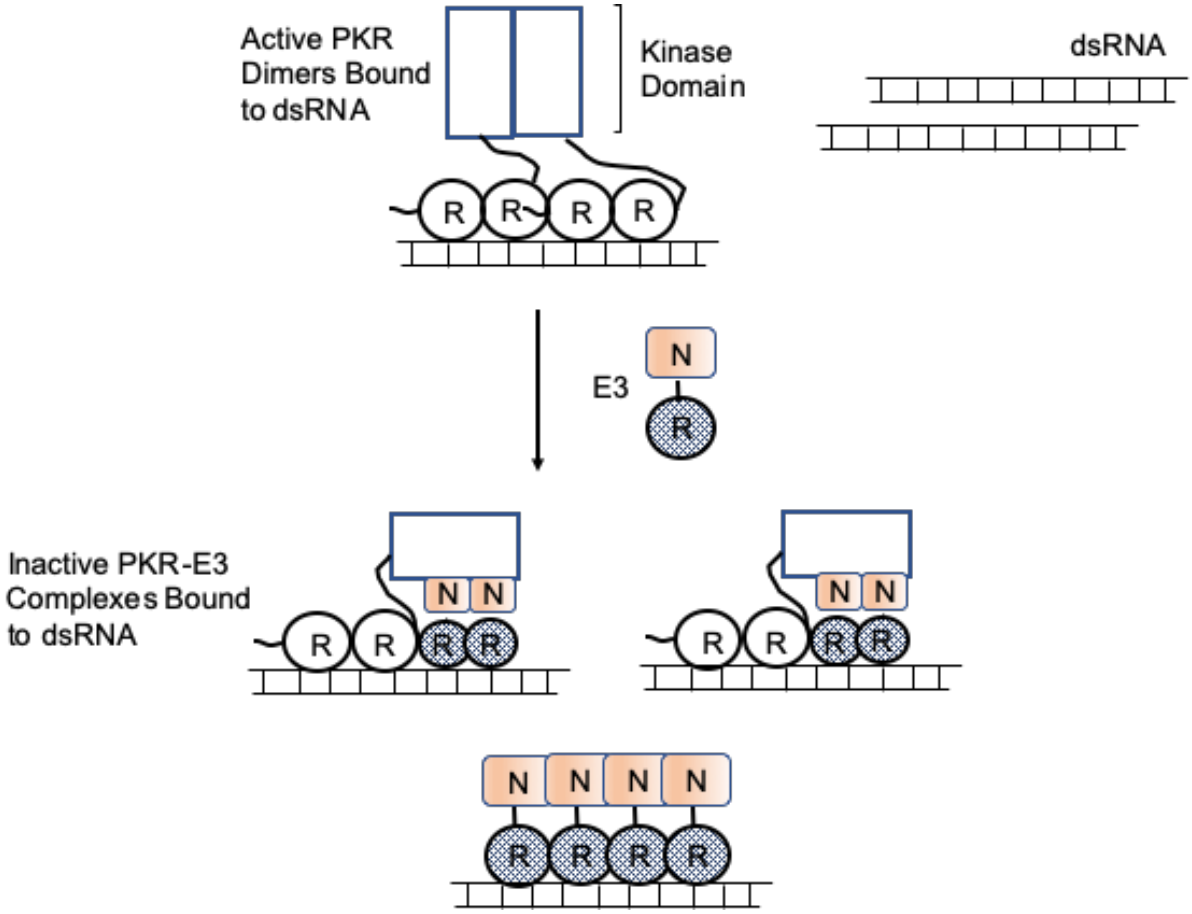

Figure 2.12. Hypothetical model for inhibition of PKR function by E3 through the formation of inactive heteromeric complexes.

PKR is shown schematically with its two DRBMs (R) and the kinase domain depicted as rectangles. E3 is depicted with its single DRBM (R) hatched and the N-terminal domain (N) shaded. The active form of PKR is depicted as a dimer bound to dsRNA, with dimerization mediated by interactions involving the N-terminal region containing the DRBMs, the kinase domain, and the region from residues 244 to 296 and by binding to the same dsRNA molecule. E3 is shown inhibiting PKR by forming inactive heterocomplexes, disrupting PKR homodimers. In addition, the N-terminal domain of E3 is shown interacting with the kinase domain of PKR, interfering with some aspect of kinase function. Binding to dsRNA by E3 greatly contributes to the stability of the PKR-E3 complex. E3 can also inhibit kinase activation by sequestering dsRNA molecules. Figure adapted from reference [13].

CHAPTER III

METHODOLOGY

3.1. ***Mutations of VACV E3 protein***

Different single (I110A, K109A, W113A, I122A, F148A, R131A, K167A, Y125A, R168A, A174V, A175V, I154A, and F159A) and double mutations (L182A L183A, R131A I110A and R131A F159A) of E3 were developed. Forward and reverse primers designed for the specific targeted mutation were purchased from Integrated DNA Technologies (IDT, IL). PCR was set up with wildtype E3 as a template, mutation specific primers, high fidelity KOD DNA polymerase designed for PCR amplification of DNA templates (Millipore Sigma, MA) and a total reaction volume of 50 μL. PCR conditions were set as follows; initial denaturation at 95°C for 30 seconds, denaturation step at 95°C for 30 seconds (16 cycles), annealing for 1 minute at 55°C and finally extension at 68°C for 2 minutes with no final extension step. PCR amplified products were mixed with DpnI restriction enzyme (New England BioLabs, MA) and incubated for an hour at 37°C to digest the parental DNA (nonmutated supercoiled dsDNA). DpnI digested products were then transformed into *E.coli* BL21 (DE3) competent cells (New England BioLabs, MA) by electroporation. BL21 (DE3) cells are B strains of *E.coli* and are deficient in Lon protease (cytoplasm) and OmpT protease (outer membrane). These competent cells contain the λDE3 lysogen that carries the gene for T7 RNA polymerase

under the control of lacUV5 promoter. In order to induce the expression of T7 RNA polymerase to a maximum effect, IPTG (Isopropyl β-D-1-thiogalactopyranoside) is required which then expresses the recombinant genes cloned downstream of a T7 promoter [77].

Electroporated cells were grown at 37°C for an hour and later were plated on kanamycin containing LB agar plates. LB agar plates were incubated overnight at 37°C. Colonies obtained from the plates were submitted for sequencing which confirmed the presence of single point mutations in E3 DNA sequence. The protocol for mutagenesis was obtained from Stratagene QuickChange® Site-Directed Mutagenesis Kit.

3.2. ***Protein expression and purification of VACV E3 mutants***

VACV E3 mutants were cloned into a modified pET28b vector that expressed maltose binding protein (MBP) with an N-terminal 6-histidine-tag and a C-terminal tobacco etch virus (TEV) protease recognition site (Glu-Asn-Leu-Tyr-Phe-Gln/Gly). A cassette containing the coding sequence for E3 mutants under the control of a T7 promoter was inserted into the vector (Fig. 3.1). The 6x histidine tag on the fusion protein allows a single step purification of protein whereas the MBP tag helps in producing very high yield of fusion protein that are soluble and properly folded. The plasmid containing the E3 mutants were expressed in *E. coli* BL21 (DE3) cells with kanamycin. Small-scale expression studies were conducted with 50 mL of LB media grown at 37°C to test the different E3 mutants. IPTG at a final concentration of 1 mM was added to induce expression of fusion protein when the optical density (OD_{600nm}) of the culture reached ~0.8. The temperature for growing the LB cultures was reduced to 18°C. After growing the cultures overnight at 18°C, the cells were collected by centrifuging at 4713 x g and kept frozen in -20°C for future use.

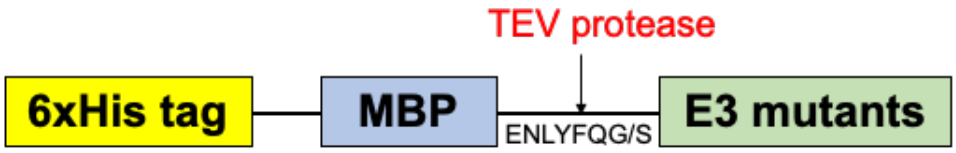

Figure 3.1. Plasmid map for E3 mutants in pMBP28b+ vector.

A 6x histidine tag on the N-terminal followed by maltose binding protein with E3 mutants on the C-terminal separated by TEV protease cleavage site. Both the single mutants and double mutants of E3 were cloned in the MBP plasmid.

Cell pellet was homogenized and filtered supernatant was passed through a Ni-NTA (Nickel-nitrilotriacetic acid) affinity column (Qiagen, MD). E3 mutants expressed along with MBP are highly soluble and because of the 6-histidine tag on the N-terminal, the fusion protein bound to the Ni-NTA column. The Ni column was washed multiple times with wash buffer and fusion protein that remained bound to the column was eluted using buffer containing 250 mM imidazole concentration. The elute from the column was subjected to TEV protease digestion which removed the His-MBP tag from the fusion protein and E3 protein was collected as a flow-through of a second Ni-NTA purification. E3 protein was further purified using size exclusion chromatography (SEC) (Superdex 200 Increase 10/300 GL column, GE Healthcare, MA). Large-scale expression and purification of E3 single and double mutants were optimized and conducted in a similar manner as small-scale expression.

3.3. ***Protein expression and purification of human PKR kinase domain (PKR-KD)***

The full length kinase domain of PKR (amino acids 258-551) was cloned into various vectors such as a modified pET28b vector that expressed maltose binding protein (MBP) with an N-terminal 6-histidine-tag and a C-terminal tobacco etch virus (TEV) protease

recognition site (ENLYFQG/S) (Fig. 3.2). A modified pET22b vector consisting of Glutathione S-transferase (GST) protein along with the TEV protease recognition site was also used for cloning the full length PKR-KD (Fig. 3.2). A cassette containing the coding sequence for PKR-KD under the control of a T7 promoter was inserted into this vector. The GST tag helps in a single step purification of PKR-KD by using a column of immobilized glutathione. A shorter PKR-KD (258-541) with the last 10 amino acids from the C-terminal deleted was also cloned into MBP vector. A double mutant of full length PKR-KD (H412N, C551A) was cloned into both MBP and GST vectors. A single mutant of the shorter PKR-KD (H412N) was cloned into both MBP and GST vectors. A construct of PKR-KD which was used for solving the crystal structure of PKR-KD and eIF2α complex had two mutations (H412N and C551A) and a 13 amino acid deletion of a protease sensitive β4 - β5 loop (residues 338-350) [45]. This crystallizable construct was also cloned into both the MBP and GST vectors. Different constructs were used for expression and purification of PKR-KD in an effort to use these PKR-KD proteins for complex formation with E3 proteins.

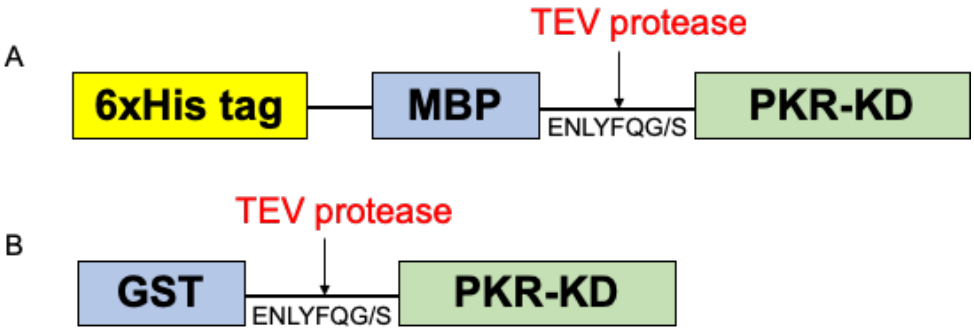

Figure 3.2. Plasmid maps for PKR-KD in pMBP28b+ and pGST vector.

(A) A 6x histidine tag on the N-terminal followed by maltose binding protein with PKR-KD on the C-terminal separated by TEV protease cleavage site. (B) A glutathione-s-transferase tag on the N-terminal and C-terminal PKR-KD separated by TEV protease cleavage site.

The plasmid containing the PKR-KD in GST and MBP vectors were expressed in *E. coli* BL21 (DE3) cells with ampicillin and kanamycin respectively. Large-scale cultures were grown in 1 liter of LB media at 37°C. IPTG at a final concentration of 1 mM was added to induce expression of fusion proteins when the optical density (OD_{600nm}) of the culture reached ~0.8. The temperature for growing the LB cultures was reduced to 18°C. After growing the cultures overnight at 18°C, the cells were collected by centrifuging at 4713 x g and kept frozen in -20°C for future use. Cell pellets were homogenized and the supernatant was filtered and passed through Ni-NTA affinity column.

Clones with GST fusion protein were loaded on to a glutathione column. GST fusion protein specifically bound to the column. Protein loosely bound to the column were cleaned out of the column by a wash buffer. Fusion protein was eluted by adding reduced glutathione that displaced the target protein out of the column. The fusion protein was digested by adding TEV protease that separated PKR-KD from GST protein.

In case of the pMBP28b+ vector, a Ni-NTA affinity column was utilized for purification. The method of purification followed was similar to the procedure of E3-MBP fusion protein purification where 1st Ni purification followed a SEC purification. Fractions from SEC purification (Superdex 200 column) containing clean fusion protein were pooled and digested with TEV protease to remove MBP from PKR-KD followed by another SEC purification. All the buffers used after fusion protein digestion had 40mM maltose to prevent

non-specific binding of MBP to PKR-KD and 10% glycerol to prevent precipitation of protein at higher concentrations.

*3.4. **Protein expression and purification of yeast eIF2α***

The N-terminal of yeast eIF2α_{4_175} was cloned into a pSKB3 vector that expressed a N-terminal 6-histidine-tag followed by a tobacco etch virus (TEV) protease recognition site (ENLYFQG/S) (Fig. 3.3). A cassette containing the coding sequence for eIF2α under the control of a T7 promoter was inserted into the vector.

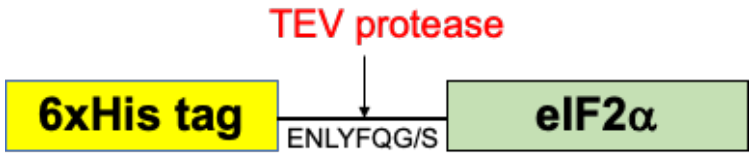

Figure 3.3. Plasmid map for yeast eIF2α in pSKB3 vector.

A 6x histidine tag on the N-terminal and eIF2α on the C-terminal separated by TEV protease cleavage site.

The plasmid containing the eIF2α gene were expressed in *E. coli* BL21 (DE3) cells with kanamycin. Large-scale cultures were grown in 1 liter of LB media at 37°C. IPTG at a final concentration of 1 mM was added to induce expression of fusion proteins when the optical density (OD_{600nm}) of the culture reached ~0.8. The temperature for growing the LB cultures was reduced to 18°C. After growing the cultures overnight at 18°C, the cells were collected by centrifuging at 4713 x g and kept frozen in -20°C for future use. Cell pellets were homogenized and the supernatant was filtered and passed through a Ni-NTA affinity column. The fusion protein bound to the column due to the presence of 6-Histidine tag on the

N-terminal was eluted out of the column using a buffer consisting of 250 mM imidazole. The eluted protein was passed through a SEC Superdex 200 column as a final step of purification. The fusion protein was used for in vitro kinase assays without removal of the 6-histidine tag.

3.5. ***Protein characterization***

The final purified proteins of E3 and PKR-KD were characterized by dynamic light scattering (DLS) (Zetasizer μV, Malvern Panalytical, UK) and size exclusion chromatography. DLS was used to detect aggregation state of the purified E3 mutants and the monomeric/dimeric state of PKR-KD. The data from DLS also provided information regarding the oligomeric state of SEC fractions along with mono or polydisperse nature of the E3 proteins. Molecular weight of protein was also estimated by SEC using a standard provided by the manufacturer (catalog # 1511901, BIO-RAD, CA).

3.6. ***Thermal shift assay of E3 proteins using Real-Time PCR (RT-PCR)***

Thermal shift assays involve incubation of natively folded proteins with fluorescent dye in a 96 well PCR plate. The thermal denaturation of a protein in many conditions can be detected simultaneously by increasing the temperature systematically while monitoring the fluorescence emission. The increase in melting temperatures in different conditions give rise to a 'thermal shift' that quantifies the stabilization of the protein under different buffer or additive conditions [78].

The stability of E3 protein with different additives was tested by conducting real-time PCR. SYPRO orange (catalog # S5692, Millipore Sigma, MA) was used as a fluorescent dye in the reaction mixture. SYPRO Orange dye has an excitation wavelength of

470 nm, emission at 570 nm and undergoes a significant increase in quantum yield when it binds to hydrophobic regions in denatured proteins yet it is compatible with filter sets found in real-time PCR equipment for detecting protein thermal denaturation assays [79]. An additive screen with 96 different conditions (catalog # HR2-428, Hampton Research) was used for the thermal shift assay. Total reaction volume of 50 μL had buffer (20mM TrisHCl, 150mM NaCl, pH 7.5), E3 protein, different additives and SYPRO orange dye. A 96 well PCR plate was used for setting up the reactions. The stability of E3 protein was scanned over the temperatures of 25°C to 95°C with an increment of 1°C. The raw fluorescence emission data from real-time PCR machine was converted to a first derivative as a function of temperature and plotted against the different temperatures used.

3.7. ***In vitro binding assay between PKR-KD and E3 proteins***

E3 and PKR-KD proteins were purified separately and added in a molar ratio of 2:1 or 1:1 along with 1 mg/mL of AMP (Adenosine monophosphate). AMP was added to activate PKR protein. The protein mixture was incubated at 4°C for an hour and was applied to Superdex 200 SEC column in a buffer containing either 500 mM or 300 mM NaCl. The chromatogram from the SEC purification was compared to the individual purification chromatograms of E3 and PKR-KD to determine the formation of a complex between these proteins. SDS-PAGE and native gels on fractions of complex purification were used for evaluation.

3.8. ***Pull down assay for E3 and PKR-KD protein interaction***

E3 fusion protein (HisMBPE3[R131A]) with 6x-His-MBP tag was used for pull down assays with PKR-KD. E3 fusion protein and PKR-KD were added in a molar ratio of 2:1 and incubated at 4°C for an hour. This protein mixture was applied to a 200µL Ni-NTA column. Flow-through from the column was collected. Wash buffer containing 5 mM imidazole was passed through the column twice and the washes were collected. Protein binding to the column was eluted by a buffer containing 250 mM imidazole. The collected fractions from the Ni column purification were added with SDS loading buffer, boiled and electrophoresed on 15% SDS-PAGE gels. The SDS gels were transferred to polyvinylidene difluoride (PVDF) membrane (Immobilon -P, Millipore Sigma, MA) and blotted with an antibody that recognizes PKR residues 435 to 449 (catalog # PA1-990, Invitrogen, CA). A chemiluminescent substrate (catalog # 34077, Thermo scientific, IL) was added to the membranes and visualized under chemiluminescence (FluorChem E, Proteinsimple, CA). A control reaction was set up with a fusion his-MBP tagged STF protein and PKR-KD. STF is an unrelated plant protein that has no known binding with PKR. Similar procedure was followed as before and chemiluminescence was visualized and documented. The entire procedure was also conducted for PKR-KD only to eliminate the possibility of non-specific binding of PKR-KD to Ni column. The western blot membranes were quantified using Image J software.

3.9. ***In-vitro kinase assay between E3 and PKR-KD***

Purified PKR-KD (monomer) or GST-PKR-KD (dimer) were diluted in a kinase reaction buffer made up of 17 mM $MgCl_2$, 60 mM HEPES [pH 7.0], 0.2 mM DTT. The PKR

proteins were then incubated with equimolar quantities of His-tagged eIF2α_{4_175} recombinant protein and varying amounts of E3[R131A] mutant in the presence 500 μM ATP. The total reaction volume was 50 μL with the final concentrations of PKR-KD, GST-PKR-KD and His-eIF2α_{4_175} as 1 μM in the reaction mixture. The final E3 concentrations were set up as 0, 3.2, 6.4, 12.9, 25.7 and 51.4 μM. After 25 minutes of incubation at 4°C, samples were mixed with SDS loading buffer, boiled and electrophoresed on 15% SDS-PAGE gels, transferred onto a polyvinylidene difluoride membrane (PVDF) (Immobilon -P, Millipore Sigma, MA) and blotted with anti-phospho-ser51 eIF2α antibody (catalog # PA5-37800, Invitrogen, CA) or anti-his antibody (catalog # MA1-80218, Invitrogen, CA). A chemiluminescent substrate (catalog # 34077, Thermo scientific, IL) was added to the membranes and visualized under chemiluminescence (FluorChem E, Proteinsimple, CA). The western blot membranes were quantified using Image J software.

3.10. ***In-vitro autophosphorylation assay***

Purified PKR-KD (monomer) or GST-PKR-KD (dimer) were diluted in a kinase reaction buffer made up of 17 mM $MgCl_2$, 60 mM HEPES [pH 7.0], 0.2 mM DTT. The PKR proteins were then incubated with equimolar quantities of His-tagged eIF2α_{4_175} recombinant protein and varying amounts of E3[R131A] mutant in the presence 100 μM cold ATP supplemented with 5 μCi of γ^{32}P ATP. The total reaction volume was 50 μL with the final concentrations of PKR-KD, GST-PKR-KD and His-eIF2α_{4_175} as 1 μM in the reaction mixture. The final E3 concentrations were set up as 0, 3.2, 6.4, 12.9, 25.7 and 51.4 μM. After 25 minutes of incubation, samples were mixed with SDS loading buffer, boiled and electrophoresed on 15% SDS-PAGE gels.

A phosphorimager (Typhoon TRIO, GE Healthcare) was used for visualizing the radioactive gels that were exposed to a phosphor imager screen (catalog # 00314394 8x10, Amersham Biosciences) for a week. The phosphor imager screens were exposed to visible light (Image Eraser, Amersham Biosciences) to erase any latent image from previous radiation exposure. These phosphor imager screens are used for recording and quantifying radioactive gels [80]. The screens are made up of crystals of BaFBr:Eu^{+2} and when exposed to ionizing radiation such as α, β or γ, oxidation of Eu^{+2} to Eu^{+3} occur which form a latent image on the screen. The luminescence produced during Eu^{+3} reverting back to Eu^{+2} gets collected during scanning at 633 nm and released as the latent image from the screen [81]. The image was viewed through the phosphorimager and quantified using ImageJ software.

3.11. ***Crystal screen set-up of E3 proteins***

The dimeric E3[R131AI110A] protein in 20 mM TrisHCl, pH 7.5 and 500 mM NaCl was concentrated to approximately 3mg/mL (0.125 μM) and was used for setting up crystal trays using three different crystal screen kits. The kits used were PEG/ION Screen (HR2-098, Hampton Research), Index (HR2-144, Hampton Research) and The BCS Screen (MD1-104, Molecular Dimensions). Each reservoir in the crystal tray was filled with 50 μL of screen kit solution and each crystal drop had 0.5 μL of protein with 0.5 μL of solution from the reservoir. A sitting drop vapor diffusion technique was used for setting up crystal trays in this case and the trays were stored at room temperature. A total of 288 conditions were tested with each screen kit containing 96 different reagents.

3.12. ***Scanning of crystal trays***

The crystal trays with the dimeric E3[R131AI110A] protein were scanned for protein crystal formation. The scanning of trays were conducted using a compound microscope and the schedule for observation was set as every day for a week after the day of setting the tray, once every two weeks and once a month thereafter. The trays were scanned for protein crystals under the microscope. Each droplet was examined carefully and the observations were recorded accordingly.

CHAPTER IV

PURIFICATION OF VACV E3 MUTANTS

4.1. ***Introduction***

A major gap in the knowledge of E3 protein is the understanding of its structure. E3 plays a major role in antagonizing the host immune response. With a broad host range, it makes a perfect candidate for drug development and viral vectors, for treating other diseases. Understanding the structure of E3 protein would be a path forward in that direction. Our goal in this study was to determine the x-ray structure of the full-length E3 protein to provide a more complete structural framework. It would provide us with a better understanding of the functional aspects of E3.

A distinctive property of the full-length E3 protein is its inherent ability to oligomerize in solution. This helps the E3 protein to enter into the nuclear compartment of the host cell with, either directly altering the physical state of the protein or indirectly preventing the export of cytoplasmic E3 proteins into the nucleus [15]. An early study on physical and chemical characteristics of E3 reported that the extent of oligomerization of E3 at equilibrium is governed by solution conditions, particularly ionic strength. Sedimentation analysis suggested that the native form of E3 at 1 M NaCl is likely to be a dimer. This was supported by the formation of crosslinked E3 dimers upon incubation with glutaraldehyde. It was also estimated from gel filtration and sedimentation data that

E3 behaved, on average, as a trimer at 0.5 M NaCl [16]. The oligomerization state is dependent on protein concentration, thus the experimental data from the above mentioned study, that used a lower concentration of 0.25 mg/mL may not be reproducible for a higher concentration of E3 protein.

Crystallization studies require a protein to be highly soluble, pure, homogenous and monodispersed (of a single multimerization state). Wild type E3 proteins is highly soluble but purifies as an aggregate which is a big problem for protein crystallization. The idea of using protein engineering to alleviate aggregation towards structural studies, is motivated from a recent success on a non-related difficult protein project conducted by a group at Baylor College of Medicine, Texas [17]. NS1 protein from H5N1 influenza virus suppresses antiviral interferon (IFN) induction in the host cells but how the protein antagonizes the IFN response was unknown [18]. NS1 protein remains in an aggregated form in the cytoplasm of the host cell similar to E3 protein. Aiming to solve the atomic structure of NS1 by crystallography, the group performed a series of single point mutations where they determined two single mutations that completely removed aggregation. The approach allowed them to crystallize the NS1 protein and perform structural analysis of the crystal [17]. Similarly, it was predicted that single/double point mutations of E3 proteins might mitigate the problem of aggregation and thus help in the structural studies of this protein through x-ray crystallography. Alanine scanning or valine substitution (in the case of alanine residues) mutagenesis on the DRBD (Double stranded RNA inding Domain) of E3 protein was performed to reduce the problem of aggregation during protein purification.

4.2. ***Results and Discussion***

4.2.1. E3 mutants purify as an aggregate except for two mutants R131A and F148A

The inherent nature of E3 protein is to remain in an aggregated form in solution. In this study, we predicted that single point mutations in the DRBD would abrogate E3 aggregation. In order to test this prediction, alanine scanning or valine substitution (in the case of alanine residues) mutagenesis on the DRBD of E3 protein was performed. These mutants were chosen based on their dsRNA binding ability and host range function in a different study [14]. The different E3 mutants were individually expressed in bacterial cells and purified using various purification methods. Molecular weight and aggregation level of E3 protein purified were measured and characterized by size exclusion chromatography (Table 4.1). It was observed that most of the mutants purified as aggregates (a high molecular weight protein eluting in the void volume of the size exclusion chromatography column) similar to wildtype E3 protein. The E3 mutants R131A and F148A purified as lower molecular weight oligomers with some aggregates. These amino acid residues must be involved in stabilizing the protein aggregates and thus mutating them led to aggregation destabilization.

*Table 4.1. Purification of E3 mutants and their ability for dsRNA binding and host range function. (*data obtained from reference [14]).*

E3 Mutants	Single/Double mutation	E3 purified protein state	Poly (I.C) binding*	Host range*
Wildtype	No	Aggregate	Yes	Yes
I105A	Single	Aggregate	No	Limited capacity
K109A	Single	Aggregate	No	No
W113A	Single	Aggregate	No	No
I122A	Single	Aggregate	No	No
F148A	Single	Some aggregate and also lower oligomeric state E3 proteins	No	Limited capacity
R131A	Single	Some aggregate and also lower oligomeric state E3 proteins	No	No
K167A	Single	Aggregate	No	No
Y125A	Single	Aggregate	No	Limited capacity
R168A	Single	Aggregate	No	No
A174V	Single	Aggregate	No	No
A175V	Single	Aggregate	No	No
I154A	Single	Aggregate	No	No
F159A	Single	Aggregate	No	Limited capacity
L182A, L183A	Double	Aggregate	No	No

The SEC chromatograms of the final purification step of E3[R131A] and other E3 mutants were compared (Fig. 4.1). As all of the other mutants except for R131A and F148A, had a similar chromatogram profile, just one of the chromatogram was compared with R131A as a representative. The SDS-PAGE gels on the SEC fractions indicate the presence of E3 and maltose binding protein (MBP) protein based on their molecular weights (Fig. 4.1). A non-specific binding of MBP with E3 led to the presence of MBP in the final purification step. Optimization of the purification process was conducted to obtain a clean and homogeneous protein which could be used for x-ray crystallography.

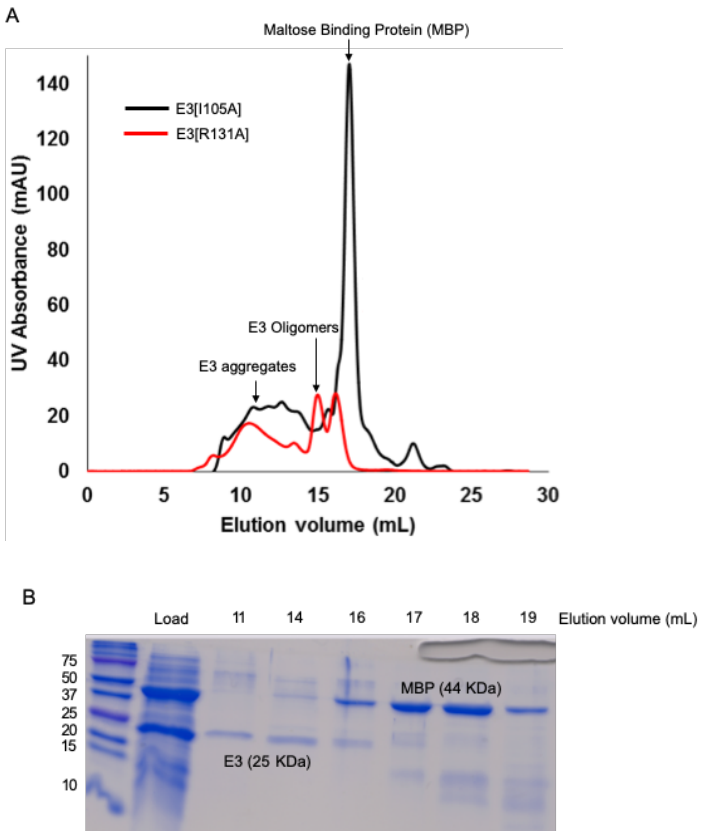

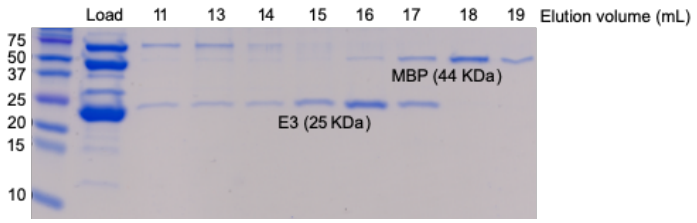

Figure 4.1. Comparison of size exclusion chromatograms of E3[R131A] and E3[I105A] mutants.

(A) SEC profiles of the E3[R131A] which purified as a lower oligomeric E3 proteins (red chromatogram) as compared to E3[I105A] that purified as an aggregate and eluted mostly in void volume of size exclusion chromatography purification (black chromatogram). Most of the E3 mutants except for E3[R131A] and E3[F148A] purified as aggregates and only one of the chromatograms was used for comparison. (B) Corresponding SDS-PAGE gels for the fractions collected from the chromatograms mentioned in A. The 1st SDS gel on top represents the E3 mutants that eluted as aggregates whereas the 2nd gel on bottom represents the fractions from E3[R131A] SEC purification. The 1st lane of the gels is the protein ladder, 2nd lane is the sample that was loaded on the SEC, lanes corresponding to E3 aggregates are the fractions from the void volume, lanes showing E3 oligomers for E3[R131A] gel represent the peak for E3 oligomeric protein and finally the fractions with MBP are the last few lanes in the gel.

4.2.2. Optimization of purification steps for E3[R131A] mutant

Based on the small-scale expression studies, E3[R131A] mutant was used for optimizing the purification process for large-scale production of the protein (Fig. 4.2). Large-scale production of E3[R131A] was conducted to purify a lower molecular weight oligomer, which could be used for crystallization studies. Multiple optimization steps were performed during the purification process.

Optimization was performed to avoid the non-specific binding of MBP to E3 protein during purification. Since MBP is a maltose binding protein, the natural target was to add maltose to the purification buffers. Different concentrations of maltose were tested ranging from 10 mM to 100 mM in buffers for E3 purification. An optimum concentration was determined to be 40 mM maltose. The concentration of 40 mM maltose was maintained in all

of the buffers used for E3 purification steps. Flow-through from affinity purification after digestion of fusion protein should contain only E3 protein and MBP which still has the 6x His-tag should stay bound to the nickel column. A big difference in quality of the flow through was observed with and without 40 mM maltose in purification buffers (Fig. 4.3).

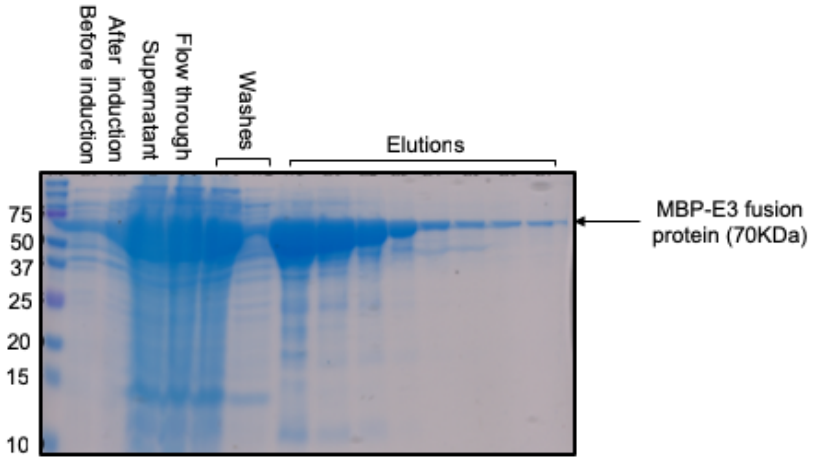

Figure 4.2. SDS-PAGE gel for affinity purification of the fusion protein.

1st lane of the SDS-PAGE gel is the protein marker denoted in KDa, 2nd and 3rd lane corresponds to before and after induction with IPTG samples respectively of cell culture, 4th represents the filtered supernatant that was passed through the nickel column,5th is the flow-through, 6th and 7th are the washes with buffer containing 1M NaCl, rest of the lanes are fractions of fusion protein eluted by using buffer containing 250mM imidazole.

The binding capacity of a nickel column is 20 – 40 μmoles Ni^{2+}/ml resin (Qiagen). A loss of binding capacity of the nickel resin was observed with multiple usage for purification. It was observed, while purifying the E3 mutants, that the same column used for more than two times led to MBP eluting with the target protein due to the loss of binding capacity. Regenerating the Ni-NTA column did not improve the binding capacity. Using a fresh Ni-NTA column with every affinity purification solved the problem of MBP eluting with E3 protein.

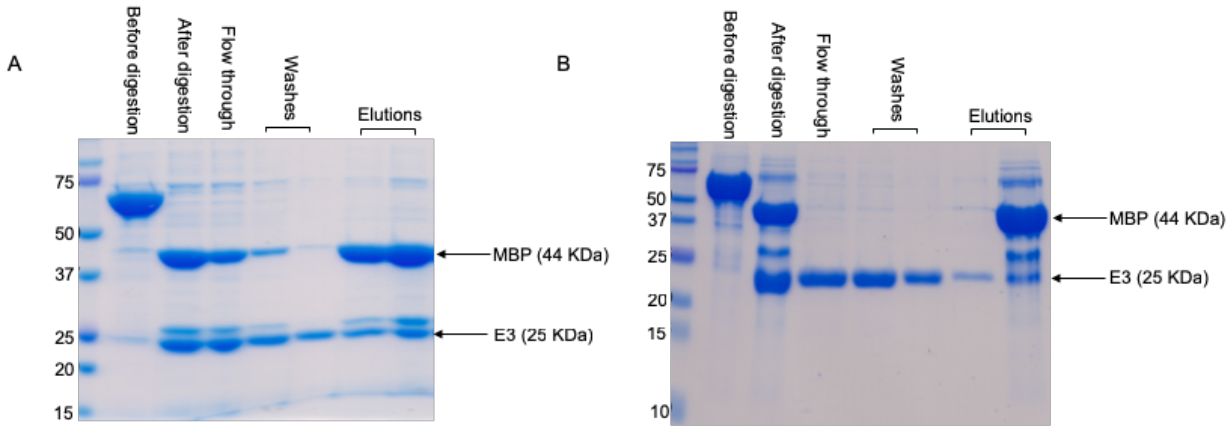

Figure 4.3. SDS-PAGE gels for affinity purification of E3 protein after digestion of MBP tag with and without 40mM maltose in purification buffers.

(A) SDS gel for fractions from an affinity purification after digestion of the MBP tag from the fusion protein (MBP-E3 protein) with no maltose in the purification buffers. The 1st lane corresponds to fusion protein before digestion (70 KDa), 2nd lane is the fusion protein after digestion with 2 different proteins (MBP = 44 KDa and E3 = 25 KDa), 3rd is the flow through which should have only E3 but has both MBP and E3, 4th and 5th lanes are washes with buffer containing 5mM imidazole and 6th and 7th lanes are fractions from elutions with 250mM imidazole. (B) SDS gel for fractions from an affinity purification after digestion of the MBP tag from the fusion protein (MBP-E3 protein) with 40mM maltose in the purification buffers. The lanes represents the fractions exactly like the gel shown in A. The flow through have a cleaner E3 protein as compared to the flow through without maltose as shown in A.

As a final step of purification, the flow-through and washes from the affinity purification of digested fusion protein consisting of E3 protein were subjected to SEC using a Superdex 200 column. The chromatogram of the SEC showed a broad peak which encompassed some aggregates and oligomers calculated to range from eighteen E3 molecules to dimers/trimers (Fig 4.4) based on the elution volumes relative to standards and DLS (Table 4.2).

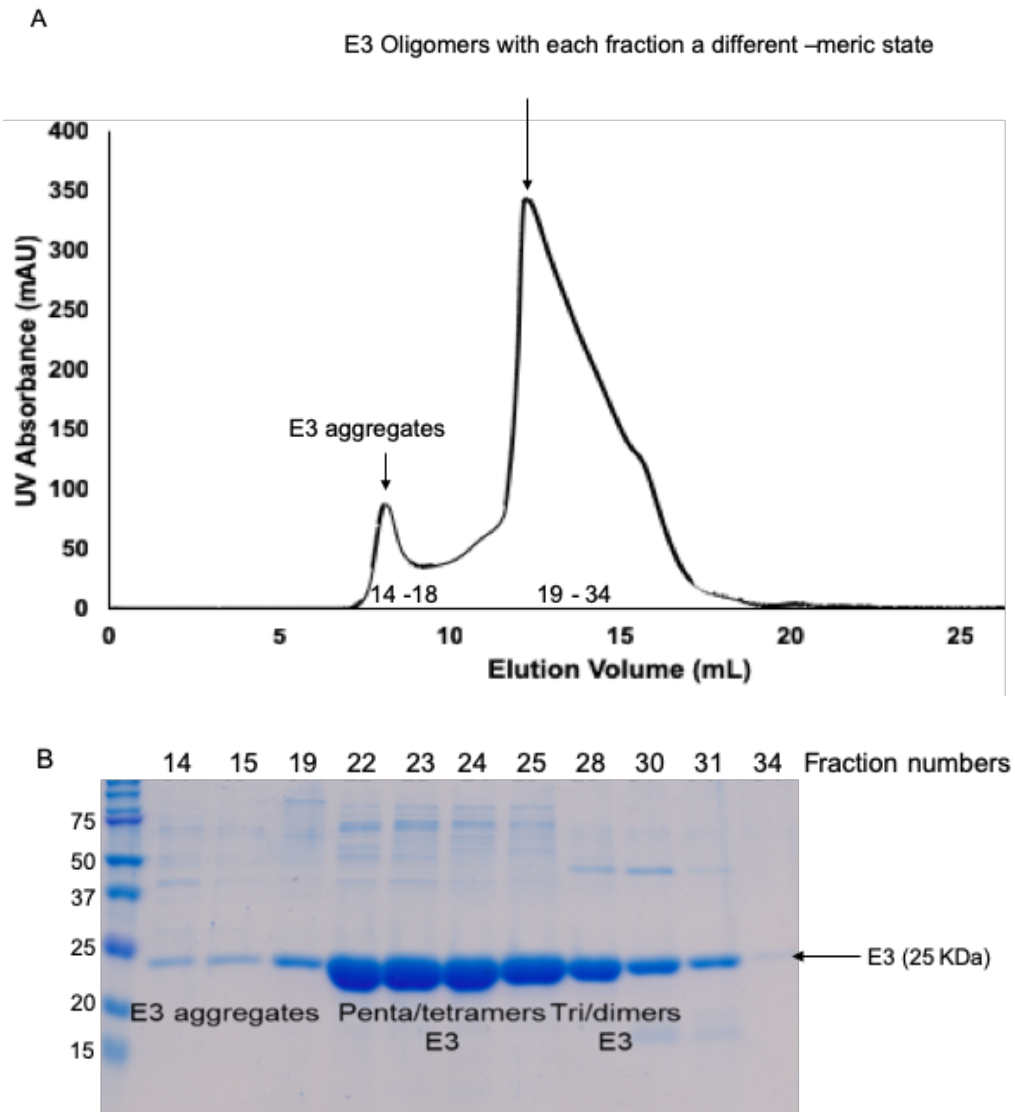

Figure 4.4. SEC chromatogram and its corresponding SDS-PAGE gel for the fractions.

(A) Chromatogram of the SEC for the last step of purification of E3 protein with buffer containing 500mM NaCl and 40mM maltose. The broad peak contained different oligomeric state of E3 along with a small amount of aggregates. (B) SDS-PAGE gel of the chromatogram shown in A with fractions from the SEC. E3 protein was observed at the expected molecular weight of ~25 KDa.

Table 4.2. Estimated molecular weight of different fractions of SEC purification of E3[R131A] protein.

Molecular weight was determined by SEC and DLS.

Protein (E3 R131A)	Mol. Weight SEC (KDa)	Mol. Weight DLS (KDa)
Fraction # 16	1028.4	26900.0 ± 6240.0
Fraction # 22	199.4	203.9 ± 35.8
Fraction # 23	152.5	196.7 ± 21.4
Fraction # 24	116.7	146.1 ± 30.0
Fraction # 25	89.2	124.3 ± 24.5
Fraction # 26	67.1	123.8 ± 34.4
Fraction # 27	50.5	83.1 ± 21.9
Fraction # 28	39.1	90.3 ± 20.5
Fraction # 29	29.1	54.3 ± 15.7
Fraction # 30	22.6	41.1 ± 10.4
Fraction # 31	17.0	24.5 ± 10.8

The fractions with different oligomeric states of the E3[R131A] mutant were homogenous. It was observed that each of these fractions if taken individually and concentrated to protein concentration required for crystallographic studies, caused aggregation. Another condition where these fractions reverted back from dimers/trimers to aggregate was storage of the fractions in -80°C (long-term storage). It has been observed that the expression and purification of recombinant proteins could be considerably improved with the addition of stabilizing solutions or additives that reduce the tendency of proteins to unfold or aggregate during purification and storage in vitro [78]. Also, increasing stability could lead to increased crystallizability of recombinant proteins [82-84].

In order to improve the stability of the E3[R131A] fractions, thermal shift assays were conducted using real-time PCR to scan different additives and solutions (Table 4.3). A selection of 96 different additives were tested, and the raw data from real-time PCR was converted into a 1st derivative of the fluorescence emission as a function of temperature. It was found that addition of salts such as 100 mM ammonium sulfate, 100 mM sodium citrate tribasic dihydrate and 100 mM sodium malonate pH 7.0, increased the melting temperature (T_m) of E3[R131A] protein (Fig. 4.5). In addition to the three salts, few other salts such as 100 mM potassium chloride, 200 mM sodium thiocyanate, 100 mM potassium sodium tartrate tetrahydrate and 100 mM cesium chloride, also had an insignificant effect on the T_m of E3. An increased melting temperature correlates to increased stability of a protein. With addition of the above mentioned salts to E3[R131A] fractions leads to an increased stability of the protein. Thus, buffers containing these salts could be used to purify E3 to obtain homogenous and stable protein.

The other additives or solutions either had no or negative effect on the T_m (individual graphs are shown in Appendix section). Fluorescence emission was not observed in case of detergents, reducing agents and co-factors suggesting, denaturation or precipitation of the protein in presence of these additives. These additives should not be used for E3 purification to avoid denaturation of the protein.

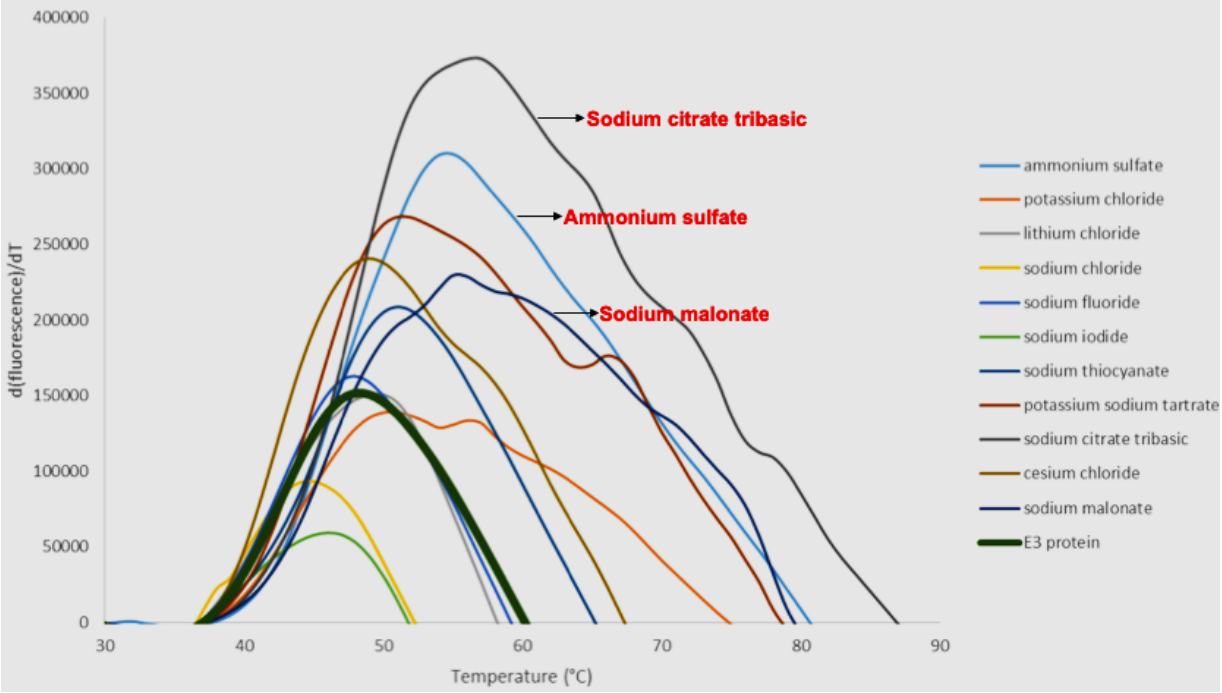

Figure 4.5. Thermal shift analysis of protein stability in different salt solutions.

The x-axis represents the increasing temperature during thermal shift assays whereas the y-axis corresponds to the first derivative of the fluorescence emission as a function of temperature (d[fluorescence]/dT). The melting temperature (Tm) is represented as the highest part of the curve. The solid green curve represents the Tm of E3[R131A] protein without any additives. The additives that had a prominent increased effect on the protein were 100 mM sodium citrate tribasic dihydrate, 100 mM sodium malonate pH 7, 100 mM ammonium sulfate as pointed on the graph.

Table 4.3. Different additives (Additive screen, HR2-428, Hampton Research) used for thermal shift assay on E3[R131A] protein.

Tray position	Salt	Classification	Concentraion in reaction mixture
A1	0.1 M Barium chloride dihydrate	Multivalent	10 mM
A2	0.1 M Cadmium chloride hydrate	Multivalent	10 mM
A3	0.1 M Calcium chloride dihydrate	Multivalent	10 mM
A4	0.1 M Cobalt (II) chloride hexahydrate	Multivalent	10 mM
A5	0.1 M Copper (II) chloride dihydrate	Multivalent	10 mM
A6	0.1 M Magnesium chloride hexahydrate	Multivalent	10 mM
A7	0.1 M Mangenese (II) chloride tetrahydrate	Multivalent	10 mM
A8	0.1 M Strontium chloride hexahydrate	Multivalent	10 mM
A9	0.1 M Yttrium (III) chloride hexahydrate	Multivalent	10 mM
A10	0.1 M Zinc chlroride	Multivalent	10 mM
A11	0.1 M Iron (III) chloride hexahydrate	Multivalent	10 mM
A12	0.1 M Nickel (II) chloride hexahydrate	Multivalent	10 mM
B1	0.1 M Chromium (III) chloride hexahydrate	Multivalent	10 mM
B2	0.1 M Praseodymium (III) acetate hydrate	Multivalent	10 mM
B3	1 M Ammonium sulfate	Salt	100 mM
B4	1 M Potassium chloride	Salt	100 mM
B5	1 M Lithium chloride	Salt	100 mM
B6	2 M Sodium chloride	Salt	200 mM
B7	0.5 M Sodium fluoride	Salt	50 mM
B8	1 M Sodium iodide	Salt	100 mM
B9	2 M Sodium thiocyanate	Salt	200 mM
B10	1 M Potassium sodium tartrate tetrahydrate	Salt	100 mM
B11	1 M Sodium citrate tribasic dihydrate	Salt	100 mM
B12	1 M Cesium chloride	Salt	100 mM
C1	1 M Sodium Malonate pH 7.0	Salt	100 mM
C2	0.1 M L-Proline	Amino Acid	10 mM
C3	0.1 M Phenol	Dissociating Agent	10 mM
C4	30% v/v Dimethyl sulfoxide	Dissociating Agent	3.00%
C5	0.1 M Sodium bromide	Dissociating Agent	10 mM
C6	30% w/v 6-Aminohexanoic acid	Linker	3.00%
C7	30% w/v 1,5-Diaminopentane dihydrochloride	Linker	3.00%
C8	30% 1,6-Diaminohexane	Linker	3.00%
C9	30% w/v 1,8-Diaminooctane	Linker	3.00%
C10	1 M Glycine	Linker	100 mM
C11	0.3 M Glycyl-glycyl-glycine	Linker	30 mM
C12	0.1 M Taurine	Linker	10 mM
D1	0.1 M Betaine hydrochloride	Linker	10 mM
D2	0.1 M Spermidine	Polyamine	10 mM
D3	0.1 M Spermine tetrahydrochloride	Polyamine	10 mM
D4	0.1 M Hexammine cobalt (II) chloride	Polyamine	10 mM
D5	0.1 M Sarcosine	Polyamine/ Osmolyte	10 mM
D6	0.1 M Trimethylamine hydrochloride	Chaotrope	10 mM
D7	1 M Guanidine hydrochloride	Chaotrope	100 mM
D8	0.1 M Urea	Chaotrope	10 mM
D9	0.1 M β-Nicotinamide adenine dinucleotide hydrate	Co-factor	10 mM
D10	0.1 M Adenosine-5'-triphosphate disodium salt hydrate	Co-factor	10 mM
D11	0.1 M TCEP hydrochloride	Reducing Agent	10 mM
D12	0.01 M GSH (L-Glutathione reduced), 0.01 M GSSG (L-Glutathione oxidized)	Reducing Agent	1 mM

Table 4.3. (Continued) Different additives (Additive screen, HR2-428, Hampton Research) used for thermal shift assay on E3[R131A] protein.

Tray position	Salt	Classification	Concentraion in reaction mixture
E1	0.1 M Ethylenediaminetetraacetic acid disodium salt dihydrate	Chelating agent	10 mM
E2	5% w/v Polyvinylpyrrolidone K15	Polymer	0.50%
E3	30% w/v Dextran sulfate sodium salt (M_r 5,000)	Polymer	3.00%
E4	40% v/v Pentaerythritol ethoxylate (3/4 EO/OH)	Polymer	4.00%
E5	10% w/v Polyethylene glycol 3,350	Polymer	1.00%
E6	30% w/v D-(+)-Glucose monohydrate	carbohydrate	3.00%
E7	30% w/v Sucrose	carbohydrate	3.00%
E8	30% Xylitol	carbohydrate	3.00%
E9	30% w/v D-Sorbitol	carbohydrate	3.00%
E10	12% w/v myo-Inositol	carbohydrate	1.20%
E11	30% w/v D-(+)-Trehalose dihydrate	carbohydrate	3.00%
E12	30% w/v D-(+)-Galactose	carbohydrate	3.00%
F1	30% v/v Ethylene glycol	Polyol	3.00%
F2	30% v/v Glycerol	Polyol	3.00%
F3	3 M NDSB-195	Non-detergent	300 mM
F4	2 M NDSB-201	Non-detergent	200 mM
F5	2 M NDSB-211	Non-detergent	200 mM
F6	2 M NDSB-221	Non-detergent	200 mM
F7	1 M NDSB-256	Non-detergent	200 mM
F8	0.15 mM CYMAL® -7	Amphiphile	0.015 mM
F9	20% w/v Benzamidine hydrochloride	Amphiphile	2.00%
F10	5% w/v n-dodecyl-N,N-dimethylamine-N-oxide (LDAO, DDAO)	Detergent	0.50%
F11	5% w/v n-Octyl-β-D-glucoside	Detergent	0.50%
F12	5% w/v n-Dodecyl-β-D-maltoside	Detergent	0.50%
G1	30% w/v Trimethylamine N-oxide dihydrate	Osmolyte	3.00%
G2	30% w/v 1,6-Hexanediol	Organic, Non-volatile	3.00%
G3	30% v/v (+/-)-2-Methyl-2,4-pentanediol	Organic, Non-volatile	3.00%
G4	50% v/v Polyethylene glycol 400	Organic, Non-volatile	5.00%
G5	50% v/v Jeffamine * M-600 * pH 7.0	Organic, Non-volatile	5.00%
G6	40% v/v 2,5-Hexanediol (mixture of isomers)	Organic, Non-volatile	4.00%
G7	40% v/v (±)-1,3-Butanediol	Organic, Non-volatile	4.00%
G8	40% v/v Polypropylene glycol P 400	Organic, Non-volatile	4.00%
G9	30% v/v 1,4-Dioxane	Organic, Volatile	3.00%
G10	30% v/v Ethanol	Organic, Volatile	3.00%
G11	30% v/v 2-Propanol	Organic, Volatile	3.00%
G12	30% v/v Methanol	Organic, Volatile	3.00%
H1	10% v/v 1,2-Butanediol	Organic, Volatile	1.00%
H2	40% v/v tert-Butanol	Organic, Volatile	4.00%
H3	40% v/v 1,3-Propanediol	Organic, Volatile	4.00%
H4	40% v/v Acetonitrile	Organic, Volatile	4.00%
H5	40% v/v Formamide	Organic, Volatile	4.00%
H6	40% v/v 1-Propanol	Organic, Volatile	4.00%
H7	5% v/v Ethyl acetate	Organic, Volatile	0.50%
H8	40% v/v Acetone	Organic, Volatile	4.00%
H9	Buffer+SYPRO orange+Protein	Control	
H10	Buffer+SYPRO orange	Control	
H11	Buffer+Protein	Control	
H12	Only buffer	Control	

Our goal was to purify E3 protein with homogenous fractions that does not form aggregates at higher protein concentration. To achieve this goal, purification of E3[R131A], was performed with buffers containing salts that increased the T_m of the protein such as 100 mM ammonium sulfate [$(NH_4)_2SO_4$], 100 mM sodium citrate tribasic dihydrate ($Na_3C_6H_5O_7$) or 100 mM sodium malonate ($C_3H_2O_4Na_2$) pH 7, instead of 500 mM NaCl. After purification, the molecular weight of E3 protein (fraction # 19) of each SEC purification using different buffers was determined by DLS and compared with the fraction # 19 of SEC purification using 500 mM NaCl (Table 4.4).

Table 4.4. Estimated molecular weight of fraction # 19 of SEC purification of E3[R131A] protein using different buffers.

Protein	MW (Kda) from DLS	Monodisperse/Polydisperse
E3 R131A fraction #19 with 500mM NaCl	**472.2 ± 93.6**	**Monodisperse**
E3 R131A fraction #19 with 100mM $(NH_4)_2SO_4$	4.36e+3 ± 4.11e+3	Polydisperse
E3 R131A fraction #19 with 100mM $Na_3C_6H_5O_7$	594.4 ± 141.9	Polydisperse
E3 R131A fraction #19 with 100mM $C_3H_2O_4Na_2$	534.4 ± 134.4	Polydisperse

The DLS data demonstrated that E3 purified in buffers other than 500 mM NaCl tend to aggregate and remain polydispersed. These salt additives increased the melting temperature and stability of E3 but at the same time increased the heterogeneity of the protein. Buffer containing 100 mM ammonium sulfate had the maximum aggregation. Buffers with 100 mM sodium citrate tribasic dihydrate and 100 mM sodium malonate although were comparable to buffer with 500 mM NaCl, an increase in heterogeneity of the protein was undesirable for crystallographic studies. Heterogeneity is referred to as the

polydisperse or monodisperse (homogeneous) state of the protein in the above mentioned table. Based on these results, subsequent purification and optimization of E3[R131A] was conducted with 500 mM NaCl without any additives added to the buffer.

To test another strategy for obtaining E3[R131A] homogeneous protein, a single fraction (fraction # 24) from SEC purification of E3[R131A] was processed through SEC column again for resizing (Fig. 4.6).

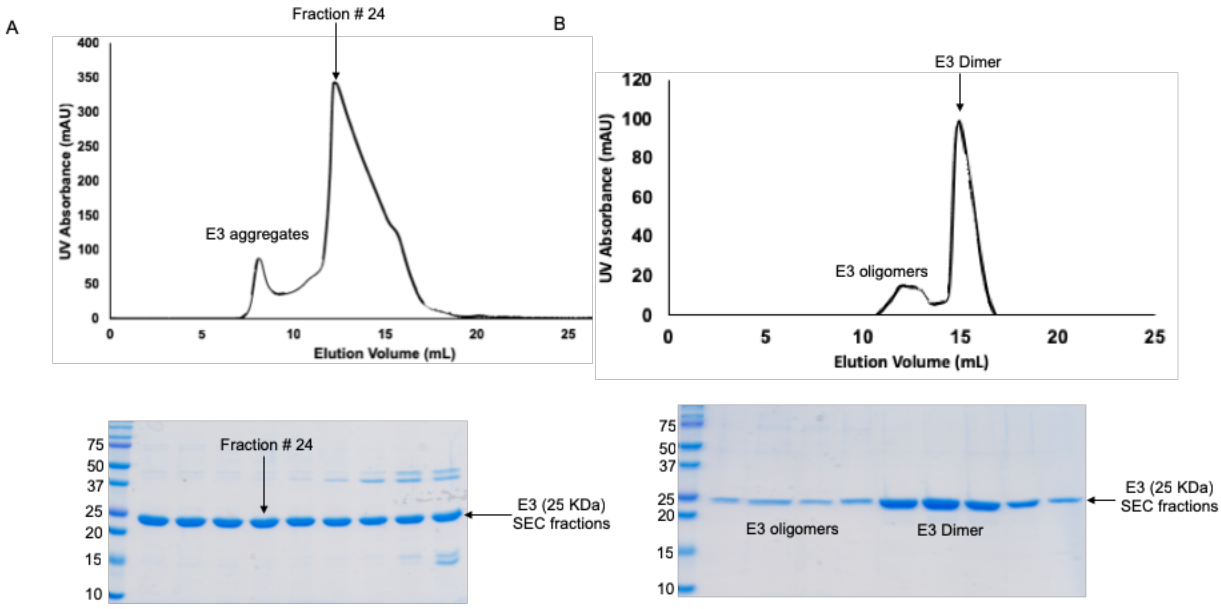

Figure 4.6. Resizing of E3[R131A] fraction

(A) Chromatogram of the SEC for the last step of purification of E3 protein with buffer containing 500mM NaCl and 40mM maltose. The broad peak contained different oligomeric state of E3 along with a small amount of aggregates. SDS-PAGE gel under the chromatogram represents the different fractions from the broad E3 purification peak. (B) Chromatogram of SEC conducted on fraction # 24 of the broad peak in SEC shown in A in a buffer containing 500mM NaCl. The chromatogram represents a sharp peak of E3 dimers and some E3 oligomers. The corresponding SDS-PAGE gel is shown under the chromatogram and E3 protein was observed at the expected molecular weight of ~25 KDa.

The estimated molecular weight of fraction # 24 of the SEC purification of E3[R131A] mutant was measured using SEC standards and DLS. It was found to be around 120 KDa which corresponds to approximately five E3 molecules. Results from the resizing of fraction # 24 show that E3 eluted as a dimer (MW confirmed with SEC standards) with a small amount of E3 oligomers. Due to the sharp peak in the chromatogram, it was assumed that the E3 dimers are in a homogeneous state. These results suggested progress towards the effort for crystallization of E3 proteins. Unfortunately, when these resized fractions were concentrated to near saturation, aggregation (confirmed by DLS) was observed.

Although these samples were not used for setting up crystal screening of E3 proteins, a procedure was developed for protein purification of E3 mutants that could lead to low molecular weight homogeneous oligomeric protein without aggregation. With further optimization, these E3 dimers and trimers could effectively be used for crystallization studies.

4.2.3. Purification of E3[R131AI110A] mutant

Purification of the double mutant E3[R131AI110A] was conducted similarly as performed for single mutant E3[R131A], in an effort to obtain stable and homogenous E3 protein. SEC fraction (fraction # 27) was passed through Superdex 200 column for resizing (Fig. 4.7).

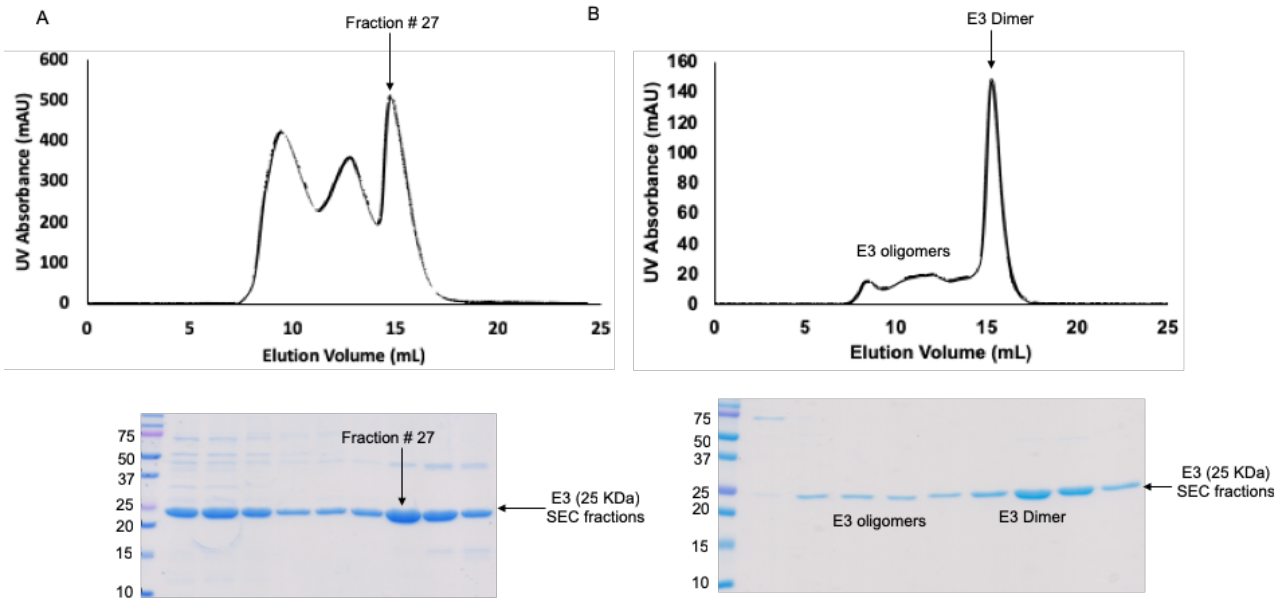

Figure 4.7. Resizing of E3[R131AI110A] fraction

(A) Chromatogram of the SEC for the last step of purification of E3 protein with buffer containing 500mM NaCl and 40mM maltose. The multiple peaks contained different oligomeric state of E3 along with aggregates. SDS-PAGE gel under the chromatogram represents the different fractions from multiple E3 purification peaks. (B) Chromatogram of SEC conducted on fraction # 27 of the last peak in SEC shown in A in a buffer containing 500mM NaCl. The chromatogram represents a sharp peak of E3 dimers and some E3 oligomers. The corresponding SDS-PAGE gel is shown under the chromatogram and E3 protein was observed at the expected molecular weight of ~25 KDa.

Results showed that the fraction # 27 of E3[R131AI110A] had a molecular weight of 44 KDa which corresponds to approximately two E3 molecules. The resizing of fraction # 27 of E3[R131AI110A] led to the elution of E3 as a dimer (MW confirmed with SEC standards) with a small amount of E3 oligomers. Due to the sharp peak in the chromatogram, it was assumed that the E3 dimers are in a homogeneous state. When these resized fractions were concentrated to ~3mg/mL, the protein remained as a dimer (confirmed by DLS) as compared to E3[R131A] that aggregated upon concentration. Mass spectrometry analysis of the protein

from the SDS-PAGE gel of resizing fractions was conducted to confirm the identity of the protein and was found to be E3 from VACV (Appendix).

These results are an important progress towards the effort for crystallization of E3 proteins. The concentrated dimeric protein samples were proceeded for crystallization set up with various crystal screening kit available commercially.

4.3. ***Conclusion***

Various surface mutations were conducted in an effort to reduce the inherent nature of E3 to aggregate. Two mutants (R131A and F148A) were successfully expressed and purified to produce lower oligomeric protein but did not completely abrogate the problem of aggregation. Optimization of purification led to a procedure that could potentially produce homogeneous dimeric proteins. An E3 double mutant (E3[R131AI110A]) displayed the best results when purified and concentrated to a desired concentration for crystallization. Unlike E3 single mutants, the double mutant had better stability and was a likely candidate for crystallization screening process. Crystal screening was conducted with the double mutant samples with various commercially available kits.

CHAPTER V

PHYSICAL INTERACTION OF VACV E3 AND HUMAN PKR-KD

5.1. Introduction

The human PKR protein is an important dsRNA-dependent serine/threonine protein kinase, which activates the innate immune response during viral infections. Due to its vital function, viruses implement numerous strategies to eliminate PKR's immune response activity. One of these strategies include VACV E3 proteins that are produced early in the viral replication cycle to prevent activation of dsRNA-activated PKR.

Models proposed in previous studies suggested that E3 inhibited PKR activity in a yeast system and this inhibition correlated with the physical interaction between the two proteins [13, 75]. A more recent study have shown physical interactions between these two proteins in vivo in HeLa cells and in vitro using GST pull down assay and correlated the interaction with the dsRNA binding capacity of E3 proteins [14]. There has to be a physical interaction between E3 and PKR to prevent PKR from inducing the immune response. Different predicted models have hypothesized that E3 forms an inactive heterodimer with PKR in the presence of dsRNA, which eventually leads to inhibition of PKR activity [13, 75].

PKR activation starts with dimerization of the protein, which occurs via the N-terminal domain of PKR containing two DRBDs. It has been shown in studies that

dsRNA binding to the N-terminal leads to dimerization and thus activation of PKR but a second patch of residues (amino acids 244-296) in the kinase domain is also known to be essential for dimerization [67]. A study indicated that multiple deletions within the patch of amino acids 244 and 296 in the kinase domain interfered with the dimerization of PKR and thus its activation [85]. The kinase domain of PKR is important during activation as the orientation of two kinase domains in a parallel, back-to-back manner leads to autophosphorylation which is the next step of PKR activation. All these facts emphasize the importance and self-sufficiency of kinase domain in PKR activation.

In this study, we hypothesized that E3 physically interacts with PKR kinase domain and the interaction does not depend on the dsRNA binding ability of either E3 or PKR. To test this hypothesis, we conducted in vitro binding and pull down assays with E3 and PKR-KD to determine the physical interaction between the two proteins and also the stoichiometry of this interaction.

5.2. Results and Discussion

5.2.1. PKR-KD purifies in a monomer-dimer equilibrium state

Purification of the individual protein was required to test for the physical interactions between E3 and PKR-KD. It was observed that expression of the full kinase domain (residues 258-551) in *E.coli* cells resulted in cell toxicity. Previous studies had shown that amino acids, histidine 412 and cysteine 551 on kinase domain of PKR, caused toxicity of PKR-KD expression in bacterial cells. Mutations H412N and C551A reduced the amount of cell toxicity by lessening catalytic activity and eliminating oxidation induced protein

instability, respectively [45, 86]. We used a shorter construct of kinase domain (residues 258-541) in this study, which reduced cell toxicity but had a low protein yield.

To obtain PKR-KD protein, MBP or GST tagged PKR-KD constructs with the double mutations were expressed and purified. The MBP-tagged protein purified as dimer and monomer (Fig 5.1) whereas GST-tagged protein purified mainly as dimer. A construct with double mutation and a 13 amino acid deletion (residues 338-350, β4 - β5 loop) cloned into GST vector was used also used for expression and purification. Purification of this construct led to PKR-KD dimer protein (Fig 5.1). The different constructs and the corresponding purified oligomeric state are mentioned in Table 5.1.

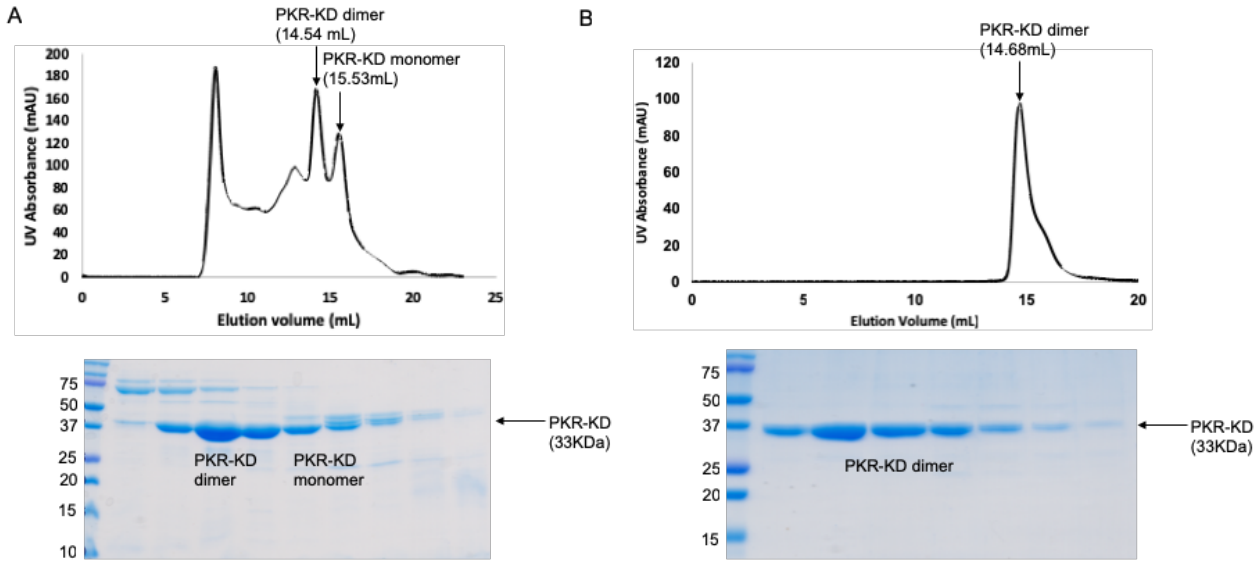

Figure 5.1. Purification of PKR-KD protein

(A) Chromatogram of the SEC for the last step of purification of PKR-KD258_551[H412N/_ C551A] (MBP vector) protein with buffer containing 500 mM NaCl and 40 mM maltose. Protein purified in an equilibrium of monomer and dimer along with aggregates eluted in the void volume of SEC column. SDS-PAGE gel (under the chromatogram) of the fractions collected in SEC show the presence of PKR-KD protein at ~37 KDa. (B) Chromatogram of SEC for the last step of purification of PKR-KD258_551[H412N/_ C551A/_ Δ338-350] (GST

vector) protein with buffer containing 150mM NaCl and 5mM DTT. Protein purified mainly as a dimer with no aggregates eluting in void volume of SEC column. SDS-PAGE gel (under the chromatogram) of the fractions collected in SEC show the presence of PKR-KD protein at ~37 KDa.

SDS-PAGE gels were loaded with the SEC fractions to measure the molecular weight of monomeric PKR-KD, which is approximately 33 KDa but as observed on the SDS-PAGE gels shown in Figure 5.1, the protein electrophorized at ~37 KDa. The reason for the higher molecular weight in SDS-PAGE gels could be the presence of phosphorylated PKR-KD. The phosphorylated protein moves slower than unphosphorylated protein in a gel.

Table 5.1. Different constructs of PKR-KD with the vectors used and the purified state of protein (Dimer or monomer).

PKR-KD Construct	Vector used	Dimer/Monomeric protein
PKR 258-551	pMBP28b+	High cell toxicity
PKR 258-551	pGST22b+	High cell toxicity
PKR 258-541	pMBP28b+	Dimeric and monomeric proteins
PKR 258-541	pGST22b+	Dimeric protein only
PKR 258-551 H412N, C551A	pMBP28b+	Dimeric and monomeric proteins
PKR 258-551 H412N, C551A	pGST22b+	Dimeric protein only
PKR 258-541 H412N	pMBP28b+	Dimeric and monomeric proteins
PKR 258-541 H412N	pGST22b+	Dimeric protein only

The PKR-KD in pMBP28b+ vectors purified in a weak equilibrium of dimers and monomers which upon long term storage in -80°C or short term storage in 4°C/-20°C led to PKR-KD dimerization.

5.2.2. Pull down assay displays the interaction of E3 and PKR-KD

Pull down assays were performed to determine the physical interactions between E3 and PKR-KD in the absence of dsRNA binding ability for both proteins. These assays were performed for both monomeric and dimeric PKR-KD separately to determine the difference in interaction with E3. The protein mix of His-MBP-E3 and monomeric PKR-KD were passed through 200 μL of Ni-NTA column. Fractions from flow-through, washes and elution were electrophoresed in SDS-PAGE gels. Protein bands corresponding to the molecular weights of His-MBP-E3 and PKR-KD were observed on the SDS-PAGE gels (Fig. 5.2, Panel A). This suggested that monomeric PKR-KD eluted along with His-MBP-E3 protein due to a physical interaction between these proteins.

As a negative control, only monomeric PKR-KD protein was passed through a Ni-NTA column. SDS-PAGE gels on these fractions showed the presence of PKR-KD in flow-through and washes but not in the elution (Fig. 5.2, Panel B). PKR-KD does not bind non-specifically to the column.

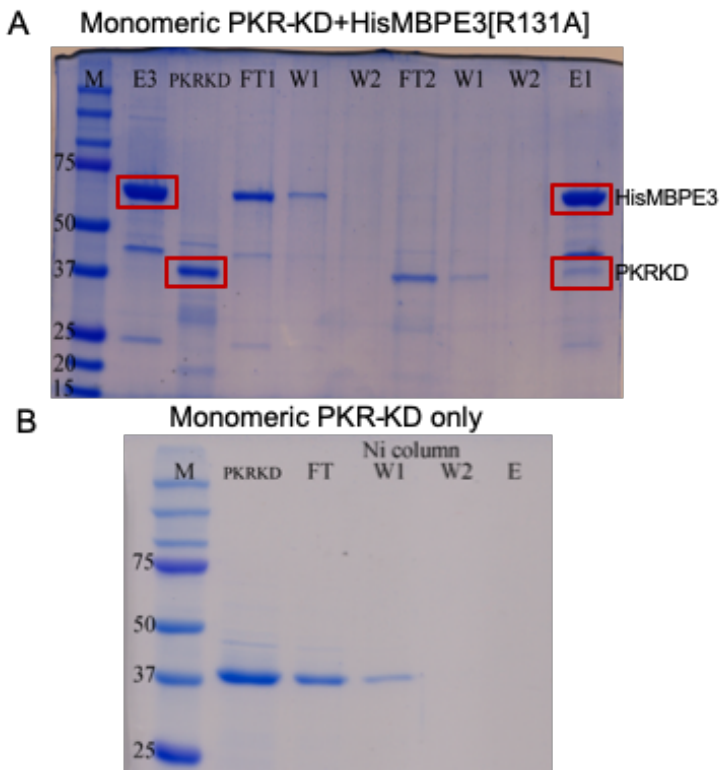

Figure 5.2. Pull down assay of monomeric PKR-KD with His-MBP-E3 protein

(A) SDS-PAGE gel of the pull down assay of PKR-KD and His-MBP-E3[R131A]. The 1st lane on the SDS-PAGE gel corresponds to His-MBP-E3 protein followed by PKR-KD. FT1 represents the flow-through collected after His-MBP-E3 protein was added to the column. The column was washed with buffer containing 5mM imidazole which is represented as W1 and W2. FT2 represents the flow-through collected after monomeric PKR-KD protein was added to the column. The column was washed again with buffer containing 5mM imidazole which is represented as W1 and W2. Proteins were eluted off the column by using a buffer with 250mM imidazole and shown on the figure as E1. (B) SDS-PAGE gel of pull down assay of only PKR-KD. The fractions on the gel are similar to the fractions described in panel A.

Dimeric form is an activated state of PKR-KD, which is formed against viral infections to trigger the immune response. Pull down assay was conducted to test whether dimeric PKR-KD physically interacted with E3. SDS-PAGE gel on the pull down assay fractions showed the absence of PKR-KD in the elution fractions along with His-MBP-E3 (Fig. 5.3, Panel A). Dimeric PKR-KD passed through the affinity column, eluted out as flow-

through and in washes. These results suggested that dimeric PKR-KD and E3 protein do not interact with each other.

A negative control with only dimeric PKR-KD was conducted. The SDS-PAGE gel showed an absence of dimeric PKR-KD in the elution fraction suggesting a lack of non-specific binding of dimeric PKR-KD to the Ni-NTA column (Fig. 5.3, Panel B).

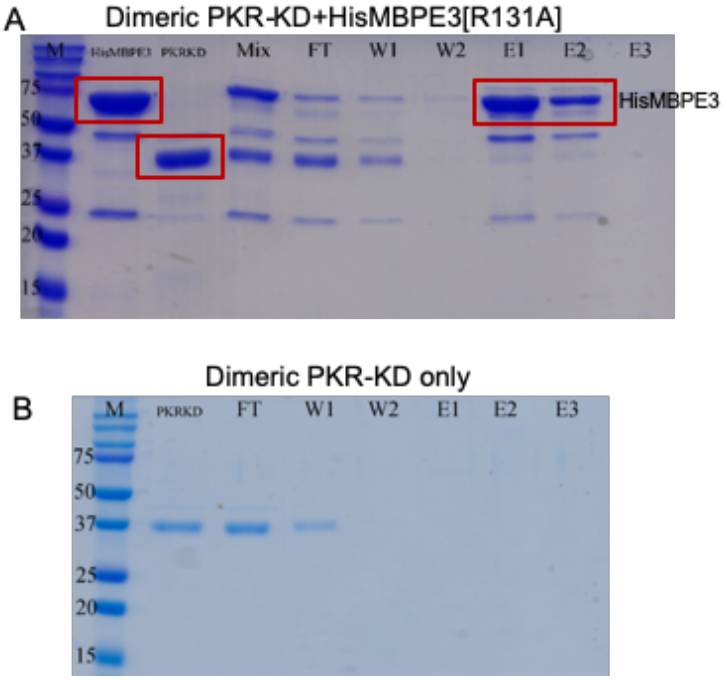

Figure 5.3. Pull down assay of dimeric PKR-KD with His-MBP-E3 protein

(A) SDS-PAGE gel of the pull down assay of PKR-KD and His-MBP-E3[R131A]. The mixture of monomeric PKR-KD and His-MBP-E3[R131A] protein was passed through a Ni-NTA column. The 1st lane on the SDS-PAGE gel corresponds to His-MBP-E3 protein followed by PKR-KD. The protein mix was loaded on the 3rd lane. FT represents the flow-through collected after the protein mix was added to the column. The column was washed with buffer containing 5mM imidazole which is represented as W1 and W2. Proteins were eluted off the column by using a buffer with 250mM imidazole and shown on the figure as E1, E2 and E3. (B) SDS-PAGE gel of pull down assay of only PKR-KD. The fractions on the gel are similar to the fractions described in panel A.

Western blot analysis of the pull down assays were conducted to confirm the results observed in the SDS-PAGE gels shown in figure 5.2 and 5.3. Pull down assays were conducted for both monomeric (Fig. 5.4, Panel A) and dimeric PKR-KD (Fig. 5.5, Panel A) with His-MBP-E3 proteins individually. The SDS-PAGE gels were transferred to a PVDF membrane and blotted against an anti-PKR-KD antibody. It was observed that monomeric PKR-KD eluted along with His-MBP-E3 whereas dimeric PKR-KD did not elute with His-MBP-E3. Unbound PKR-KD protein was observed in the flow-through fractions and also in washes. These results suggested that there is a physical interaction between E3 and monomeric PKR-KD but absent in case of dimeric PKR-KD. This interactions between E3[R131A] and monomeric PKR-KD does not require the dsRNA binding ability of either protein, which is a contradiction from previous models proposed on PKR and E3 interactions.

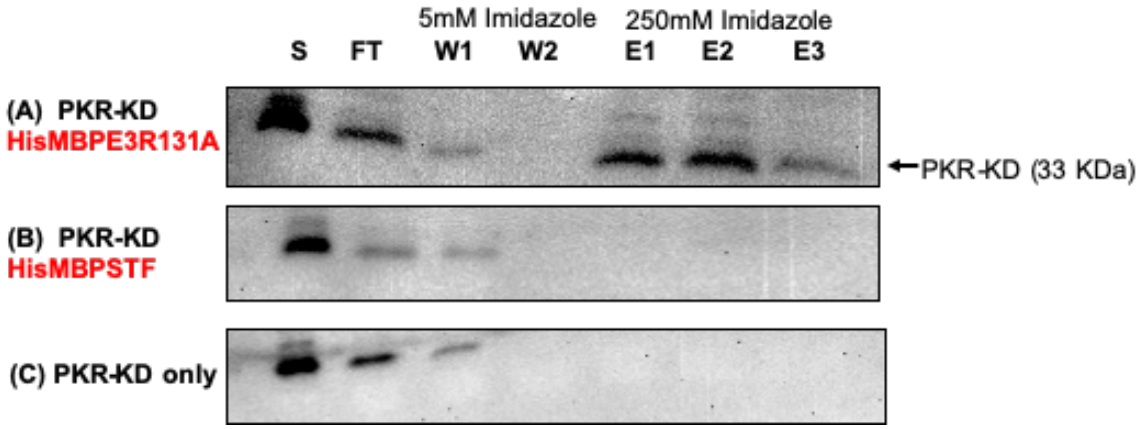

Figure 5.4. Western blots of pull down assay of monomeric PKR-KD with His-MBP-E3[R131A]

(A) Pull down assay of PKR-KD and HisMBPE3[R131A] and blotted against antibody that recognizes PKR residues 435 to 449). The mixture of monomeric PKR-KD and HisMBPE3[R131A] protein was passed through a Ni-NTA column. The 1st fraction on the western blot corresponds to the protein mix or supernatant (S) followed by the flow-through (FT). The column was washed with buffer containing 5mM imidazole which is represented as

W1 and W2. Proteins were eluted off the column by using a buffer with 250mM imidazole and shown on the figure as E1, E2 and E3. (B) Pull down assay of PKR-KD and His-MBP-STF. The fractions on the western blot were similar to the fractions described in panel A. (C) Pull down assay for PKR-KD only. PKR-KD protein was passed through the column (S) and the flow-through (FT) fraction was collected, washes W1, W2 had PKR-KD protein but elution fractions E1, E2 and E3 did not have any PKR-KD protein.

A negative control experiment was conducted with His-MBP-STF and monomeric/dimeric PKR-KD. STF (Stenofolia)) is a DNA binding plant protein and has no known association with human PKR protein. Monomeric/dimeric PKR-KD and His-MBP-STF were added in a molar ratio of 1:2, incubated for an hour at 4°C and passed through 200 µL of Ni-NTA column. Most of the PKR-KD proteins were observed in flow-through and wash fractions but nothing eluted along with His-MBP-STF, indicating the non-interaction of STF and PKR-KD (Fig. 5.4, Panel B and Fig. 5.5, Panel B). A second negative control experiment was also conducted with only monomeric/dimeric PKR-KD. Absence of PKR-KD in the elution fractions, as observed in the western blots, suggested lack of non-specific binding of PKR-KD to the Ni-NTA column (Fig. 5.4, Panel C and Fig. 5.5, Panel C).

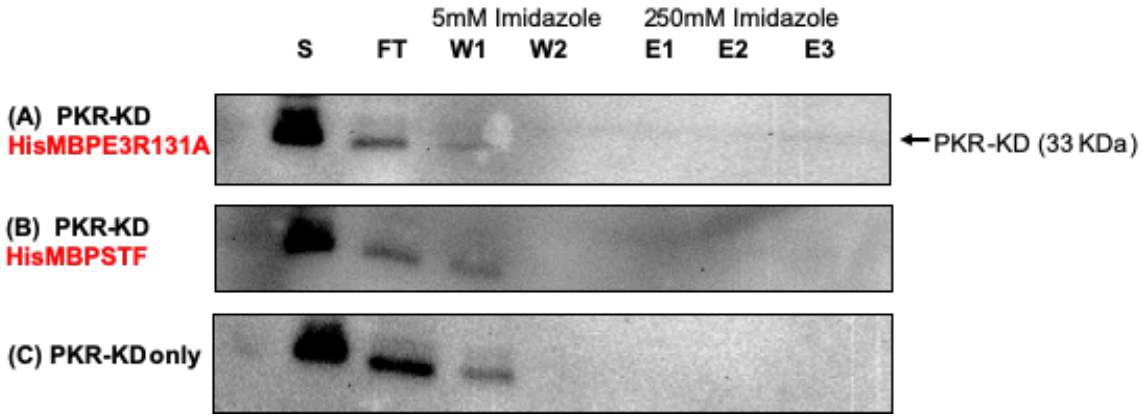

Figure 5.5. Pull down assay of dimeric PKR-KD with His-MBP-E3[R131A]

(A) Pull down assay of PKR-KD and HisMBPE3[R131A] and blotted against antibody that recognizes PKR residues 435 to 449). The mixture of dimeric PKR-KD and HisMBPE3[R131A] protein was passed through a Ni-NTA column. The 1st fraction on the western blot corresponds to the protein mix or supernatant (S) followed by the flow-through (FT). The column was washed with buffer containing 5mM imidazole which is represented as W1 and W2. Proteins were eluted off the column by using a buffer with 250mM imidazole and shown on the figure as E1, E2 and E3. Elution fractions do not show the presence of PKR-KD protein. (B) Pull down assay of PKR-KD and His-MBP-STF. The fractions on the western blot were similar to the fractions described in panel A. (C) Pull down assay for PKR-KD only. PKR-KD protein was passed through the column (S) and the flow-through (FT) fraction was collected, washes W1, W2 had PKR-KD but elution fractions E1, E2 and E3 did not have any PKR-KD protein.

5.2.3. In-vitro binding assays of E3 and PKR-KD

In order to detect a physical interaction in the absence of dsRNA binding ability between monomeric or dimeric PKR-KD with E3[R131A], in vitro binding assays were conducted. Monomeric or dimeric PKR-KD was added to E3[R131A] protein in a molar ratio of 1:2 respectively along with 1mg/mL of AMP. This protein mixture was incubated for 1 hour at 4°C and passed through SEC column. Different constructs of PKR-KD in pMBP28b+ vector were used for complex formation with E3 proteins. A shorter construct of PKR-KD ($PKR\text{-}KD_{258\_541}$) was used for the complex formation with E3[R131A] protein. It was observed in the SEC chromatogram that a protein with higher molecular weight in comparison to monomeric or dimeric PKR-KD or E3 protein eluted from the column (Fig. 5.6, A). The elution volume of the protein mix eluted at 14.23 mL as compared to E3[R131A] that eluted at 14.91 mL, dimeric PKR-KD at 14.54 mLand monomeric PKR-KD at 15.53 mL. DLS was used to determine the estimated molecular weight of the protein complex, which was approximately 90 KDa. The results from the SEC chromatograms suggested the formation of PKR-KD-E3 complex and this interaction does not depend on the dsRNA binding ability of both protein.

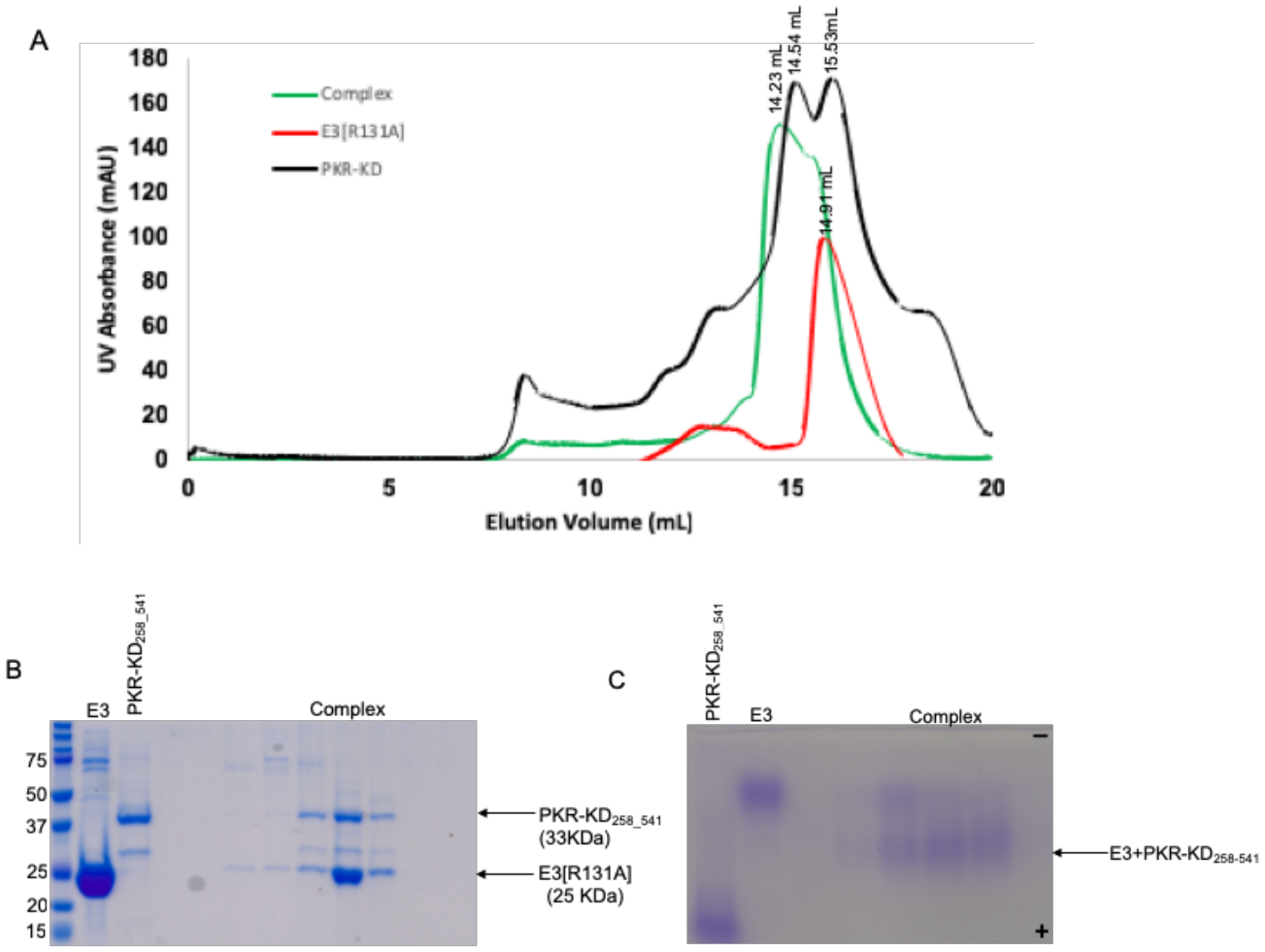

Figure 5.6. Binding assay of monomeric PKR-KD258_541 with E3[R131A].

(A) Chromatograms of E3-PKR-KD complex, E3 and PKR-KD proteins overlapped. The green chromatogram represents the E3-PKR-KD complex, the black chromatogram represents PKR-KD protein and the red chromatogram represents E3[R131A] protein. A shift in elution volume of the complex as compared to E3 and PKR-KD proteins was observed. (B) SDS-PAGE gel of the complex chromatogram shown in A. The fractions from the green chromatogram had both the proteins E3 and PKR-KD. Protein bands corresponding to the molecular weight of E3 (25 KDa) and PKR-KD proteins (33 KDa). (C) 1% agarose gel with complex fractions from the green chromatogram shown in A. Agarose gel was run in 1X TAE buffer at 90 volts for 2 hours and protein migrated from negative to positive terminal. The migration of E3-PKR-KD complex was different from E3 and PKR-KD proteins individually.

In order to test the fractions obtained from the SEC purification of the protein mix, SDS-PAGE and agarose gel. Protein bands corresponding to the molecular weight of both E3 and PKR-KD were observed in the SEC fractions of the protein mix electrophoresed in SDS-PAGE gel (Fig. 5.6, B). The SEC fractions of the protein mix were electrophoresed on the non-denaturing gel (1% agarose gel) shown in figure 5.6, C. Protein bands corresponding to the protein mix fractions migrated differently than E3 or PKR-KD protein when individually electrophoresed on the agarose gel. An excess of E3 protein was added not involved in the complex formation with PKR-KD. The results from the SDS-PAGE and agarose gels indicated the formation of a complex between E3 and PKR-KD. The complex formation between these proteins does not depend on their ability to bind to dsRNA. Based on the molecular weight calculations, the stoichiometry of the protein complex was estimated to be two molecules of E3 and one molecule of PKR-KD protein.

Similar experiments were conducted with dimeric PKR-KD and E3[R131A] proteins to detect the interactions between these protein. A different construct of PKR-KD was used for the complex formation. PKR-KD$_{258_551}$ H412N, C551A Δ338-350 in a GST vector was purified as a dimer and added in a 1:2 molar ratio with E3[R131A] protein. The protein mixture was passed through a SEC column. It was observed that the protein mixture eluted at 15.03 mL in comparison to E3[R131A] that eluted at 14.91 mL and dimeric PKR-KD at 14.68 mL (Fig. 5.7, A). The lack of shift in elution volume of the protein mixture compared to the individual proteins suggested that protein complex was not formed between dimeric PKR-KD and E3 as a higher molecular weight protein would have had a higher elution volume than the individual proteins.

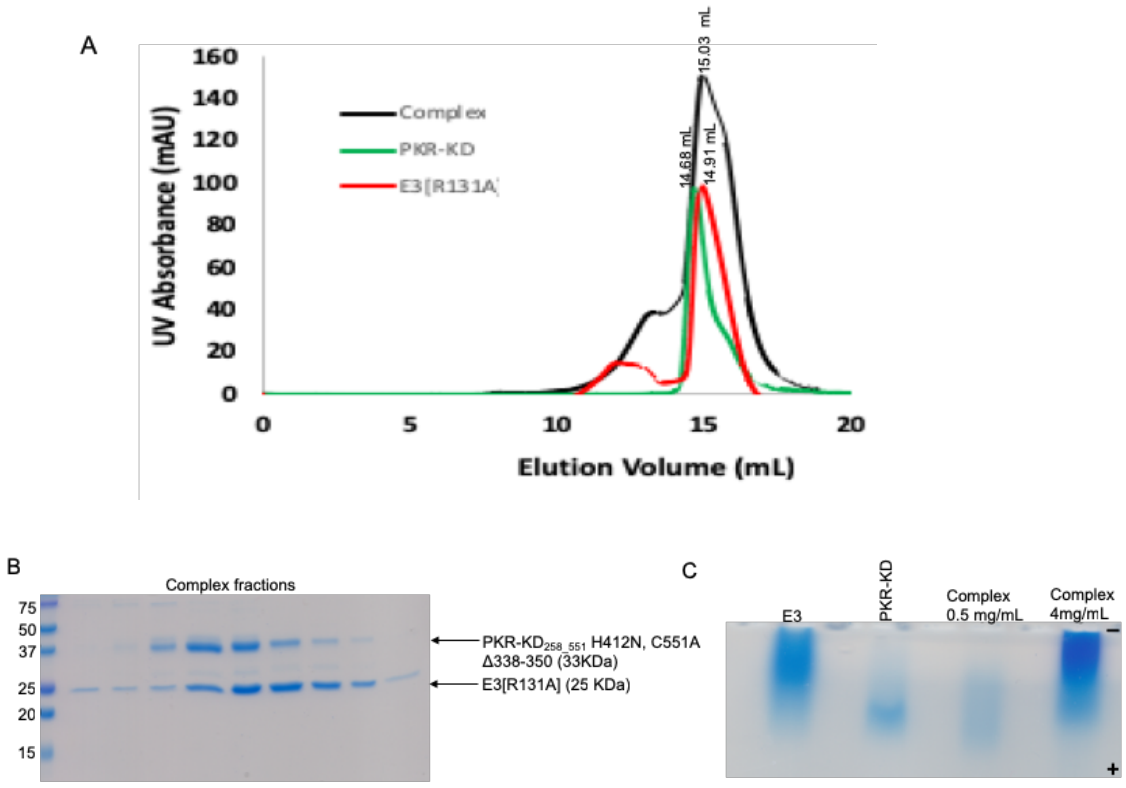

Figure 5.7. Binding assay of dimeric PKR-KD with E3[R131A].

(A) Chromatograms of E3-PKR-KD complex, E3 and PKR-KD proteins overlapped. The black chromatogram represents the E3-PKR-KD complex, the green chromatogram represents PKR-KD protein and the red chromatogram represents E3[R131A] protein. No shift in elution volume of the complex was observed as compared to E3 and PKR-KD proteins. (B) SDS-PAGE gel of the complex chromatogram shown in A. The fractions from the black chromatogram had both the proteins E3 and PKR-KD. Protein bands corresponding to the molecular weight of E3 (25 KDa) and PKR-KD proteins (33 KDa). (C) 1% agarose gel with complex fractions from the black chromatogram shown in A. Agarose gel was run in 1X TAE buffer at 90 volts for 2 hours and protein migrated from negative to positive terminal. The migration of E3-PKR-KD complex had similar pattern as individual E3 and PKR-KD proteins.

SDS-PAGE and agarose gels were used to detect the SEC fractions obtained from the protein mix of E3 and dimeric PKR-KD. The SDS-PAGE gel of the protein mix SEC fractions indicated the presence proteins bands corresponding to both E3 and PKR-KD (Fig.

5.7, B). The agarose gel indicated that the SEC fractions from the protein mix migrated as E3 and PKR-KD independent of each other, instead of a single protein band as observed in monomeric PKR-KD-E3 complex (Fig. 5.7, C). This suggested that dimeric PKR-KD and E3 does not interact with each other to form a protein complex. The SEC chromatograms, SDS-PAGE and agarose gels results combinedly suggested that dimeric PKR-KD and E3 proteins do not form a protein complex.

A dimeric GST-tagged PKR-KD_{258_551} H412N, C551A protein was also used for binding assays with E3 proteins showed similar results as the dimeric PKR-KD. As a negative control, the N-terminal of PKR protein (PKR-N_{1_201} in GST vector) was used for binding assay with E3[R131A] protein. The GST tagged PKR-N_{1_201} was added to E3[R131A] and purified with SEC following a similar procedure. There was no interaction observed between PKR-N terminal and E3 proteins which was evident from the SEC chromatograms and SDS-PAGE gel (Fig 5.8).

Unfortunately, the results from binding assays between monomeric PKR-KD_{258_541} and E3[R131A] protein were not reproducible. Various constructs of PKR-KD in MBP or GST vectors were used for binding assays with E3 protein (Table 5.2). Protein interaction between these two protein was not observed for any of the conditions or different constructs of PKR-KD. The amount of salt in the buffer for complex purification in SEC was varied from 500 mM NaCl to 300 mM NaCl to improve the chances of protein interaction but it led to precipitation of E3 proteins and no complex formation. Similarly, different molar ratios for PKR-KD and E3 mixture were tried but none of the conditions resulted in a purified complex.

Table 5.2. Different constructs of PKR-KD used for complex formation with E3[R131A] protein.

PKR Construct	PKR-KD purification state	Makes complex with E3[R131A] (Yes/No)	SEC purification (Superdex 200)	Native gel (1% Agarose)
$PKR\text{-}KD_{258\_541}$ in pMBP28b+ vector	Dimer and monomer	Yes	Yes	Yes
$PKR\text{-}KD_{258\_551}$ H412N, C551A in pMBP28b+ vector	Dimer and monomer	No *Used different conditions	Yes	Yes
$PKR\text{-}KD_{258\_551}$ H412N, C551A Δ338-350 in pGST22b+ vector	Dimer	No	Yes	Yes
$PKR\text{-}KD_{258\_551}$ H412N, C551A Δ338-350 in pMBP28b+ vector	Dimer and monomer	No	Yes	Yes
$PKR\text{-}KD_{258\_541}$ H412N in pMBP28b+ vector	Dimer and monomer	No	Yes	Yes

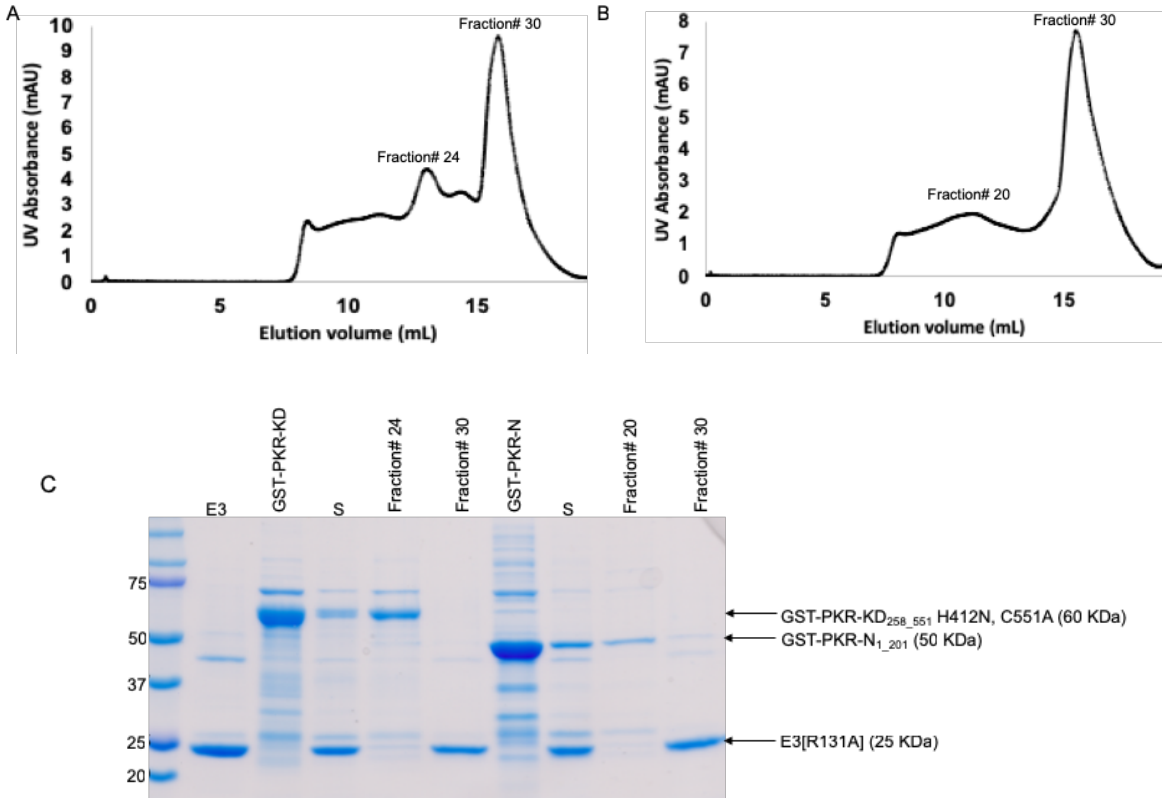

Figure 5.8. Binding assay of dimeric GST-PKR-KD/GST-PKR-N with E3[R131A].

(A) Chromatogram of E3-GST-PKR-KD complex. Both the proteins elute at different elution volumes based on their molecular weight suggesting a complex of these proteins was not formed. (B) Chromatogram of E3-GST-PKR-N complex. Both the proteins elute at different elution volumes based on their molecular weight suggesting a complex of these proteins was not formed. (C) SDS-PAGE gel of the fractions collected from chromatograms A and B. The protein mixture loaded on the SEC column was also ran on SDS-PAGE and labeled as S (supernatant). Fractions 24 and 30 were from chromatogram A and fractions 20 and 30 were from chromatogram B.

5.3. Conclusion

Physical interaction between PKR and E3 proteins have been observed in yeast cells [13, 75]. A recent study has also shown the interaction between these two proteins in in-vitro pull down assays and in-vivo assays [14]. In this study, we demonstrated the interaction between PKR-KD and E3 mutants in the absence of the dsRNA binding ability for both

proteins. Pull down assays and complex formation with SEC assays were used for testing the interaction between PKR-KD and E3 proteins. PKR-KD activates by undergoing dimerization, hence it was important to determine whether the E3 proteins interacted with PKR-KD monomers or dimers after activation. It was determined that E3 mutants that lack dsRNA binding ability physically interacted with monomeric PKR-KD as observed in pull down assays and in vitro binding assays with SEC. A physical interaction between E3 and dimeric PKR-KD could not be observed either in pull down assays or binding assays which could be indicative of the absence of interaction between the E3 and dimeric PKR-KD. Because of the weak interaction between E3 and PKR-KD, it was considered that SEC was not a very robust method to determine the interactions between these protein.

CHAPTER VI

E3 PROTEIN INHIBITS PKR ACTIVITY

6.1. Introduction

A study conducted on VACV E3 provided genetic evidence of E3 inhibiting PKR activity in yeast through potential complex formation [13]. A recent study on various E3 mutants also reported a suppression of PKR activation in VACV infected HeLa cells. In this study, the authors measured the levels of PKR and eIF2α phosphorylation in HeLa cells infected with wildtype E3 or E3 mutant recombinant viruses [14]. Mechanism of E3 inhibition of PKR activity had been predicted by Romano et al., and Sharp et al. These models suggested a physical interaction of E3 proteins to PKR dimers and a formation of inactive heterodimer, which eventually inhibits the PKR activity. The activation process of PKR starts with dimerization followed by autophosphorylation and phosphorylation of its substrate, eIF2α. E3 is known to affect the dimerization process but this mechanism has not been experimentally shown in any in vitro or in vivo studies.

In this study, we attempted to understand the mechanism of E3 inhibition of PKR activity. The effect of E3 was analyzed on the catalytic domain or kinase domain of PKR rather than the full protein. It was predicted that E3 would inhibit the PKR-KD activity in the absence of dsRNA binding ability of both proteins. To test the prediction, various concentrations of E3 mutants that do not possess dsRNA binding ability were added to

the kinase domain of PKR and the phosphorylation of PKR-KD and eIF2α was monitored. It was observed that E3 affected the autophosphorylation of PKR-KD and the phosphorylation of eIF2α. These results contradict the previously proposed models of E3-PKR interaction, which suggested the importance of dsRNA binding for E3 to inhibit PKR activity.

6.2.Results and Discussion

6.2.1. Purification of yeast eIF2α protein

The yeast eIF2α_{4_175} protein was expressed in *E.coli* bacterial cells and purified using affinity chromatography and SEC. The fusion protein was purified without digesting the his-tag to aid in the in vitro phosphorylation assays along with E3 and PKR-KD proteins. The purified fusion protein had an expected molecular weight of 24 KDa (Fig. 6.1). The proteins expressed well and purified with an yield of 110 mg of total protein per liter of cell culture.

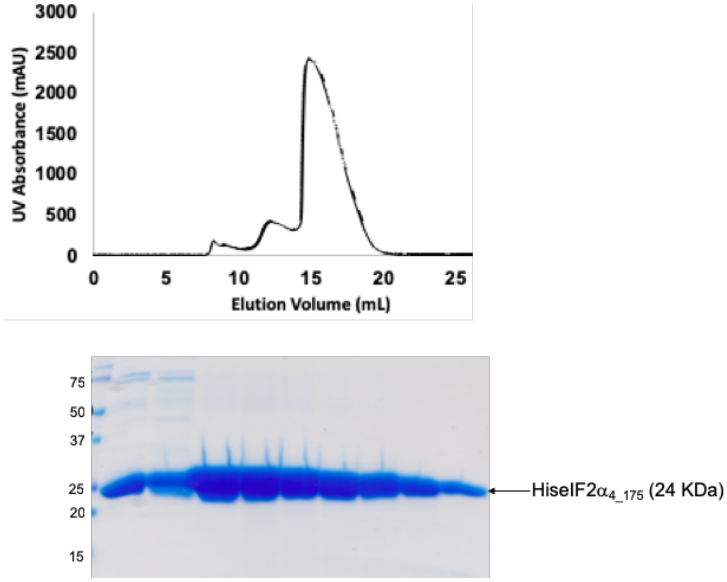

Figure 6.1. Size exclusion chromatogram and corresponding SDS-PAGE gel of His-eIF2α_{4_175} protein.

SEC profile of the fusion protein showed the presence of a predominant single peak and the fractions were electrophoresed on 15% SDS-PAGE gel. The fusion proteins were visualized on the gel at an expected molecular weight of approximately 24 KDa.

6.2.2. E3 inhibits the autophosphorylation of PKR-KD

The in vitro autophosphorylation assay was designed to determine the effect of E3 proteins on the activation of PKR-KD proteins. Both monomeric (PKR-KD) and dimeric PKR-KD (GST-PKR-KD) proteins were utilized in the assay to understand the mechanism of E3 deactivation of PKR-KD. Various concentration of E3[R131A] were added to a protein mixture of monomeric/dimeric PKR-KD, eIF2α and ATP in a kinase reaction buffer. It was observed that E3 inhibited autophosphorylation of both monomeric and dimeric PKR-KD in a dose dependent manner (Fig. 6.2, Panel A). Increasing the dose of E3[R131A] in the reaction mixture eventually led to complete inhibition of autophosphorylation of PKR-KD and GST-PKR-KD. An amount of 13 μM of E3 protein completely inhibited the autophosphorylation of PKR-KD whereas the highest amount of E3 at 51 μM was required for complete inhibition of dimeric GST-PKR-KD. These assays were repeated three times for statistical significance and the gels were quantified using ImageJ software. Quantified data were plotted against the concentrations of E3 used in the assay (Fig. 6.3). E3 had an IC_{50} value of 2.2 μM in case of PKR-KD whereas 9.5 μM for GST-PKR-KD. A significant difference ($p < .001$) was found between the inhibition of monomeric PKR-KD and dimeric GST-PKR-KD by E3[R131A] protein.

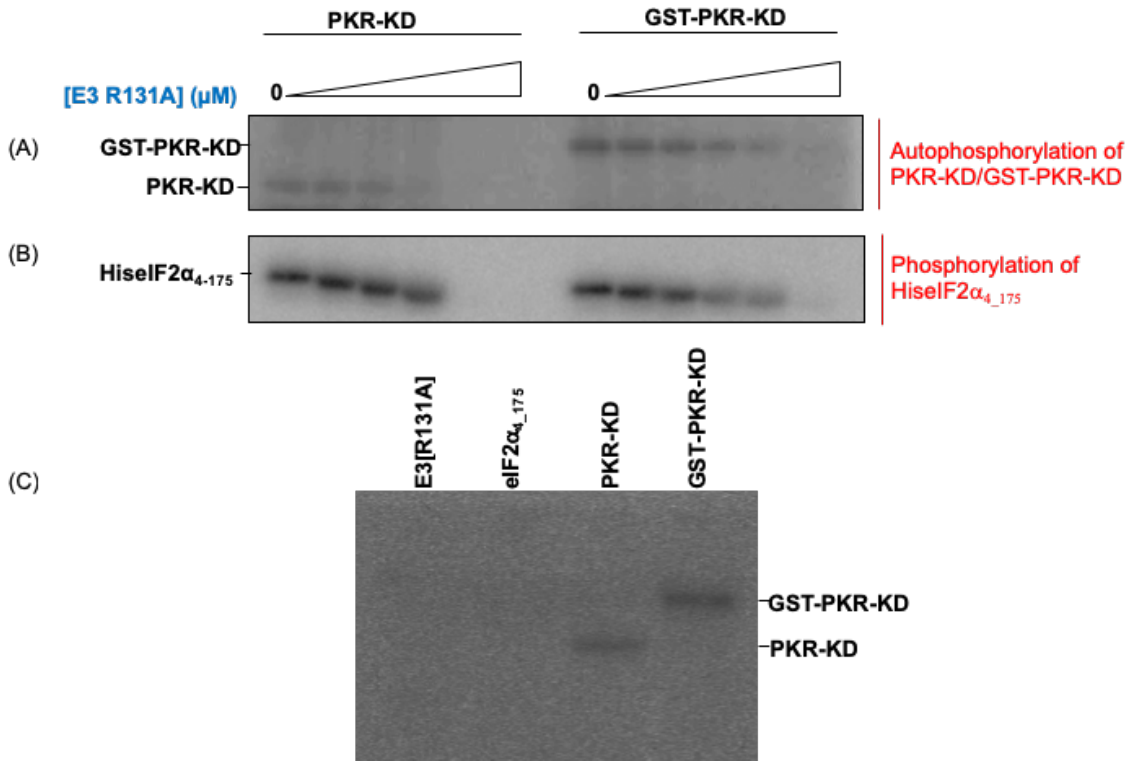

Figure 6.2. In-vitro autophosphorylation assay indicating the inhibitory effect of E3[R131A] on PKR-KD/GST-PKR-KD activity.

(A) Scanned radioactive gel displaying the phosphorylated PKR-KD and GST-PKR-KD and their inhibition with increase in E3 concentration. (B) The same scanned radioactive gel shown in A also displayed phosphorylated HiseIF2α_{4_175} and an inhibition of phosphorylated HiseIF2α_{4_175} with increase in E3 concentration was observed. (C) Radioactive scanned gel for control assay with individual proteins and 100 μM cold ATP supplemented with 5 μCi of γ^{32}P ATP. The 1st lane had E3[R131A] protein with ATP indicated no band, 2nd lane had HiseIF2α_{4_175} with ATP also indicated no band, 3rd and 4th lanes had PKR-KD and GST-PKR-KD respectively with ATP that underwent autophosphorylation indicating the presence of γ^{32}P ATP.

In order to detect the effect of E3 on phosphorylation of eIF2α, the phosphorylation of eIF2α was monitored in the in vitro autophosphorylation assay. The inhibition of His-

eIF2α followed a similar pattern as observed in autophosphorylation of PKR-KD and GST-PKR-KD by E3[R131A] (Fig. 6.2, Panel B).

To test if the phosphorylation observed in the assay blots are due to the phosphorylation of PKR-KD and GST-PKR-KD, a control assay was conducted with individual proteins (E3[R131A], HiseIF2α_{4_175}, PKR-KD and GST-PKR-KD) with 100 μM cold ATP supplemented with 5 μCi of γ^{32}P ATP. Radioactive signals were not observed in case of E3[R131A] and HiseIF2α_{4_175} indicating that these proteins do not undergo autophosphorylation simply in the presence of ATP (Fig. 6.2, Panel C). PKR-KD and GST-PKR-KD on the other hand underwent phosphorylation validating the results obtained in the above mentioned autophosphorylation assays.

Based on the results from the in vitro autophosphorylation assay, it was suggested that E3 proteins inhibit the autophosphorylation of PKR-KD and without the requirement of dsRNA binding. The difference in inhibitory effect of E3 on PKR-KD and GST-PKR-KD was indicative of two pathways that E3 followed for PKR-KD inhibition: first with monomeric PKR-KD which is in the process of dimerization and second with activated and dimerized GST-PKR-KD. A physical interaction between E3 and monomeric PKR-KD had already been established and the results from monomeric PKR-KD autophosphorylation assay together support the model that E3 physically binds to monomeric PKR-KD which disrupts its dimerization process and thus autophosphorylation and phosphorylation of eIF2α. Similarly, a physical interaction between E3 and dimeric PKR-KD was not observed which could be due to lack of interaction or a very weak interaction between these two proteins. The autophosphorylation assay displayed a lower inhibition effect of E3 on dimeric GST-PKR-KD. Based on these observations, a second pathway was suggested by which E3

disrupts the already dimerized PKR-KD, inhibits its autophosphorylation and thus phosphorylation of eIF2α.

(A)

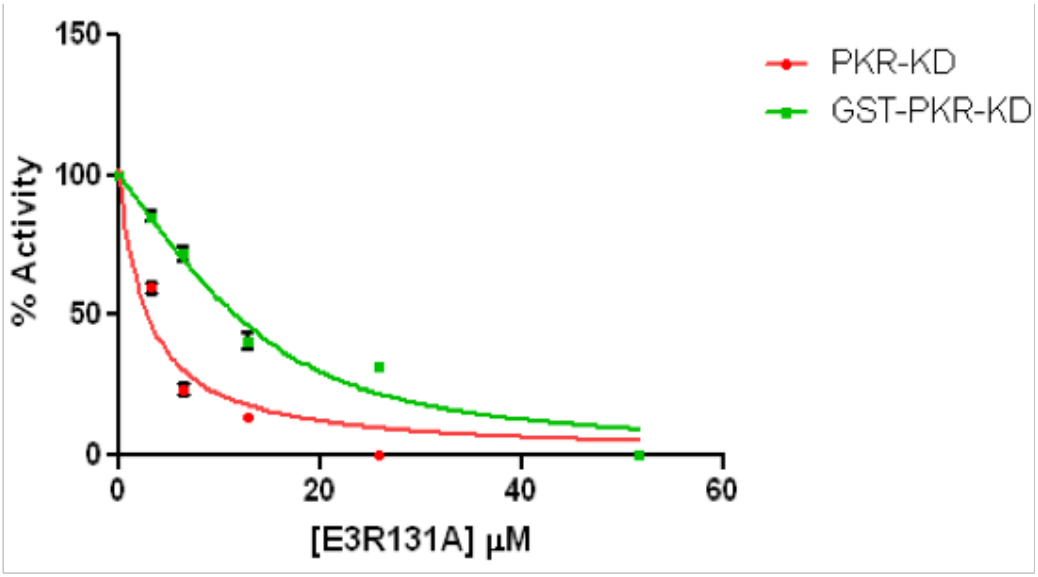

(B)

Protein	IC_{50} value of E3 (µM)	IC_{50} value of E3 (µM)	IC_{50} value of E3 (µM)	Average IC_{50} value	P value
PKR-KD (Monomer)	2.185	2.087	2.454	2.242	< .001
GST-PKR-KD (Dimer)	10.58	8.415	9.595	9.53	

Figure 6.3. Quantitative analysis of in-vitro autophosphorylation assay with E3[R131A] and PKR-KD/GST-PKR-KD.

(A) The graph represents the quantitative analysis of the autophosphorylation gels conducted in triplicates. The densitometry data from the gels in Figure 6.2 were obtained using ImageJ software. The x-axis represents the concentration of E3[R131A] used in the assays and the y-axis represents the percent PKR-KD/GST-PKR-KD activity. (B) The IC50 values of the triplicate assays performed for PKR-KD/GST-PKR-KD with E3 protein. IC50 values were calculated using GraphPad Prism version 5.0 for Windows, GraphPad Software, La Jolla California USA, www.graphpad.com. The p-value for the difference in inhibition of PKR-KD and GST-PKR-KD by E3 was calculated using GraphPad QuickCalcs Web site.

6.2.3. E3 inhibits the phosphorylation of eIF2α by PKR-KD

In vitro kinase assays were performed to determine the effect of E3 on the phosphorylation of eIF2α without the dsRNA binding ability of either E3 or PKR-KD. PKR-KD proteins purify in a weak equilibrium of monomeric and dimeric state and upon long term storage in -80°C, the monomeric fractions had converted to PKR-KD dimers. Hence, to combat this problem, all the in-vitro kinase assays were performed with freshly purified E3 and PKR-KD proteins. Dimeric or trimeric E3 fractions were used for the assays to ensure the inhibitory effects of E3 on PKR-KD activity. These criteria and conditions were followed for all the in-vitro kinase assays to remain consistent through-out.

The E3[R131A] protein inhibited phosphorylation of His-eIF2α_{4_175} in case of both monomeric PKR-KD and dimeric GST-PKR-KD. Consistent with the His-eIF2α_{4_175} phosphorylation results obtained in autophosphorylation assay, inhibition of His-eIF2α_{4_175} phosphorylation was observed more in monomeric PKR-KD than dimeric GST-PKR-KD (Fig. 6.4, Panel A). A different western blot with the same in vitro kinase assay reactions were blotted with anti-His antibody to demonstrate the loading control in these assays. As observed in figure 6.4, an equal amount of His-eIF2α_{4_175} was added to each reactions and the inhibition of His-eIF2α_{4_175} phosphorylation was due to increased concentration of E3[R131A] protein. An amount of 26 μM of E3 protein inhibited the phosphorylation of HiseIF2α_{4_175} completely in monomeric PKR-KD reactions whereas 52 μM of E3 was needed for inhibition in case of dimeric GST-PKR-KD. The calculated IC_{50} value for E3[R131A] protein for inhibiting phosphorylation of His-eIF2α_{4_175} in an assay with monomeric PKR-KD was 5.4 μM and for dimeric GST-PKR-KD was 6.5 μM. A *p*-value of less than 0.05 was calculated which suggested statistically significant difference was found

between E3[R131A] inhibition of His-eIF2α_{4_175} phosphorylation led by PKR-KD and GST-PKR-KD (Fig. 6.5).

To validate the inhibition of phosphorylated His-eIF2α_{4_175} by E3[R131A] proteins, a control assay was performed similar to the in vitro kinase assay with Bovine Albumin Serum (BSA) protein instead of E3. BSA was unable to inhibit the phosphorylation of HiseIF2α_{4_175} suggesting that the inhibition observed in these assays represent the actual result of E3 and PKR-KD interactions (Fig. 6.4, Panel B). Higher oligomers of E3 (10-15 E3 molecules) or aggregates did not have any effect on the PKR-KD activity (Data not shown).

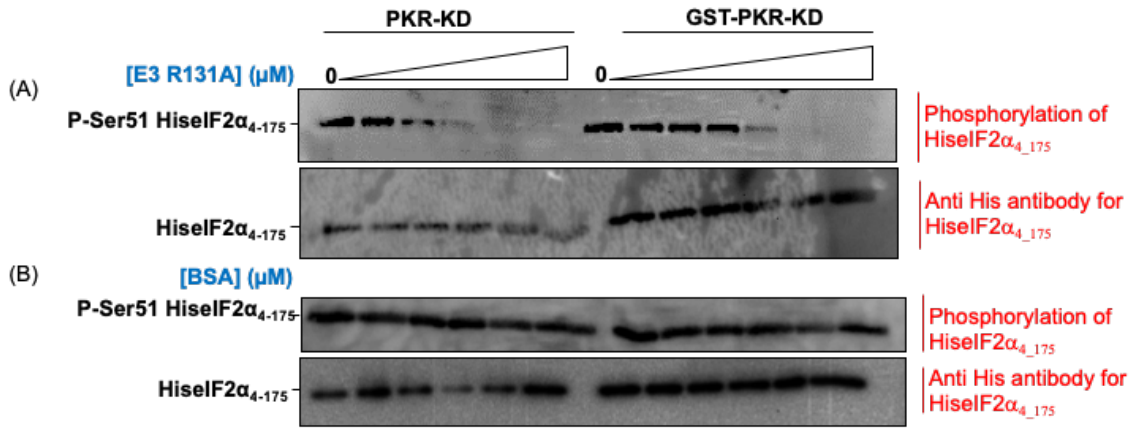

Figure 6.4. In-vitro kinase assay indicating the inhibitory effect of E3[R131A] on phosphorylation of HiseIF2α_{4_175} led by PKR-KD/GST-PKR-KD and control in-vitro assay with BSA.

(A) Western blot of in-vitro assay of E3[R131A] protein shows the inhibition of HiseIF2α_{4_175} phosphorylation with increased concentration of E3 and blotted with anti-phospho-serine51-eIF2α antibody. The 1st six reactions are assembled with monomeric PKR-KD and the 2nd six reactions with dimeric GST-PKR-KD with different concentrations of E3[R131A] protein. The panel underneath is a separate blot that represents the loading control blotted with anti-His antibody with protein reactions used in the in vitro kinase assays. (B) Control assay with BSA protein instead of E3 shows no inhibition of HiseIF2α_{4_175} phosphorylation in case of both PKR-KD and GST-PKR-KD. The gels were

blotted with anti-phospho-serine51-eIF2α antibody and the loading control gel underneath was blotted with anti-His antibody.

(A)

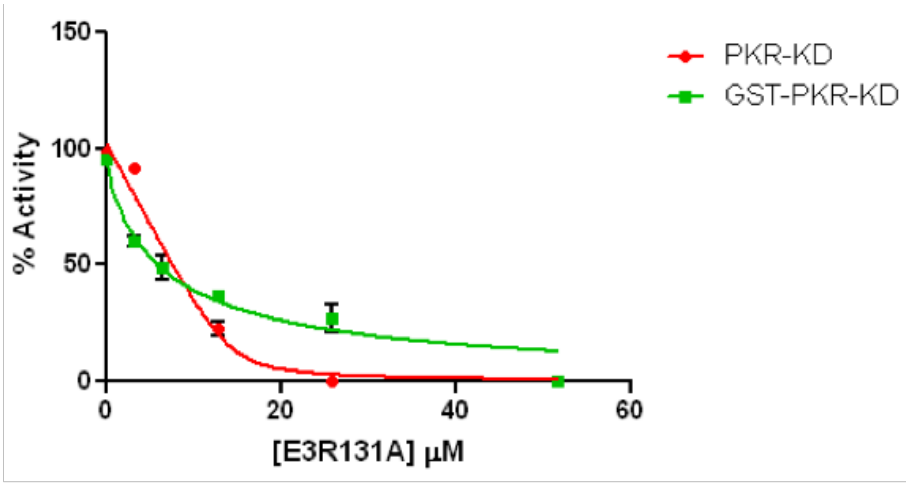

(B)

Protein	IC_{50} value of E3 (µM)	IC_{50} value of E3 (µM)	IC_{50} value of E3 (µM)	Average IC_{50} value	P value
PKR-KD (Monomer)	5.425	5.218	5.679	5.4	< .05
GST-PKR-KD (Dimer)	6.449	6.051	6.884	6.5	

Figure 6.5. Quantitative analysis of in-vitro kinase assay to measure the inhibition of HiseIF2α$_{4_175}$ phosphorylation by E3[R131A].

(A) The graph represents the quantitative analysis of the western blots conducted in triplicates. The densitometry data from the gels in figure 6.4 were obtained using ImageJ software. The x-axis represents the concentration of E3[R131A] used in the assays and the y-axis represents the percent PKR-KD/GST-PKR-KD activity as a correlation to HiseIF2α$_{4_175}$ phosphorylation. (B) The IC50 values of the triplicate assays performed for PKR-KD/GST-PKR-KD with E3 protein. IC50 values were calculated using GraphPad Prism version 5.0 for Windows, GraphPad Software, La Jolla California USA, www.graphpad.com. The p-value for the difference in inhibition of PKR-KD and GST-PKR-KD by E3 was calculated using GraphPad QuickCalcs Web site.

To test a difference in the ability to inhibit the phosphorylation of HiseIF2α$_{4_175}$, a different E3[F148A] mutant was used. Results showed that E3[F148A] inhibited phosphorylation of HiseIF2α$_{4_175}$ by PKR-KD and GST-PKR-KD (Fig. 6.6). An amount of 52 µM of E3[F148A] protein was required to completely inhibit the phosphorylation of

HiseIF2α_{4_175} for both PKR-KD and GST-PKR-KD reactions. The calculated IC_{50} values of E3[F148A] for these assays were 6.3 μM and 6.5 μM for PKR-KD and GST-PKR-KD respectively (Fig. 6.7). The *p*-value was calculated to be more than 0.05 which demonstrated the non-significant difference between PKR-KD and GST-PKR-KD reactions.

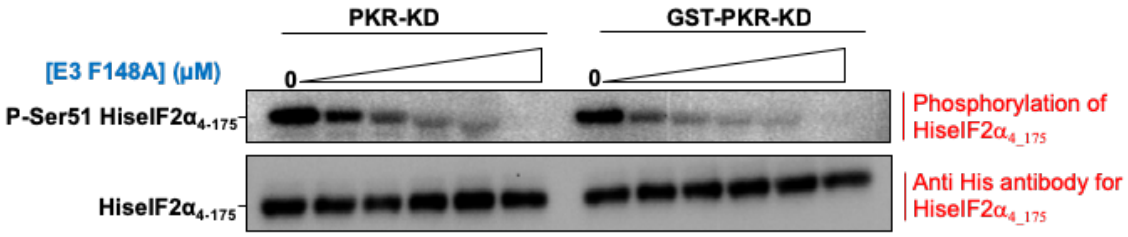

Figure 6.6. In-vitro kinase assay indicating the inhibitory effect of E3[F148A] on phosphorylation of HiseIF2α_{4_175} *led by PKR-KD/GST-PKR-KD.*

Western blot of in-vitro assay of E3[F148A] protein shows the inhibition of HiseIF2α_{4_175} *phosphorylation with increased concentration of E3 and blotted with anti-phospho-serine51-eIF2*α_4 *antibody. The 1st six reactions are assembled with monomeric PKR-KD and the 2nd six reactions with dimeric GST-PKR-KD with different concentrations of E3[F148A] protein. The panel underneath is a separate blot that represents the loading control blotted with anti-His antibody with protein reactions used in the in vitro kinase assays.*

E3[R131A] showed a complete inhibition of phosphorylated HiseIF2α_{4_175} at a concentration of 26 μM for monomeric PKR-KD reactions whereas for E3[F148A] protein it required 52 μM. The IC_{50} values for these assays were 5.4 μM and 6.3 μM for E3[R131A] and E3[F148A] respectively. The difference had statistical significance as the *p*-value was more than 0.05. Similarly, a comparison was made for the effect of E3[R131A] and E3[F148A] on the inhibition of HiseIF2α_{4_175} phosphorylation by dimeric GST-PKR-KD.

There were no significant differences found between the two E3 mutants for GST-PKR-KD reactions (p-value > 0.05, 6.2 μM for E3[R131A], 5.4 μM for E3[F148A]).

Based on the comparisons of the effect of E3[R131A] and E3[F148A] on the phosphorylation of eIF2α by PKR-KD or GST-PKR-KD, it was inferred that phenyl alanine residue at position 148 in E3 proteins could be an essential amino acid required for the inhibition for PKR-KD activity.

(A)

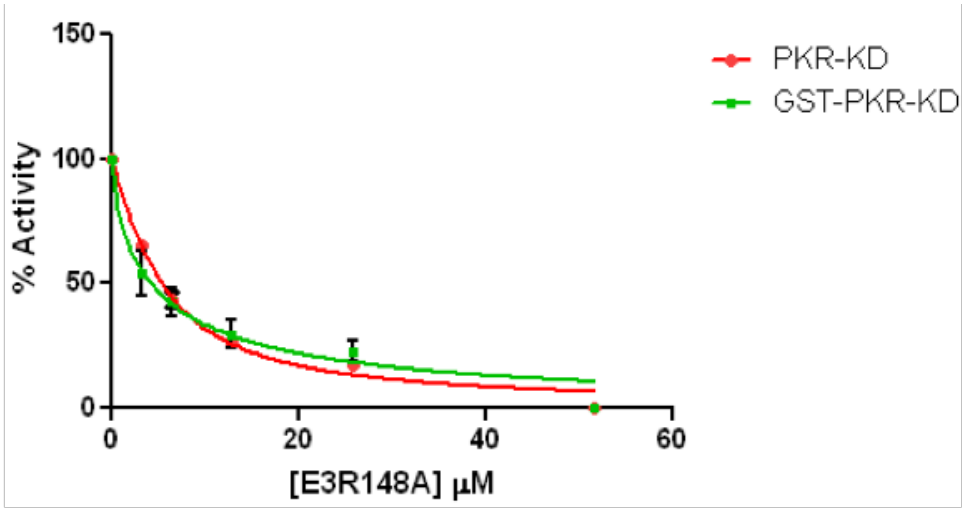

(B)

Protein	IC_{50} value of E3 (μM)	IC_{50} value of E3 (μM)	IC_{50} value of E3 (μM)	Average IC_{50} value	P value
PKR-KD (Monomer)	6.609	6.148	6.036	6.3	> .05
GST-PKR-KD (Dimer)	5.966	6.779	6.704	6.5	

Figure 6.7. Quantitative analysis of in-vitro kinase assay to measure the inhibition of HiseIF2α$_{4_175}$ phosphorylation by E3[F148A].

(A) The graph represents the quantitative analysis of the western blots conducted in triplicates. The densitometry data from the gels in figure 6.6 were obtained using ImageJ software. The x-axis represents the concentration of E3[F148A] used in the assays and the y-axis represents the percent PKR-KD/GST-PKR-KD activity as a correlation to HiseIF2α$_{4_175}$ phosphorylation. (B) The IC50 values of the triplicate assays performed for PKR-KD/GST-PKR-KD with E3 protein. IC50 values were calculated using GraphPad Prism version 5.0 for Windows, GraphPad Software, La Jolla California USA, www.graphpad.com. The p-

value for the difference in inhibition of PKR-KD and GST-PKR-KD by E3 was calculated using GraphPad QuickCalcs Web site.

6.2.4. N and C-terminals of E3 are required for PKR-KD inhibition

The predicted models for E3 and PKR interactions had advocated the importance of both N and C-terminals of E3 protein. These studies have shown the interaction of E3 and PKR (in-vivo coimmunoprecipitation assay) was dependent on both N and C-terminal of E3 [13, 75]. A physical interaction between E3 and PKR-KD has already been established in this study. This result indicates that the dsRNA binding N-terminal domain of PKR is dispensable for PKR and E3 interaction contrary to the proposed model (Fig. 2.12). To resolve this discrepancy, in vitro kinase assays were conducted with E3[R131A] N-terminal (amino acids 1-79) and C-terminal (amino acids 81- 190) protein individually.

The results from in vitro kinase assay with E3[R131A] N-terminal protein demonstrated a lack of inhibition of His-eIF2α_{4_175} phosphorylation by monomeric PKR-KD. This result was in accordance with the prediction that both N and C-terminals of E3 are required for its activity. But the results for the GST-PKR-KD reactions displayed inhibition of His-eIF2α_{4_175} phosphorylation with an increase in E3[R131A] N-terminal protein concentration (Fig. 6.8). A complete inhibition of HiseIF2α_{4_175} was observed at 26 μM of E3 [R131A] N protein with an IC_{50} value of 5.3 μM (Fig. 6.9).

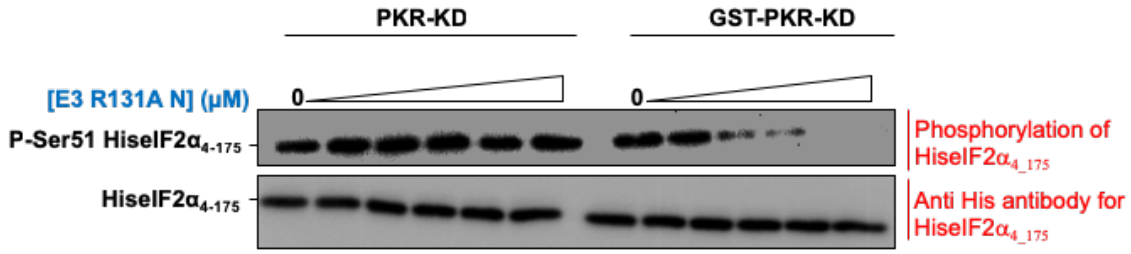

Figure 6.8. In-vitro kinase assay indicating the inhibitory effect of E3[R131A] N-terminal protein on phosphorylation of HiseIF2α$_{4_175}$ led by PKR-KD/GST-PKR-KD.

Western blot of in-vitro assay of E3[R131A] N-terminal protein shows no inhibition of HiseIF2α$_{4_175}$ phosphorylation led by PKR-KD whereas inhibition in case of GST-PKR-KD with increased concentration of E3. The membranes were blotted with anti-phospho-serine51-eIF2α antibody. The 1st six reactions are assembled with monomeric PKR-KD and the 2nd six reactions with dimeric GST-PKR-KD with different concentrations of E3[R131A] N-terminal protein. The panel underneath is a separate blot that represents the loading control blotted with anti-His antibody with protein reactions used in the in vitro kinase assays.

The results from the in vitro kinase assay of E3[R131A] N terminal protein suggested that the interaction of dimeric PKR-KD with E3 N terminal disrupted the PKR-KD dimers leading to inhibition of PKR-KD autophosphorylation and eventually inhibition of His-eIF2α$_{4_175}$ phosphorylation.

(A)

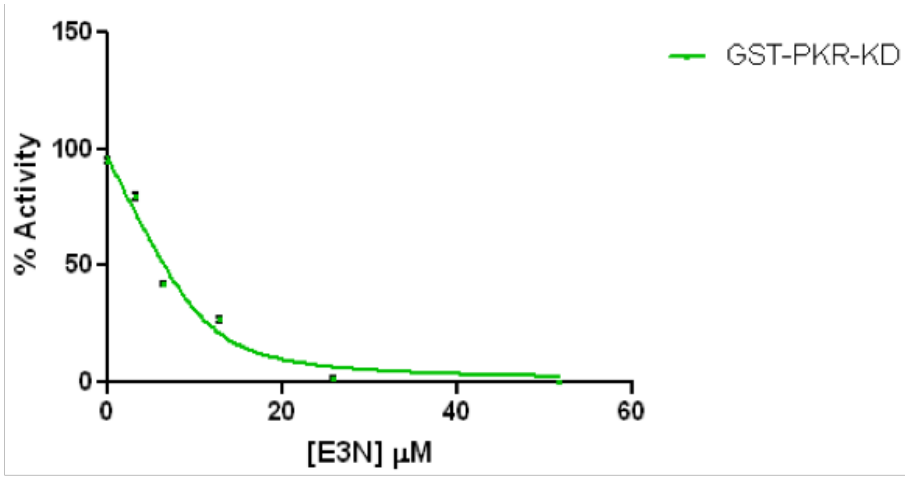

(B)

Protein	IC_{50} value of E3 (µM)	IC_{50} value of E3 (µM)	IC_{50} value of E3 (µM)	Average IC_{50} value
GST-PKR-KD (Dimer)	5.056	5.190	5.563	5.3

Figure 6.9. Quantitative analysis of in-vitro kinase assay to measure the inhibition of HiseIF2α_{4_175} phosphorylation by E3[R131A] N terminal.

(A) The graph represents the quantitative analysis of the western blots conducted in triplicates. The densitometry data from the gels in figure 6.8 were obtained using ImageJ software. The x-axis represents the concentration of E3[R131A] N protein used in the assays and the y-axis represents the percent GST-PKR-KD activity as a correlation to HiseIF2α_{4_175} phosphorylation. (B) The IC50 values of the triplicate assays performed for GST-PKR-KD with E3 protein. IC50 values were calculated using GraphPad Prism version 5.0 for Windows, GraphPad Software, La Jolla California USA.

A binding assay was conducted between E3[R131A] N and dimeric/monomeric PKR-KD protein to understand the inhibitory effect of E3 N terminal on dimeric GST-PKR-KD activity. A protein mix of E3[R131A]N and PKR-KD protein was passed through a SEC column. Both dimeric and monomeric PKR-KD failed to physically interact with E3 N terminal protein (Fig. 6.10 & 6.11). Two main peaks were observed in the SEC for both monomeric PKR-KD and dimeric PKR-KD complex formation assay with E3N protein. The elution volumes of the complex peaks corresponded to that of the individual proteins

suggesting a non-formation of complex. The results from SEC did not reveal an interaction between the two proteins. However, weak protein-protein interactions are difficult to be measured in size exclusion chromatography method, which could be a possible reason for the non-formation of complex between E3 N and dimeric PKR-KD.

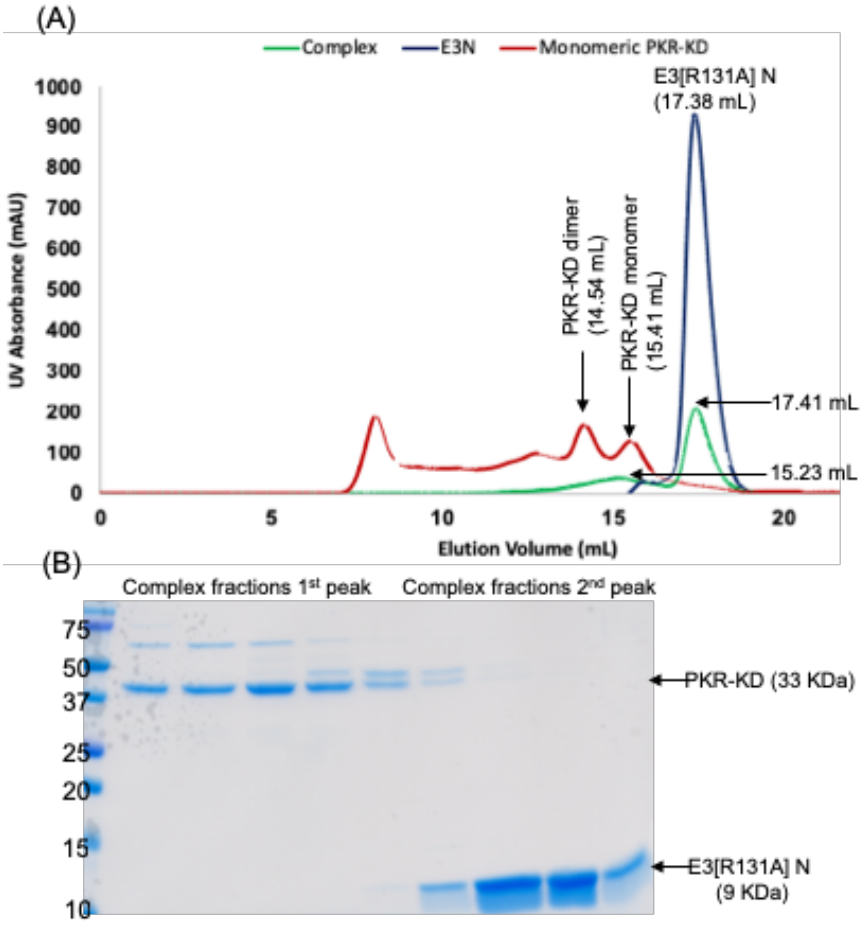

Figure 6.10. Size exclusion chromatogram of interactions between E3[R131A] N and monomeric PKR-KD with the corresponding SDS-PAGE gel of the complex formation assay.

(A) Comparison of the chromatograms for E3[R131A] N protein (Blue), PKR-KD (Red) and complex (Green). The corresponding elution volumes are mentioned along the peaks. (B) SDS-PAGE gel of fractions from the E3[R131A] N and PKR-KD complex SEC. Fractions from the main two peaks were electrophoresed on a 15% SDS-PAGE gel.

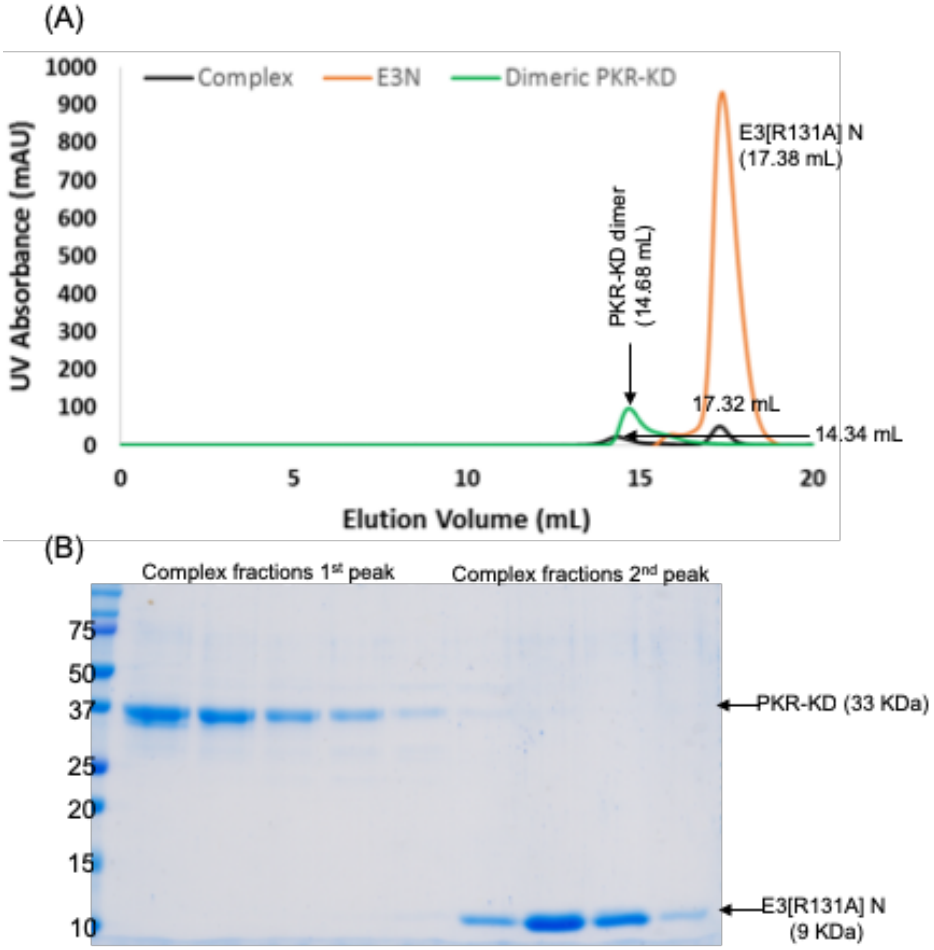

Figure 6.11. Size exclusion chromatogram of interactions between E3[R131A] N and dimeric PKR-KD with the corresponding SDS-PAGE gel of the complex formation assay.

(A) Comparison of the chromatograms for E3[R131A] N protein (Orange), dimeric PKR-KD (Green) and complex (Black). The corresponding elution volumes are mentioned along the peaks. (B) SDS-PAGE gel of fractions from the E3[R131A] N and PKR-KD complex SEC. Fractions from the main two peaks were electrophoresed on a 15% SDS-PAGE gel.

Similar to the E3 N-terminal, in-vitro kinase assay of the C-terminal of E3[R131A] protein with PKR-KD and GST-PKR-KD was conducted which displayed no inhibition in the phosphorylation of HiseIF2α_{4_175} (Fig. 6.12). E3 C-terminal did not inhibit the

monomeric or dimeric PKR-KD activity which was observed by the identical phosphorylation of HiseIF2α_{4_175} even with increasing concentration of the E3 C protein.

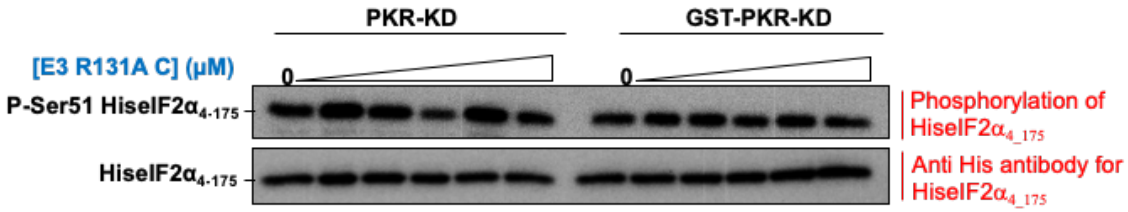

Figure 6.12. In-vitro kinase assay indicating the inhibitory effect of E3[R131A] C-terminal protein on phosphorylation of HiseIF2α_{4_175} led by PKR-KD/GST-PKR-KD.

Western blot of in-vitro assay of E3[R131A] C-terminal protein shows no inhibition of HiseIF2α_{4_175} phosphorylation led by PKR-KD and GST-PKR-KD. The membranes were blotted with anti-phospho-serine51-eIF2α antibody. The 1st six reactions are assembled with monomeric PKR-KD and the 2nd six reactions with dimeric GST-PKR-KD with different concentrations of E3[R131A] C-terminal protein. The panel underneath is a separate blot that represents the loading control blotted with anti-His antibody with protein reactions used in the in vitro kinase assays.

A binding assay was conducted to detect the interactions between E3[R131A] C-terminal protein and monomeric PKR-KD. The results indicated that a non-interaction of these proteins (Fig. 6.13). Comparison of the chromatogram of complex of E3 C and PKR-KD protein with their individual SEC purification chromatograms indicated that these proteins do not interact. A broader peak of the chromatogram had an elution volumes of 14.53 mL and 15.26 mL which corresponded to the elution volumes of dimeric and monomeric PKR-KD respectively whereas the sharp 2nd peak had an elution volume closer to E3[R131A] C protein. There was no shift in elution volumes and separate peaks corresponding to the E3 C and PKR-KD protein suggested a non-formation of complex. The

results from the complex formation assay and in-vitro kinase assay confirmed that the C-terminal of E3 does not physically interact with PKR-KD in the absence of E3 N-terminal.

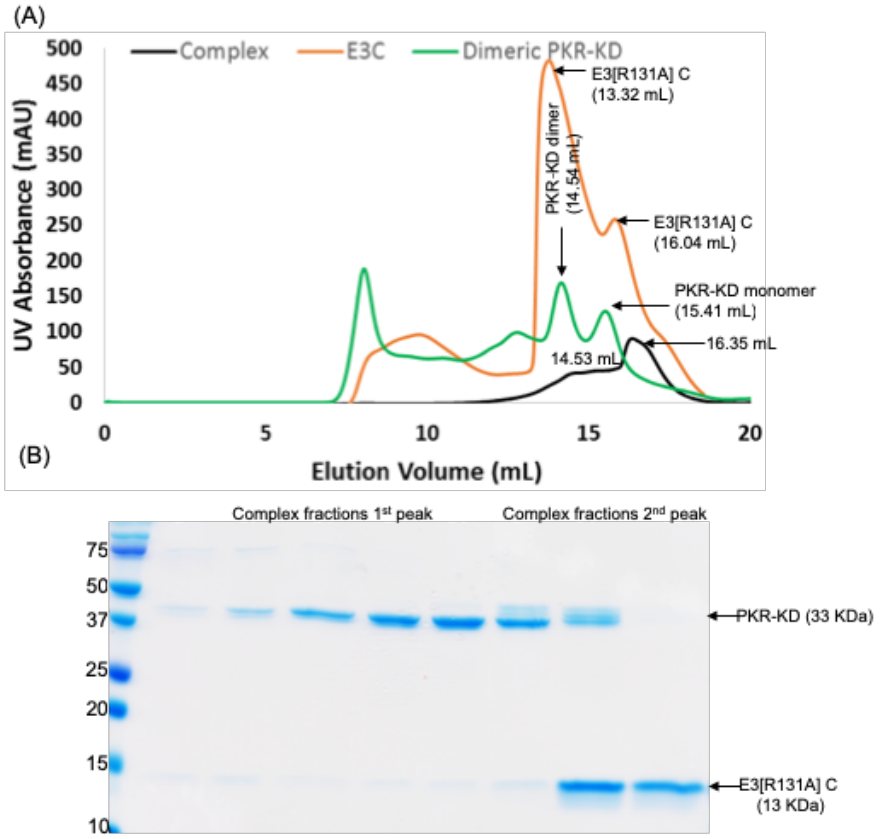

Figure 6.13. Size exclusion chromatogram of interactions between E3[R131A] C and monomeric PKR-KD with the corresponding SDS-PAGE gel of the complex formation assay.

(A) Comparison of the chromatograms for E3[R131A] C protein (Orange), PKR-KD (Green) and complex (Black). The corresponding elution volumes are mentioned along the peaks. (B) SDS-PAGE gel of fractions from the E3[R131A] C and PKR-KD complex SEC. Fractions from the main two peaks were electrophoresed on a 15% SDS-PAGE gel.

In order to detect the effects of E3 N and E3 C together on PKR-KD activity, E3[R131A] N and E3[R131A] C were added in a 1:1 molar ratio and this protein mixture was used for in vitro kinase assay. It was predicted that the E3 N and E3 C would behave as

two individual proteins rather than a full length E3 protein and the inhibition pattern would be similar to what was observed in each individual case. The results did not uphold the predictions. It was observed that no inhibition of the phosphorylation of His-eIF2α_{4_175} occurred in either monomeric PKR-KD or dimeric GST-PKR-KD even for different concentrations of the E3 N-E3 C mix (Fig. 6.14).

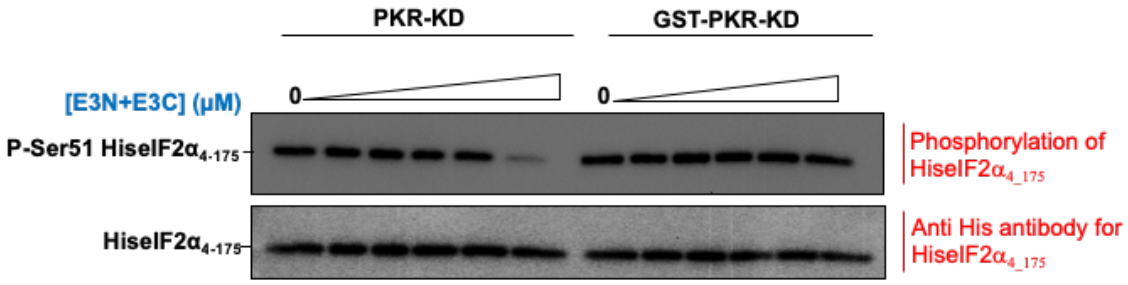

Figure 6.14. In-vitro kinase assay indicating the inhibitory effect of an equal mix of E3[R131A] N and C-terminal protein on phosphorylation of HiseIF2α_{4_175} led by PKR-KD/GST-PKR-KD.

Western blot of in-vitro assay of E3[R131A] N and C-terminal protein shows no inhibition of HiseIF2α_{4_175} phosphorylation led by PKR-KD and GST-PKR-KD. The membranes were blotted with anti-phospho-serine51-eIF2α antibody. The 1st six reactions are assembled with monomeric PKR-KD and the 2nd six reactions with dimeric GST-PKR-KD with different concentrations of E3[R131A] N and C-terminal protein. The panel underneath is a separate blot that represents the loading control blotted with anti-His antibody with protein reactions used in the in vitro kinase assays.

The in vitro kinase assay for the protein mixture was repeated to confirm the results obtained. Results showed no inhibition of phosphorylated HiseIF2α_{4_175} by PKR-KD or GST-PKR-KD, apart from a slight inhibition that was observed with 52 μM of the protein mix in the PKR-KD reaction. The E3 N protein individually had inhibited the activity of GST-PKR-KD but surprisingly this was not observed in case of the protein mixture. An

explanation for this phenomenon could be that E3 C protein binds to E3 N in the protein mixture which makes the binding surface of E3 N interacting with dimeric PKR-KD inaccessible. This leads to no inhibition of GST-PKR-KD activity by E3 N as observed earlier.

In order to detect an interaction between E3 N and E3 C proteins, a binding assay was conducted. Equal molar ratio of E3[R131A] N and E3[R131A] C protein were added and passed through a SEC column. It was observed that the SEC chromatogram of E3 N-E3 C protein mix showed a main peak with a shoulder (Fig. 6.15). The elution volume of the main peak corresponded with that of E3 N protein with a minor shift to the left whereas the shoulder had an elution volume that corresponded to E3 C protein. The SDS-PAGE gel exhibited few fractions of the main peak with both E3 N and E3 C proteins. Although the SDS-PAGE gel had fractions with both proteins, it could be due to an overlap of elution volumes because of comparable molecular weight. Based on the comparison of chromatograms from protein mix and individual proteins and the SDS-PAGE gel, it was suggested that E3 N and E3 C protein do not interact or have a weak interaction with each other.

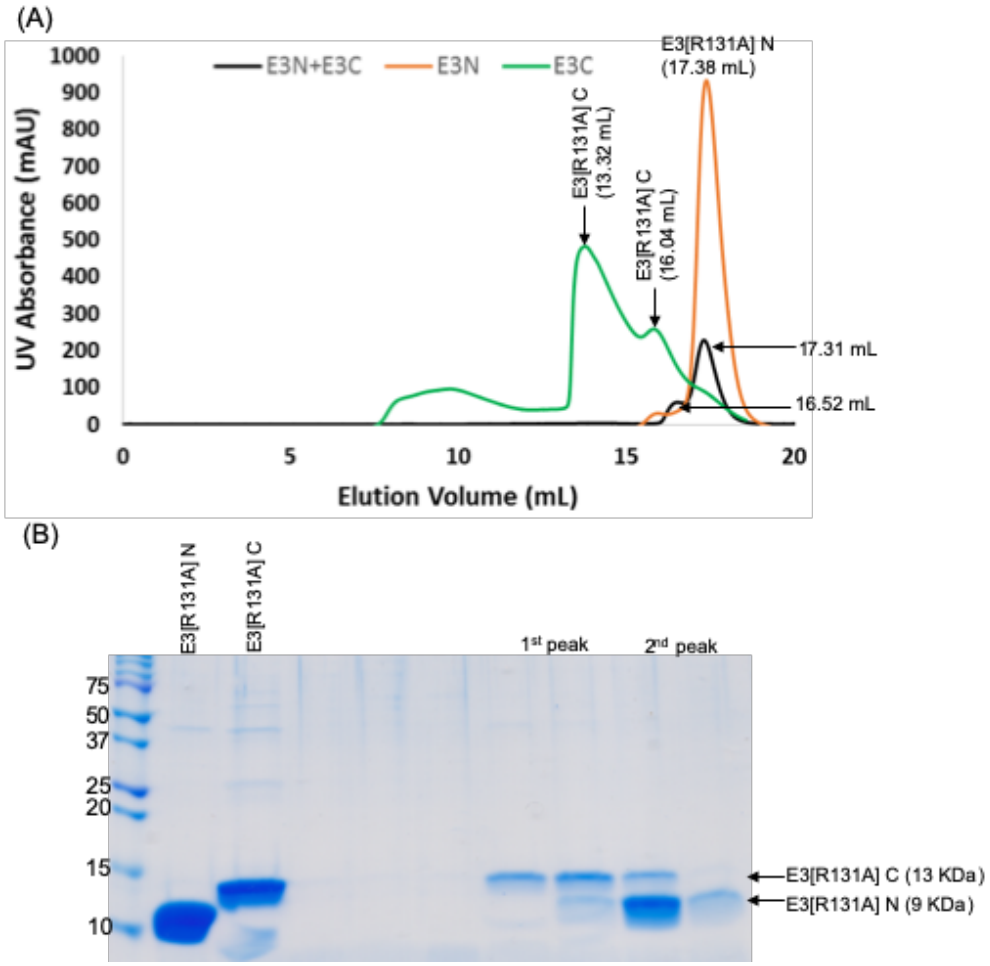

Figure 6.15. Size exclusion chromatogram of interactions between E3[R131A] N and E3[R131A] C protein with the corresponding SDS-PAGE gel of the complex formation assay.

(A) Comparison of the chromatograms for E3[R131A] N protein (Orange), E3[R131A] C (Green) and complex (Black). The corresponding elution volumes are mentioned along the peaks. (B) SDS-PAGE gel of fractions from the E3[R131A] N and E3[R131A] C complex SEC. Fractions from the main peaks were electrophoresed on a 15% SDS-PAGE gel.

6.2.5. E3 double mutants inhibit PKR-KD activity

In a recent study, a GST pull down assay with endogenous PKR in HeLa cells was used to determine the physical interaction between GST tagged E3CΔ25 and PKR where no

interaction was found between these proteins [14]. As the E3CΔ25 protein was known to not interact with PKR, it was used as a negative control to test the robustness of the in vitro kinase assays in this study. The results of the in vitro kinase assay demonstrated that E3CΔ25 did not inhibit the phosphorylation of HiseIF2α_{4_175} by monomeric PKR-KD and dimeric GST-PKR-KD (Fig. 6.16). These results suggested that E3CΔ25 does not physically interact or inhibit PKR-KD activity.

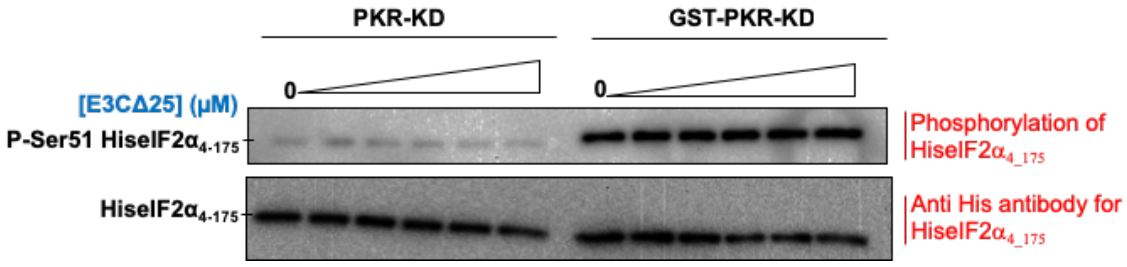

Figure 6.16. In-vitro kinase assay indicating the inhibitory effect of E3CΔ25 protein on phosphorylation of HiseIF2α_{4_175} led by PKR-KD/GST-PKR-KD.

Western blot of in-vitro assay of E3CΔ25 protein shows no inhibition of HiseIF2α_{4_175} phosphorylation led by PKR-KD and GST-PKR-KD. The lighter signal in case of PKR-KD reactions were due to the quality of protein used as compared to GST-PKR-KD. The membranes were blotted with anti-phospho-serine51-eIF2α antibody. The 1st six reactions are assembled with monomeric PKR-KD and the 2nd six reactions with dimeric GST-PKR-KD with different concentrations of E3CΔ25 protein. The panel underneath is a separate blot that represents the loading control blotted with anti-His antibody with protein reactions used in the in vitro kinase assays.

Authors in the same study as mentioned earlier, also noted that single mutants of E3 (I110A and F159A) physically interact with PKR, but do not inhibit PKR activity [14]. Double mutants incorporating these mutations were developed in E3 protein. These double mutants were tested for their ability to inhibit PKR-KD activity. An inhibition of HiseIF2α_{4_175} phosphorylation was observed in both PKR-KD and GST-PKR-KD with

increased concentration of E3[R131AI110A] protein (Fig. 6.17). The inhibition was higher in case of the GST-PKR-KD than PKR-KD reactions. A concentration of 13 μM of E3 protein was required to completely inhibit PKR-KD activity whereas only 6 μM for GST-PKR-KD.

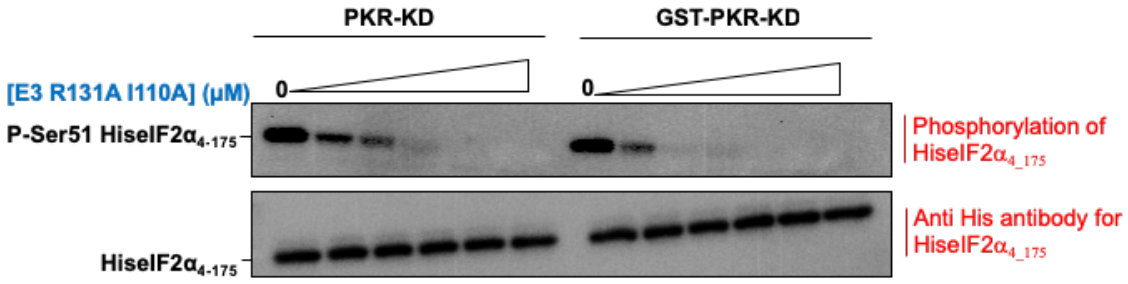

Figure 6.17. In-vitro kinase assay indicating the inhibitory effect of E3[R131AI110A] protein on phosphorylation of HiseIF2α$_{4_175}$ led by PKR-KD/GST-PKR-KD.

Western blot of in-vitro assay of E3[R131AI110A] protein shows inhibition of HiseIF2α$_{4_175}$ phosphorylation led by PKR-KD and GST-PKR-KD. The membranes were blotted with anti-phospho-serine51-eIF2α antibody. The 1st six reactions are assembled with monomeric PKR-KD and the 2nd six reactions with dimeric GST-PKR-KD with different concentrations of E3[R131AI110A] protein. The panel underneath is a separate blot that represents the loading control blotted with anti-His antibody with protein reactions used in the in vitro kinase assays.

The E3[R131AI110A] protein had a calculated IC_{50} value of 3.6 μM for inhibition of monomeric PKR-KD activity whereas only 1.6 μM for dimeric GST-PKR-KD (Fig. 6.18). The difference in the inhibitory ability of E3[R131AI110A] for PKR-KD and GST-PKR-KD was statistically significant with a *p*-value less than 0.05.

(A)

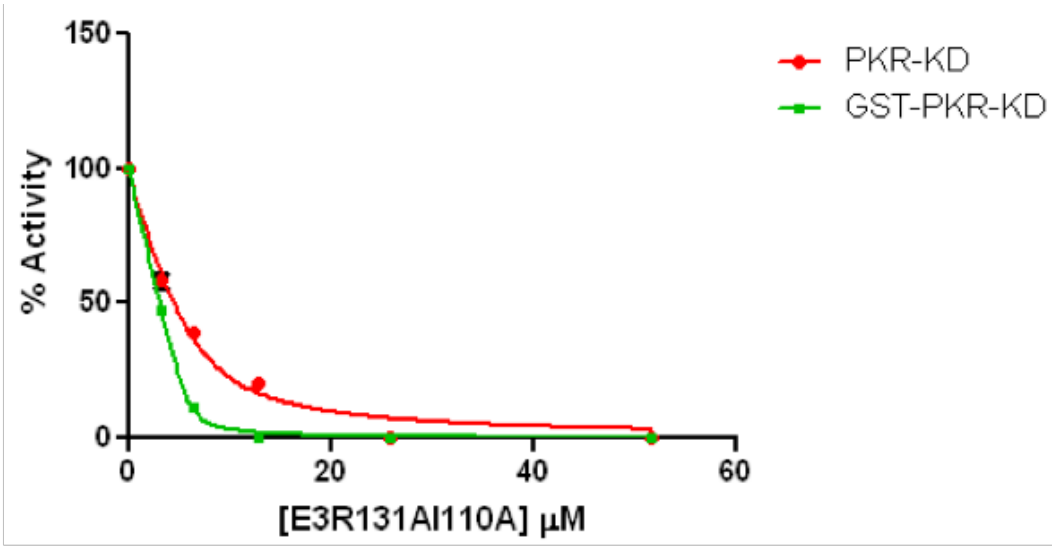

(B)

Protein	IC_{50} value of E3 (µM)	IC_{50} value of E3 (µM)	IC_{50} value of E3 (µM)	Average IC_{50} value	P value
PKR-KD (Monomer)	3.699	3.850	3.320	3.6	< .05
GST-PKR-KD (Dimer)	1.665	1.628	1.612	1.6	

Figure 6.18. Quantitative analysis of in-vitro kinase assay to measure the inhibition of HiseIF2α_{4_175} phosphorylation by E3[R131AI110A].

(A) The graph represents the quantitative analysis of the western blots conducted in triplicates. The densitometry data from the gels in figure 6.17 were obtained using ImageJ software. The x-axis represents the concentration of E3[R131AI110A] used in the assays and the y-axis represents the percent PKR-KD/GST-PKR-KD activity as a correlation to HiseIF2α_{4_175} phosphorylation. (B) The IC50 values of the triplicate assays performed for PKR-KD/GST-PKR-KD with E3 protein. IC50 values were calculated using GraphPad Prism version 5.0 for Windows, GraphPad Software, La Jolla California USA, www.graphpad.com. The p-value for the difference in inhibition of PKR-KD and GST-PKR-KD by E3 was calculated using GraphPad QuickCalcs Web site.

Due to the strong inhibition of GST-PKR-KD activity by E3[R131AI110A] mutant as observed in the in vitro kinase assays, these proteins were tested for protein-protein interactions. Binding assay was conducted by SEC on E3[R131AI110A] and dimeric PKR-

KD. The SEC chromatogram of the protein complex showed the presence of two main peaks with elution volumes of 14.40 mL and 15.51 mL. Comparison of complex SEC chromatogram with chromatograms of individual proteins demonstrated the two main peaks corresponding to dimeric PKR-KD and E3[R131AI110A] protein (Fig. 6.19). This comparison suggested that a complex was not formed between the two proteins but a slight shift of the 1st peak to a higher elution volume as compared to dimeric PKR-KD could possibly be due to the formation of a higher molecular weight complex. The main peak fractions from the SEC purification of complex was electrophoresed on a 15% SDS-PAGE gel showed the presence of both proteins in all fractions implying either a complex formation between the two proteins or an overlap of elution peaks due to similar molecular weight that disguise as a complex.

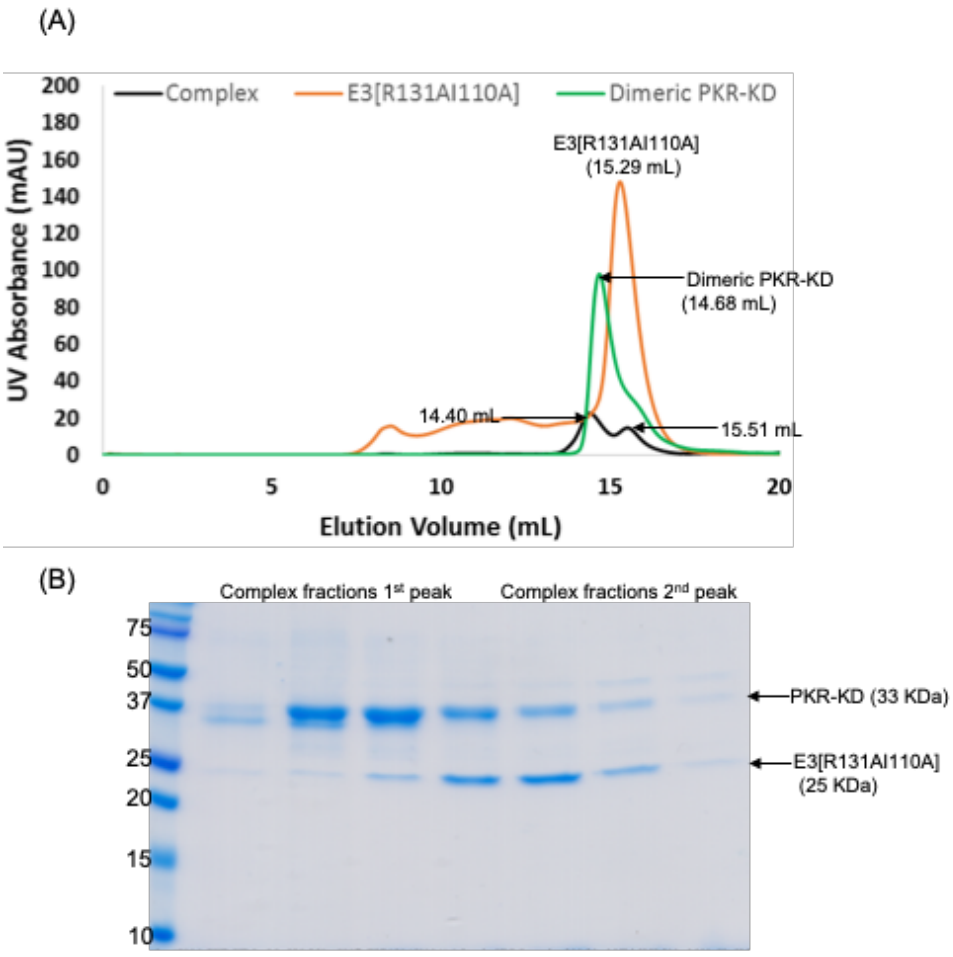

Figure 6.19. Size exclusion chromatogram of interactions between E3[R131AI110A] and dimeric PKR-KD with the corresponding SDS-PAGE gel of the complex formation assay.

(A) Comparison of the chromatograms for E3[R131AI110A] protein (Orange), dimeric PKR-KD (Green) and complex (Black). The corresponding elution volumes are mentioned along the peaks. (B) SDS-PAGE gel of fractions from the E3[R131AI110A] and PKR-KD complex SEC. Fractions from the main two peaks were electrophoresed on a 15% SDS-PAGE gel.

Another double mutant of E3 (R131A F159A) was also tested for its effect on PKR activity. An in-vitro kinase assay was conducted with E3[R131AF159A] protein with PKR-KD and GST-PKR-KD to detect the effect of E3 on phosphorylation of eIF2α, a substrate of PKR. A strong inhibition of HiseIF2α_{4_175} phosphorylation was observed in case of both

monomeric PKR-KD and dimeric GST-PKR-KD with increasing concentrations of E3[R131AF159A] protein (Fig. 6.20). A concentration of 26 μM of E3[R131AF159A] was required for complete inhibition of HiseIF2α_{4_175} phosphorylation by PKR-KD whereas 13 μM for GST-PKR-KD.

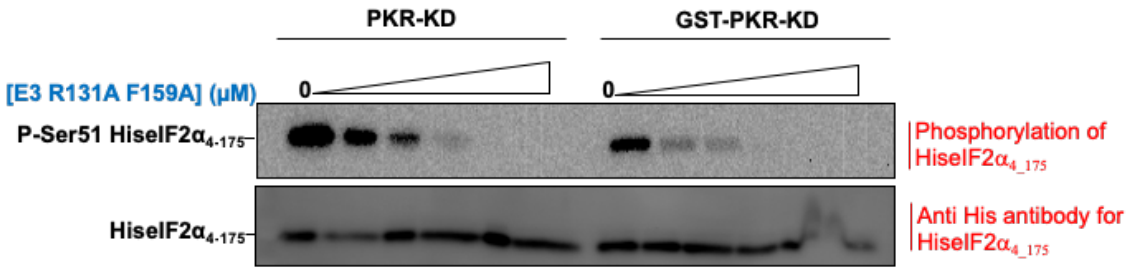

Figure 6.20. In-vitro kinase assay indicating the inhibitory effect of E3[R131AF159A] protein on phosphorylation of HiseIF2α_{4_175} led by PKR-KD/GST-PKR-KD.

Western blot of in-vitro assay of E3[R131AF159A] protein shows inhibition of HiseIF2α_{4_175} phosphorylation led by PKR-KD and GST-PKR-KD. The membranes were blotted with anti-phospho-serine51-eIF2α antibody. The 1st six reactions are assembled with monomeric PKR-KD and the 2nd six reactions with dimeric GST-PKR-KD with different concentrations of E3[R131AF159A] protein. The panel underneath is a separate blot that represents the loading control blotted with anti-His antibody with protein reactions used in the in vitro kinase assays.

E3[R131AF159A] protein had a calculated IC_{50} value of 4 μM for inhibiting phosphorylation of HiseIF2α_{4_175} by PKR-KD whereas a 2.6 μM for GST-PKR-KD reactions (Fig. 6.21). The difference between the effect of E3[R131AF159A] protein on monomeric PKR-KD and dimeric GST-PKR-KD was statistically significant with a *p*-value less than 0.05.

(A)

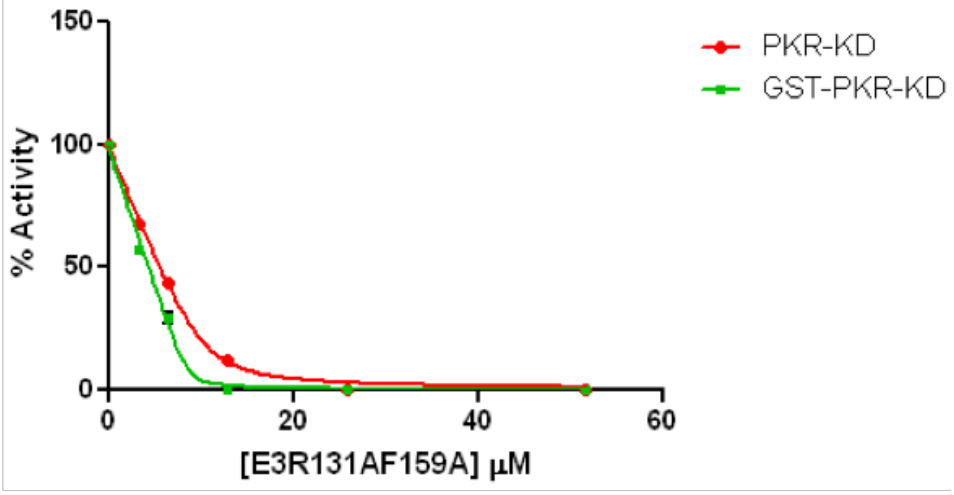

(B)

Protein	IC_{50} value of E3 (µM)	IC_{50} value of E3 (µM)	IC_{50} value of E3 (µM)	Average IC_{50} value	P value
PKR-KD (Monomer)	4.058	4.145	3.913	4.0	< .05
GST-PKR-KD (Dimer)	2.455	2.611	2.632	2.6	

Figure 6.21. Quantitative analysis of in-vitro kinase assay to measure the inhibition of HiseIF2α_{4_175} phosphorylation by E3[R131AF159A].

(A) The graph represents the quantitative analysis of the western blots conducted in triplicates. The densitometry data from the gels in figure 6.20 were obtained using ImageJ software. The x-axis represents the concentration of E3[R131AF159A] used in the assays and the y-axis represents the percent PKR-KD/GST-PKR-KD activity as a correlation to HiseIF2α_{4_175} phosphorylation. (B) The IC50 values of the triplicate assays performed for PKR-KD/GST-PKR-KD with E3 protein. IC50 values were calculated using GraphPad Prism version 5.0 for Windows, GraphPad Software, La Jolla California USA, www.graphpad.com. The p-value for the difference in inhibition of PKR-KD and GST-PKR-KD by E3 was calculated using GraphPad QuickCalcs Web site.

Both the E3 double mutants had a strong inhibitory effect on the activity of PKR-KD and GST-PKR-KD. The inhibition was observed more in case of dimeric GST-PKR-KD as compared to monomeric PKR-KD. The difference in the inhibitory effect of both E3 double mutants in case of PKR-KD activity was compared and found not to be statistically significant with a *p*-value close to 0.05. But in case of the GST-PKR-KD activity, the

difference between both the double mutants was highly significant with a *p*-value less than 0.05. These results indicated E3[R131AI110A] protein had the maximum impact on PKR-KD/GST-PKR-KD activity as compared to single mutants and other constructs of E3 used in various in-vitro kinase assays. It could be explained by suggesting that the double mutations on E3 protein could structural alter the protein to enhance its binding ability to PKR-KD proteins as compared to other E3 constructs.

A summary of all the in-vitro kinase assays performed in this study are compiled in a table along with their functional characteristics (Table 6.1). The biological properties listed in the table were obtained from this study and a recent study conducted by Dueck, 2015 [14].

Table 6.1. Results of in-vitro kinase assays for all the different E3 constructs along with their biological and functional characteristics.

E3 protein (Different mutants)	Actual results (Inhibition of Phosphorylation of eIF2α by PKR-KD)	Actual results (Inhibition of Phosphorylation of eIF2α by GST-PKR-KD)	Expected results	Physical interaction of E3 and PKR-KD	Properties of E3 protein (Different mutants)
E3 R131A	Inhibits PKR-KD activity (IC_{50}= 6.2μM)	Inhibits GST-PKR-KD activity but less than PKR-KD (IC_{50}= 6.2μM)	Inhibition of PKR activity	Yes (Based on complex formation-2018, Patnaik and GST pull down assay-2015, Dueck)	• No ds RNA binding capacity • No host range function
E3 F148A	Inhibits PKR-KD activity (IC_{50}= 5.0μM)	Inhibits GST-PKR-KD activity similar to PKR-KD (IC_{50}= 5.4μM)	Inhibition of PKR activity	Yes (GST pull down assay- 2015, Dueck)	• No ds RNA binding capacity • host range function
E3 R131A (N-terminal) 1_79 aa	No inhibition of PKR-KD activity	Inhibition of GST-PKR-KD activity (IC_{50}= 5.3μM)	No inhibition should be observed	No (Complex formation-2018, Patnaik)	• No ds RNA binding capacity • No host range function
E3 R131A (C-terminal) 81_190 aa	No inhibition of PKR-KD activity	No inhibition of GST-PKR-KD activity	No inhibition should be observed	No (Complex formation-2018, Patnaik)	• No ds RNA binding capacity • No host range function
E3 R131A (N + C terminal)	No inhibition of PKR-KD activity	No inhibition of GST-PKR-KD activity	Inhibition of PKR activity (GST-PKR-KD) as obtained in case of E3N	No	• No ds RNA binding capacity • No host range function
E3 R131AΔ25	No inhibition of PKR-KD activity	No inhibition of GST-PKR-KD activity	No inhibition should be observed	No (GST pull down assay-2015, Dueck, Complex formation-2018, Patnaik)	• No ds RNA binding capacity • No host range function • Doesn't bind to PKR-KD
E3 R131A, I110A	Inhibits PKR-KD activity (IC_{50}= 3.6μM)	Inhibits GST-PKR-KD activity but more than PKR-KD (IC_{50}= 1.6μM)	No Inhibition of PKR activity should be observed	Yes (GST pull down assay-2015, Dueck, Complex formation-2018, Patnaik)	• No ds RNA binding capacity • No host range function
E3 R131A, F159A	Inhibits PKR-KD activity (IC_{50}= 4.0μM)	Inhibits GST-PKR-KD activity but more than PKR-KD (IC_{50}= 2.6μM)	No Inhibition of PKR activity should be observed	Yes (GST pull down assay-2015, Dueck)	• No ds RNA binding capacity • No host range function

6.3. Conclusion

In an effort to understand the mechanism of E3 inhibition of PKR-KD activity, we conducted various in vitro kinase assays. All these experiments were conducted in the absence of dsRNA binding ability for both proteins. The results from the in vitro kinase assays demonstrated that E3 could inhibit PKR-KD activity by disrupting the autophosphorylation of PKR-KD, which affected the phosphorylation of eIF2α. While conducting in vitro kinase assays, it was observed that aggregated E3 proteins did not inhibit PKR-KD activity. This was an important observation, which suggested that only lower molecular weight oligomers of E3 could inhibit PKR-KD activity in vitro. In cells, E3 remains in an aggregated state, which increases the multivalence useful for a tighter binding with PKR.

Models previously proposed on the interaction of E3 and PKR suggested that a protein-protein contact occurred between the DRBD domains of PKR and E3 with a mutual binding to the same dsRNA that stabilized the complex of PKR-E3-dsRNA [13, 75]. In this study, we showed that full length E3 physically interacted with the C-terminal of PKR and this interaction occurred without the mutual binding of dsRNA to both proteins. The physical interaction between the two proteins was important for E3 to inhibit the autophosphorylation of PKR-KD. Previous models also suggested that the N-terminal of E3 interacts with the C-terminal of PKR along with interactions between the DRBDs of both proteins. Interactions between E3 and PKR required dsRNA [13]. In this study, an interaction between N-terminal of E3 and C-terminal of PKR could not be established. Results from the in vitro assays on these protein showed that E3 N protein did not affect monomeric PKR-KD activity but

inhibited dimeric PKR-KD activity. A similar inhibition of dimeric PKR-KD activity by E3 N protein has been claimed in a previous study but with no experimental evidence [13].

An importance of the N and C-terminals of E3 protein has been emphasized in previous predicted models of E3-PKR interactions. In this study, we also demonstrated that E3 protein required both its N and C terminals to inhibit PKR-KD activity. We established that the physical interaction between E3 and PKR-KD is mandatory for E3 to inhibit PKR-KD activity. In vitro assays conducted on E3CΔ25, which has been shown to physically not bind to PKR in vivo [14] and PKR-KD in vitro (in this study), and PKR-KD showed no inhibition of PKR-KD activity.

In vitro assay with E3[F148A] showed different results than E3[R131A] mutant suggesting an essential nature of the amino acid 148 for E3 to inhibit PKR-KD activity. Both the E3 double mutants had a strong inhibitory effect on the activity of monomeric and dimeric PKR-KD. The inhibition was observed more in case of dimeric as compared to monomeric PKR-KD. E3[R131AI110A] protein had the maximum impact on PKR-KD activity as compared to single mutants and other constructs of E3 used in various in-vitro kinase assays. It could be explained by suggesting that the double mutations on E3 protein could structural alter the protein to enhance its binding ability to PKR-KD proteins as compared to other E3 constructs.

Overall, this study was the first time to demonstrate the mechanism of E3 inhibition of PKR-KD by conducting in vitro studies. This study also demonstrated the inessentiality of dsRNA binding for E3 and PKR-KD to physically interact with each other and E3 to inhibit PKR-KD activity, as emphasized in previous models.

CHAPTER VII

CRYSTALLIZATION OF VACV E3 PROTEIN

7.1. Introduction

VACV E3 proteins have been studied for more than 15 years in a quest for understanding its functional and structural aspects. This protein affects the innate immune response of the host cell in multiple ways and that makes it an important protein of interest for scientist in this field. Although a well-studied protein, there are still a lot of information missing about E3 and the structure of this protein is one among many. E3 proteins stay in an aggregated form in the cytoplasm of the host cells. Aggregation helps E3 protein to enter into the nuclear compartment of the host cells by either directly altering the physical state of the protein or indirectly preventing the export of cytoplasmic E3 proteins into the nucleus [15]. Structural analysis of E3 proteins has been difficult due to the problem of aggregation. The idea of using protein engineering to alleviate aggregation towards structural studies was derived from a recent success on a non-related difficult protein project conducted by a group in Baylor College of Medicine, Texas [17]. Based on the success achieved in the above mentioned study, it was hypothesized that single/double point mutations of E3 proteins might mitigate the problem of aggregation and thus help in the structural studies of this protein via x-ray crystallography.

Expression and purification of single (E3[R131A]) and double mutants (E3[R131AI110A]) of E3 did not completely eliminate the problem of protein aggregation but obtained lower oligomeric state stable proteins that could be used for crystallization. This chapter covers the early attempts at purifying stable E3 proteins and setting up crystallization conditions using various screening kits.

7.2. Results and Discussion

7.2.1. Crystals of E3[R131AI110A]

The wildtype E3 proteins purify as aggregates which could not be used for structural analysis hence surface mutations on E3 were introduced to reduce or abrogate the problem of aggregation. Single mutant E3[R131A] reduced aggregation and purified as lower oligomeric protein but these protein were not stable. At higher concentration, the E3[R131A] protein fractions tended to form higher oligomers or aggregates. Quite contrary to the single mutant, a double mutant of E3 (R131AI110A) formed dimers even at higher protein concentration. This protein was purified to more than 95% purity and verified to be homogeneous. The crystal trays were scanned regularly for crystal formation as per the schedule. Almost 80 percent of the droplets had protein precipitate without any crystals. Out of the 288 conditions, crystal like structures were observed in one of the droplet after more than a month (Fig. 7.1). The crystallization condition was from the BCS screen kit (MD1-104, Molecular Dimensions) and had 0.15M Sodium chloride, 28% v/v PEG Smear Medium. Izit crystal dye (Hampton Research) was used for differentiating protein crystals from salt crystals. Izit is a small molecule which when added to the droplet would penetrate through large solvent

channels in the protein crystal and turn the crystal blue. But in case of salt crystals, due to the lack of large solvent channels, the crystal does not turn blue. Izit dye was added to the droplet containing the crystals. The crystals did not turn blue suggesting the formation of salt crystals rather than protein. Thin, needle shaped blue crystals appeared after the addition of the Izit dye which were crystals of the dye present in Izit. This occurs in crystallization reagents with a high relative supersaturation (Fig. 7.1).

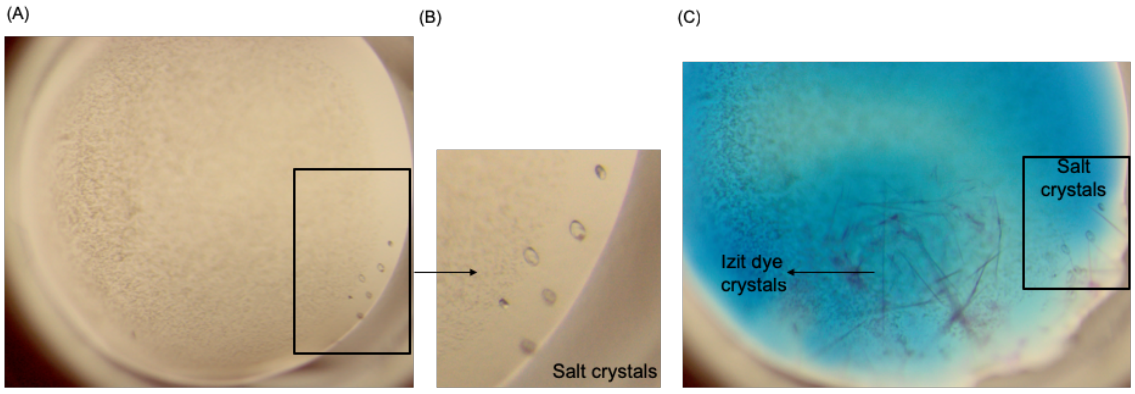

Figure 7.1. Crystallization droplet of E3[R131AI110] for one condition in the BCS screen kit.

(A) The droplet of E3[R131AI110A] with 0.15M Sodium chloride, 28% v/v PEG Smear Medium reagent showed the presence of salt crystals. (B) A closer look at the salt crystals. (C) The same droplet as shown in A but with Izit dye to identify the crystals. The salt crystals did not turn blue and needle like crystals of the Izit dye were formed in the reagent.

7.2.2. Predicted structure of E3

The secondary structure and a 3D model of VACV E3 protein were predicted using an online program, I-TASSER [87-89]. The amino acid sequence of E3 protein was provided and the software projected the best-fitted secondary structure prediction (Fig. 7.2). The sequence-based prediction of secondary structure of E3 was conducted by PSSpred (Protein Secondary Structure Prediction) assigned by ITASSER which is a simple neural network

training algorithm for accurate protein secondary structure prediction. The N-terminal of E3 (amino acids 1-79), the Z-DNA binding domain consisted mostly of coils and α-helices based on the predictions. The crystal structure of the N-terminal Z-DNA binding domain of an E3 orthologue from Yatapoxvirus had a helix-turn-helix (HTH) motif and three antiparallel β-sheets [33]. In comparison to N-terminal of Yatapoxvirus, the VACV E3 proteins did not have a α/β architecture typical of Z-DNA binding protein family as per the predicted structure but solving the structure of E3 could provide an insight to the real structural configuration of the protein. The dsRNA binding C-terminal domain of E3 (amino acids 81-190) was predicted of consisting coils, α-helices and β-sheets.

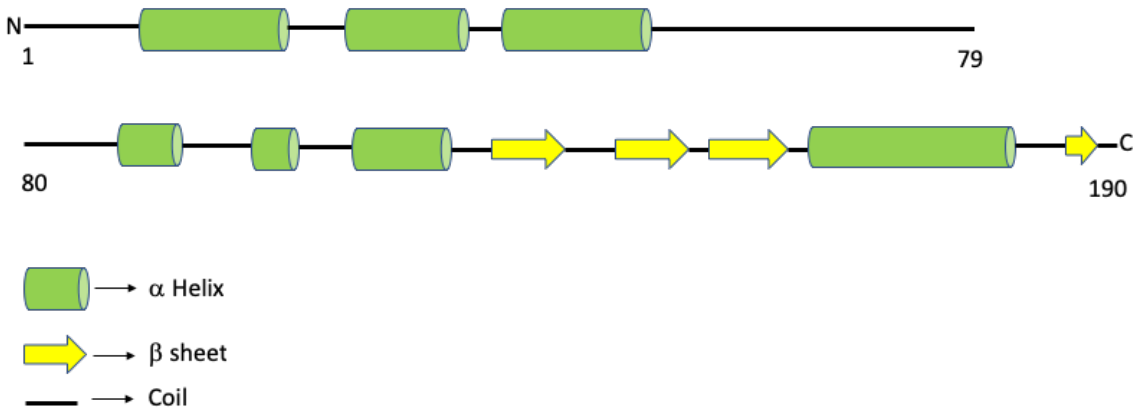

Figure 7.2. Predicted secondary structure of VACV E3 protein.

The prediction of the secondary structure was performed by ITASSER. The N-terminal consisted of coils and α-helices whereas the C-terminal was predicted to be composed of coils, α-helices and β-sheets.

The 3-D structure model of VACV E3 protein was also predicted by ITASSER. Five different models were predicted and were ranked based on their C-score. C-score is a confidence score for estimating the quality of predicted models by I-TASSER. It is calculated based on the significance of threading template alignments and the convergence parameters of the structure assembly simulations. C-score is typically in the range of [-5,2], where a C-score of higher value signifies a model with a high confidence and vice-versa [87-89]. The estimated global accuracy of the model is also based on C-score and C-score > -1.5 indicates a model of correct global topology. In this study, the model with highest C-score of -1.68 was selected (Fig. 7.3).

Figure 7.3. Predicted 3D model of VACV E3 protein. The prediction of the 3D model was performed by I-TASSER.

7.3. Conclusion

Based on the above mentioned results, the structure of VACV E3 protein could possibly be obtained from the stable and pure protein of E3[R131A/I110A] mutant. Crystal

scanning for the E3 double mutant has to be conducted by setting up various crystal screen conditions at different temperatures (room temperature and 4°C). Observation of no crystals in the crystal trays that was set up with three different screen kits at room temperature suggested the protein might not be at a saturation concentration which leads to crystal formation. Optimization of protein concentration and setting up crystal trays at different temperatures would be required for successfully solving the structure of E3 proteins. Crystal trays were also set up for PKR-KD and E3 complex but without much success. The weak interactions of PKR-KD and E3 could be a major drawback for attempting to solve the structure of the complex.

CHAPTER VIII

CONCLUSIONS AND FUTURE WORK

8.1. Conclusions

VACV E3 proteins have been studied for more than 15 years which resulted in a lot of information regarding its functional and biological characteristics. Solving the structure of the protein is an important aspect of E3 which would impart a completeness in the overall knowledge of this protein. This study focused on understanding the mechanistic aspect of E3 proteins. Various surface mutations were conducted in an effort to reduce the inherent nature of E3 aggregation. Two mutants (R131A and F148A) were successfully expressed and purified to produce lower oligomeric state of E3 proteins but did not completely abrogate the problem of aggregation. Optimization of purification of these mutants led to a procedure that could potentially produce homogeneous dimeric proteins. An E3 double mutant (R131A I110A) showed the best results when purified and concentrated to a desired concentration for crystallization (Fig. 4.7). Unlike the single E3 mutants that aggregate at higher concentration, the double mutant had better stability and were a likely candidate for crystallization screening process. Crystal screening was conducted with the E3 double mutant samples which were more than 95 percent pure, stable and homogeneous with various commercially available kits but the lack of crystals so far have led to further experimentations. Optimization of protein concentration and

setting up crystal trays at different temperatures are imperative for successfully solving the structure of E3 proteins. Produced early in the viral replication cycle, E3 protein is known for its host range function, suppression of cytokine expression, and inhibition of interferon (IFN)-induced antiviral activity [8-10]. E3 is known to downregulate PKR activity, thus inhibiting the host immune response [72].

In the event of a viral infection, PKR, a kinase protein in the host cell undergoes activation and thus start a cascade of reactions that initiate immune response against the virus. PKR exists as an inactive monomer in homeostasis but undergoes dimerization for its activation during viral infections. A study proposed an autoinhibition model for PKR activation where dsRNA produced by viruses during infections bind to the DRBD of PKR, thus inducing a conformation change which helps in dimerization of the protein [61-63]. Another study supported this autoinhibition model by proposing that PKR's second DRBD interacts with residues within the insert region (residues 328-335) to mask PKR's kinase domain [64]. Although it has been shown that dsRNA binding to DRBDs leads to PKR dimerization, evidence for a dsRNA independent mechanism also has been reported [65, 66]. A study conducted by Tan et al. found that PKR can dimerize in vivo and in vitro independently of the DRBDs and the dimerization is mediated by amino acid residues 244 to 296 [67]. The second step of PKR activation is autophosphorylation which occurs simultaneously during dimerization. A study showed that a kinase dead PKR mutant K296R impaired PKR-KD dimerization, indicating that kinase domain dimerization promotes activation segment autophosphorylation of PKR, which in turn would stabilize dimerization [68]. Hence, it is considered that autophosphorylation and dimerization are mutually protected events. Autophosphorylation of PKR leads to the phosphorylation of eIF2a at

serine 51 position. The phosphorylated eIF2α inhibits the translation initiation process and thus reduce protein synthesis [49].

VACV E3 protein inhibits the activation of PKR thus preventing the onset of immune response. An early study on vaccinia virus had reported an inhibitor of PKR autophosphorylation but the study did not specify the involvement of E3 proteins [74]. It was found in a study that the downregulation of host defense mechanisms correlated with the accumulation of E3 early in VACV infection [29, 73]. The mechanism of E3 inhibition of PKR activity has been speculated and different in vivo studies had demonstrated that E3 inhibited the dimerization of PKR by forming an inactive heterodimer of E3-PKR [13, 75]. Although the effect of E3 on PKR has been established more than two decades ago, a breakdown of this process is yet to be determined. A recent study had shown that E3 protein does not require the dsRNA binding ability to perform their biological functions [14]. Hence, in this study we attempted to understand the complete mechanism of E3 inhibition of PKR activity and it was predicted that E3 and PKR proteins would interact with each other in the absence of their dsRNA binding capacities. Hence, E3 mutants (with no dsRNA binding ability) and only the kinase domain of PKR were used in this study to understand the mechanism of their interaction. Monomeric inactive PKR-KD and dimeric activated PKR-KD were used in the assays to understand the difference in interaction with E3 protein.

Based on the in vitro and in vivo binding assays conducted by Sharp et al., two regions on PKR were known to interact with VACV E3 protein. One of the binding region involved the DRBDs of PKR and the other overlapped the region of interaction with the substrate eIF2α and the pseudosubstrate VACV K3 protein [75]. This study demonstrated that E3 could directly interact with PKR and suggested the idea that E3 downregulates PKR

by forming nonfunctional heterodimers. In vitro pull down and binding assays in this study indicated a physical interaction between E3[R131A] mutant and monomeric PKR-KD (Fig. 5.2, 5.4, 5.6). It was for the first time that the direct interaction of E3 and the catalytic domain of PKR has been demonstrated in vitro. Similar pull down and binding assays for dimeric PKR-KD demonstrated a lack of interaction between both proteins (Fig. 5.3, 5.5, 5.7). These results indicated that E3 could bind to the catalytic domain of PKR when it is in an inactive monomeric state without the dsRNA binding ability of both proteins.

In vitro kinase and autophosphorylation assays revealed the inhibitory effect of E3[R131A] mutant on the dimerization, autophosphorylation and substrate phosphorylation of PKR-KD proteins. It was detected that higher oligomers of E3 (10 to 12 E3 molecules) or high molecular weight aggregates did not have any effect on the PKR-KD activity in in vitro kinase and autophosphorylation assays. Dimeric or trimeric E3 fractions were used for the assays to ensure the inhibitory effects of E3 on PKR-KD activity. These criteria and conditions were followed for all the in vitro assays to remain consistent through-out. Based on these results, a model for the PKR-KD and E3 interaction mechanism was predicted (Fig. 8.1). According to the model, E3 interacts with PKR-KD in two ways; first when E3 encounters monomeric PKR-KD and second when it interacts with dimeric PKR-KD. The first mechanism works when a lower oligomeric state E3 protein physically binds to monomeric PKR-KD to inhibit it from undergoing autophosphorylation and thus preventing the cascade of reactions that follows to initiate the immune response. The second mechanism occurs when lower oligomeric state E3 proteins inhibit the activity of dimeric PKR-KD which are already activated due to dimerization. A weak interaction between these proteins would explain the inhibition of the dimeric PKR-KD activity by E3. Further experiments

have to be performed to understand the actual mechanism of E3 and dimeric PKR-KD interaction.

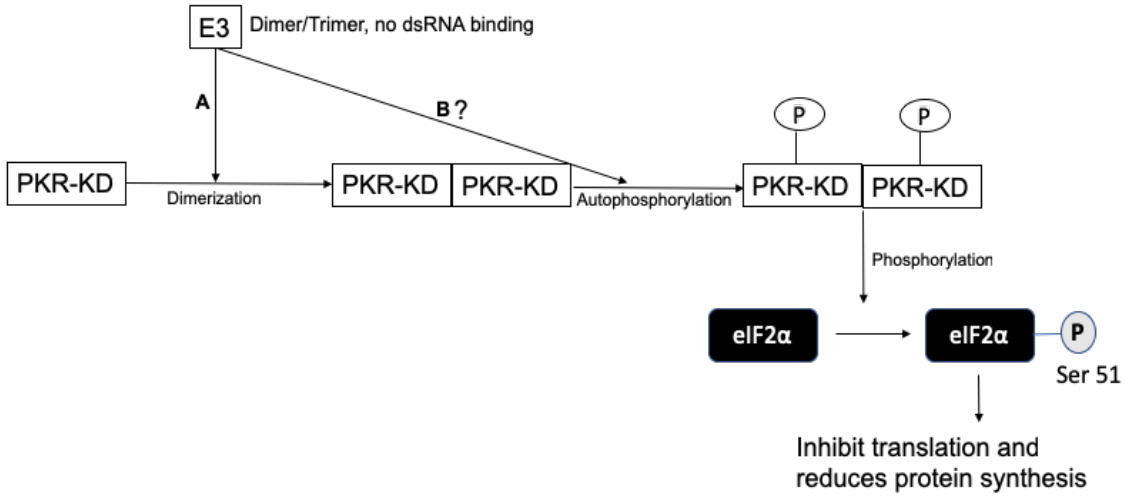

Figure 8.1. Predicted model of the mechanism by which E3 interacts and inhibits PKR-KD activity.

E3 inhibits PKR-KD by two mechanisms to ultimately continue regular protein synthesis during viral infection in host cells. Pathway A: E3 in a lower oligomeric state inhibits activation of monomeric PKR-KD protein by disrupting the dimerization process. This is achieved by direct physical interaction between E3 and PKR-KD. Pathway B: E3 in a lower oligomeric state inhibits already activated dimeric protein to regulate PKR-KD activity. A weak interaction between E3 and dimeric PKR-KD is suspected to be the method of regulation.

The C-terminal domain of E3[R131A] mutant could not inhibit either monomeric or dimeric PKR-KD activity which was due to the absence of physical interactions between these proteins (Fig. 6.12). The N-terminal of E3 had an inhibitory effect only on the dimeric PKR-KD but a physical interaction between these proteins could not be established (Fig. 6.8, 6.10, 6.11). A weak interaction between E3-N and dimeric PKR-KD that disrupts the PKR-KD dimer could explain the inhibitory effect of E3-N protein. A previous in vivo study had suggested that N-terminal of E3 interacted with the C-terminal of PKR and prevented

dimerization in the absence of dsRNA binding by E3 [13]. In spite of the statement, the study failed to show experimental data supporting their arguments for interaction of E3 N-terminal with dimeric PKR-KD. A lack of physical interaction between these protein was explained as inconsistencies that could be due to the high off rate for this interaction [13]. Our in vitro data on E3 N-terminal and dimeric PKR-KD had similar annotations as the previous study. Surprisingly, when both N- and C-terminals of E3 were added in an equal molar ratio and used for in vitro kinase assay, no inhibition of eIF2α phosphorylation was observed for monomeric and dimeric PKR-KD (Fig. 6.14). The E3 N protein individually had inhibited the activity of GST-PKR-KD but remarkably this was not observed in case of the protein mixture. An explanation for this phenomenon could be that E3 C protein binds to E3 N in the protein mixture which makes the binding surface of E3 N interacting with dimeric PKR-KD inaccessible. This leads to no inhibition of GST-PKR-KD activity by E3 N as observed earlier. An in vitro interaction assay of E3N and E3C showed a possible protein-protein interaction between these proteins (Fig. 6.15). It was deduced from these results that both the N and C-terminals of E3 protein are required for interacting and inhibiting PKR-KD as mentioned in previous studies [13, 75].

The double mutants of E3 (E3R131AI110A, E3R131AF159A) had a strong inhibitory effect on the activity of monomeric and dimeric PKR-KD (Fig. 6.17, 6.20). The inhibition was observed more in case of dimeric as compared to monomeric PKR-KD. E3[R131AI110A] protein had the maximum impact on PKR-KD activity as compared to single mutants and other constructs of E3 used in various in vitro kinase assays. This strong inhibition by E3 double mutants could be explained by suggesting that the double mutations

on E3 protein could structural alter the protein to enhance its binding ability to PKR-KD proteins as compared to other E3 constructs.

It has always been suggested that PKR and E3 interact with each other with the aid of their dsRNA binding domains. In this study, we demonstrated that E3 mutants that have completely lost the ability to bind to dsRNA could interact with the catalytic domain of PKR and inhibit its' activity. An in vitro kinase assay was developed to detect the effect of E3 mutants on autophosphorylation of PKR-KD and phosphorylation of eIF2α. The consistencies and reproducibility of these assays validate the robustness of these assays. Overall, this in vitro study was the first time to demonstrate the novel mechanisms of E3 inhibition of PKR-KD.

8.2. Recommendations for future work

Optimization of the crystallization screening with E3 double mutant (E3R131A/I110A) is an important effort required for solving the structure of E3 by x-ray crystallography. Obtaining crystals that would undergo diffraction when exposed to x-rays requires multiple optimization steps. It is important to optimize at every step of the process. Along with the E3[R131A/I110A] protein, other combinations of mutations could be tested for a stable E3 protein which could also be used for crystallization. This would increase the chances of obtaining an E3 protein crystal for structural analysis. An effort to obtain crystals of the PKR-KD and E3 complex was also made in this study. It was predicted that the E3 proteins would make a stable complex with PKR-KD. The weak interactions between the two proteins became the main deterrent of crystal formation. An artificial linker between the two proteins could possibly solve this problem. Glycine-rich linkers have been proven useful for

these types of unstable interactions, particularly where the interaction is weak and transient, by creating a covalent link between the proteins to form a stable protein–protein complex [90]. MHC class II molecules along with their antigenic peptides is an example of a protein-protein interaction that was stabilized by these artificial linkers [90]. Following this method and solving the structure of the complex could explain the interactions between E3 and PKR protein in depth. This would also explain the interaction between E3 and dimeric PKR-KD and thus the mechanism of the E3 inhibiting the dimeric PKR-KD activity.

VACV inhibits the immune response of a host cell by producing two critical host range proteins E3 and K3 early in the viral replication. The mechanism of inhibition of immune response is different in case of both the proteins. E3 binds to catalytic domain of PKR and inhibit the dimerization activation whereas K3 proteins have a limited sequence similarity to the N-terminal domain of eIF2α and are considered a pseudo-substrate for PKR proteins. A number of studies have shown that K3 inhibits phosphorylation of eIF2α by PKR both in-vitro and in-vivo [72, 86, 91]. A crystal structure of K3 protein have shown a direct interaction between the C-terminal of PKR and the region of interaction is an equivalent PKR recognition motif shared with eIF2α [86]. Binding assays with ^{35}S labeled E3 and K3 proteins with PKR have suggested that E3 binds to catalytic domain of PKR that is same or overlaps with the K3/eIF2α binding site [75]. These results could be further verified by performing competitive assays with E3, K3 and PKR-KD proteins. Structural analysis of E3 and PKR complex would shed some light on the exact nature of interaction between the two proteins and would also provide information regarding the competitiveness for binding to a similar motif on PKR as K3/eIF2α proteins. Structural analysis is of the utmost importance

for generating a complete picture on E3 protein and this study has provided a solid base which would further the research on E3 towards its ultimate goal.

REFERENCES

1. Moss, B., Vaccinia Virus: A Tool for Research and Development. Science, 1991. 252(5013): p. 1662.
2. Whitley, R.J., Smallpox: a potential agent of bioterrorism. Antiviral Research, 2003. 57(1): p. 7-12.
3. Henderson, D.A., and Moss, B. , Recombinant Vaccinia Virus Vaccines. In Vaccines (Plotkin, S. A., and Orenstein, W. A., Eds.), 1999. 3rd edition ed., Saunders, Philadelphia.
4. Cooney, E.L., et al., Safety of and immunological response to a recombinant vaccinia virus vaccine expressing HIV envelope glycoprotein. The Lancet, 1991. 337(8741): p. 567-572.
5. Graham, B.S., et al., Vaccination of vaccinia-naive adults with human immunodeficiency virus type 1 gp160 recombinant vaccinia virus in a blinded, controlled, randomized clinical trial. The AIDS Vaccine Clinical Trials Network. The Journal of infectious diseases, 1992. 166(2): p. 244.
6. Chang, H.W., J.C. Watson, and B.L. Jacobs, The E3L gene of vaccinia virus encodes an inhibitor of the interferon-induced, double-stranded RNA-dependent protein kinase. Proceedings of the National Academy of Sciences of the United States of America, 1992. 89(11): p. 4825.
7. Yang-Gyun, K., et al., A role for Z-DNA binding in vaccinia virus pathogenesis. Proceedings of the National Academy of Sciences of the United States of America, 2003. 100(12): p. 6974.
8. Werden, S.J., M.M. Rahman, and G. McFadden, Poxvirus host range genes. Adv Virus Res, 2008. 71: p. 135-71.
9. Watson, J.C., H.-W. Chang, and B.L. Jacobs, Characterization of a vaccinia virus-encoded double-stranded RNA-binding protein that may be involved in inhibition of the double-stranded rna-dependent protein kinase. Virology, 1991. 185(1): p. 206-216.
10. Perdiguero, B. and M. Esteban, The Interferon System and Vaccinia Virus Evasion Mechanisms. Journal of Interferon & Cytokine Research, 2009. 29(9): p. 581-598.
11. Katze, M.G., Regulation of the interferon-induced PKR: can viruses cope? Trends in Microbiology, 1995. 3(2): p. 75-78.
12. Samuel, C.E., et al., The PKR protein kinase--an interferon-inducible regulator of cell growth and differentiation. Int J Hematol, 1997. 65(3): p. 227-37.
13. Romano, P.R., et al., Inhibition of Double-Stranded RNA-Dependent Protein Kinase PKR by Vaccinia Virus E3: Role of Complex Formation and the E3 N-Terminal Domain. Molecular and Cellular Biology, 1998. 18(12): p. 7304.

14. Dueck, K.J., et al., Mutational Analysis of Vaccinia Virus E3 Protein: the Biological Functions Do Not Correlate with Its Biochemical Capacity To Bind Double-Stranded RNA. Journal of Virology, 2015. 89(10): p. 5382.
15. Xiang, Y., et al., Blockade of Interferon Induction and Action by the E3L Double-Stranded RNA Binding Proteins of Vaccinia Virus. The Journal of Virology, 2002. 76(10): p. 5251.
16. Ho, C.K. and S. Shuman, Physical and Functional Characterization of the Double-Stranded RNA Binding Protein Encoded by the Vaccinia Virus E3 Gene. Virology, 1996. 217(1): p. 272-284.
17. Zachary, A.B. and B.V.V. Prasad, X-ray structure of NS1 from a highly pathogenic H5N1 influenza virus. Nature, 2008. 456(7224): p. 985.
18. Hoffmann, E. and R. Webster, Lethal H5N1 influenza viruses escape host anti-viral cytokine responses. Nature Medicine, 2002. 8(9): p. 950-4.
19. Condit, R.C., N. Moussatche, and P. Traktman, In a nutshell: structure and assembly of the vaccinia virion. Adv Virus Res, 2006. 66: p. 31-124.
20. Moss, B., Poxviridae: the viruses and their replication. 2001. 2906-2945.
21. Seet, B.T., et al., Poxviruses and immune evasion. Annu Rev Immunol, 2003. 21: p. 377-423.
22. Koehler, H., et al., Inhibition of DAI-dependent necroptosis by the Z-DNA binding domain of the vaccinia virus innate immune evasion protein, E3. Proc Natl Acad Sci U S A, 2017. 114(43): p. 11506-11511.
23. Myskiw, C., et al., Comparative Analysis of Poxvirus Orthologues of the Vaccinia Virus E3 Protein: Modulation of Protein Kinase R Activity, Cytokine Responses, and Virus Pathogenicity. Journal of Virology, 2011. 85(23): p. 12280.
24. Chang, H.W., L.H. Uribe, and B.L. Jacobs, Rescue of vaccinia virus lacking the E3L gene by mutants of E3L. The Journal of Virology, 1995. 69(10): p. 6605.
25. Deng, L., et al., Vaccinia Virus Infection Attenuates Innate Immune Responses and Antigen Presentation by Epidermal Dendritic Cells. The Journal of Virology, 2006. 80(20): p. 9977.
26. García, M., et al., Anti-apoptotic and oncogenic properties of the dsRNA-binding protein of vaccinia virus, E3L. Oncogene, 2002. 21(55): p. 8379-87.
27. Chang, H.-W. and B.L. Jacobs, Identification of a Conserved Motif That Is Necessary for Binding of the Vaccinia Virus E3L Gene Products to Double-Stranded RNA. Virology, 1993. 194(2): p. 537-547.
28. Brandt, T.A. and B.L. Jacobs, Both Carboxy- and Amino-Terminal Domains of the Vaccinia Virus Interferon Resistance Gene, E3L, Are Required for Pathogenesis in a Mouse Model. The Journal of Virology, 2001. 75(2): p. 850.
29. Beattie, E., et al., Reversal of the interferon-sensitive phenotype of a vaccinia virus lacking E3L by expression of the reovirus S4 gene. The Journal of Virology, 1995. 69(1): p. 499.
30. Brandt, T., et al., The N-terminal domain of the vaccinia virus E3L-protein is required for neurovirulence, but not induction of a protective immune response. Virology, 2005. 333(2): p. 263-270.

31. White, S.D. and B.L. Jacobs, The Amino Terminus of the Vaccinia Virus E3 Protein Is Necessary To Inhibit the Interferon Response. Journal of Virology, 2012. 86(10): p. 5895.
32. Thakur, M., E.J. Seo, and T.E. Dever, Variola virus E3L Zα domain, but not its Z-DNA binding activity, is required for PKR inhibition. RNA (New York, N.Y.), 2014. 20(2): p. 214.
33. Ha, S. and N. Lokanath, A poxvirus protein forms a complex with left-handed Z-DNA: Crystal structure of a Yatapoxvirus Zalpha bound to DNA. Proceedings of the National Academy of Sciences of the United States of America, 2004. 101(40): p. 14367-14372.
34. Myskiw, C., et al., Vaccinia Virus E3 Suppresses Expression of Diverse Cytokines through Inhibition of the PKR, NF-{kappa}B, and IRF3 Pathways. The Journal of Virology, 2009. 83(13): p. 6757.
35. Shors, T., et al., Complementation of Vaccinia Virus Deleted of the E3L Gene by Mutants of E3L. Virology, 1997. 239(2): p. 269-276.
36. Rivas, C., et al., Vaccinia Virus E3L Protein Is an Inhibitor of the Interferon (IFN)-Induced 2-5A Synthetase Enzyme. Virology, 1998. 243(2): p. 406-414.
37. Stark, G.R., et al., HOW CELLS RESPOND TO INTERFERONS. Annual Review of Biochemistry, 1998. 67(1): p. 227-264.
38. Colby, C. and M.J. Chamberlin, The specificity of interferon induction in chick embryo cells by helical RNA. Proceedings of the National Academy of Sciences of the United States of America, 1969. 63(1): p. 160.
39. Jacobs, B.L. and J.O. Langland, When two strands are better than one: the mediators and modulators of the cellular responses to double-stranded RNA. Virology, 1996. 219(2): p. 339.
40. Nanduri, S., et al., Structure of the double-stranded RNA-binding domain of the protein kinase PKR reveals the molecular basis of its dsRNA-mediated activation. EMBO Journal, 1998. 17(18): p. 5458-5465.
41. Garcia, M.A., et al., Impact of Protein Kinase PKR in Cell Biology: from Antiviral to Antiproliferative Action. Microbiology and Molecular Biology Reviews, 2006. 70(4): p. 1032.
42. Pindel, A. and A. Sadler, The Role of Protein Kinase R in the Interferon Response. Journal of Interferon & Cytokine Research, 2011. 31(1): p. 59-70.
43. Lu, B., et al., Novel role of PKR in inflammasome activation and HMGB1 release. Nature, 2014. 488(7413).
44. Feng, G.S., et al., Identification of double-stranded RNA-binding domains in the interferon-induced double-stranded RNA-activated p68 kinase. Proceedings of the National Academy of Sciences of the United States of America, 1992. 89(12): p. 5447.
45. Dar, A.C., T.E. Dever, and F. Sicheri, Higher-Order Substrate Recognition of eIF2α by the RNA-Dependent Protein Kinase PKR. Cell, 2005. 122(6): p. 887-900.
46. Nolen, B., S. Taylor, and G. Ghosh, Regulation of Protein Kinases: Controlling Activity through Activation Segment Conformation: Controlling Activity through Activation Segment Conformation. Molecular Cell, 2004. 15(5): p. 661-675.
47. Johnson, L.N., M.E. Noble, and D.J. Owen, Active and inactive protein kinases: structural basis for regulation. Cell, 1996. 85(2): p. 149.

48. Kimball, S.R., Eukaryotic initiation factor eIF2. International Journal of Biochemistry and Cell Biology, 1999. 31(1): p. 25-29.
49. Hinnebusch, A.G., Mechanism and regulation of initiator methionyl-tRNA binding to ribosomes. 2000. 185-244.
50. Chakrabarti, A. and U. Maitra, Release and recycling of eukaryotic initiation factor 2 in the formation of an 80 S ribosomal polypeptide chain initiation complex. The Journal of biological chemistry, 1992. 267(18): p. 12964.
51. Lapointe, J. and L. Brakier-Gingras, Translation mechanisms. 2003, Georgetown, Tex. : New York: Georgetown, Tex. : Eurekah.com : Landes Bioscience, New York : Kluwer Academic/Plenum Publishers.
52. Bommer, U.A., et al., Amino acid sequence analysis of the beta - and gamma - subunits of eukaryotic initiation factor eIF-2. Identification of regions interacting with GTP. Biochimica et Biophysica Acta: Protein Structure and Molecular Enzymology, 1991. 1079(3): p. 308-315.
53. Dhaliwal, S. and D.W. Hoffman, The Crystal Structure of the N-terminal Region of the Alpha Subunit of Translation Initiation Factor 2 (eIF2α) from Saccharomyces cerevisiae Provides a View of the Loop Containing Serine 51, the Target of the eIF2α-specific Kinases. Journal of Molecular Biology, 2003. 334(2): p. 187-195.
54. Chen, J.J., Heme-regulated eIF2α kinase. 2000. 529-546.
55. Kaufman, R., Double-stranded RNA-activated protein kinase PKR. 2000. 503-528.
56. Dever, T.E., et al., Phosphorylation of initiation factor 2α by protein kinase GCN2 mediates gene-specific translational control of GCN4 in yeast. Cell, 1992. 68(3): p. 585-596.
57. Hinnebusch, A.G. and K. Natarajan, Gcn4p, a Master Regulator of Gene Expression, Is Controlled at Multiple Levels by Diverse Signals of Starvation and Stress. Eukaryotic Cell, 2002. 1(1): p. 22.
58. Ron, D. and H. Harding, "PERK and translational control by stress in the endoplasmic reticulum. 2000.
59. Nonato, M.C., J. Widom, and J. Clardy, Crystal structure of the N-terminal segment of human eukaryotic translation initiation factor 2alpha. The Journal of biological chemistry, 2002. 277(19): p. 17057.
60. Murzin, A.G., OB(oligonucleotide/oligosaccharide binding)-fold: common structural and functional solution for non-homologous sequences. The EMBO journal, 1993. 12(3): p. 861.
61. Vattem, K.M., K.A. Staschke, and R.C. Wek, Mechanism of activation of the double-stranded-RNA-dependent protein kinase, PKR: role of dimerization and cellular localization in the stimulation of PKR phosphorylation of eukaryotic initiation factor-2 (eIF2). European journal of biochemistry, 2001. 268(13): p. 3674.
62. Nanduri, S., et al., A dynamically tuned double-stranded RNA binding mechanism for the activation of antiviral kinase PKR. EMBO Journal, 2000. 19(20): p. 5567-5574.
63. Wu, S. and R.J. Kaufman, A model for the double-stranded RNA (dsRNA)-dependent dimerization and activation of the dsRNA-activated protein kinase PKR. The Journal of biological chemistry, 1997. 272(2): p. 1291.
64. Shoudong, L., et al., Molecular basis for PKR activation by PACT or dsRNA. Proceedings of the National Academy of Sciences, 2006. 103(26): p. 10005.

65. Ortega, L.G., et al., Mechanism of Interferon Action: Biochemical and Genetic Evidence for the Intermolecular Association of the RNA-Dependent Protein Kinase PKR from Human Cells: Biochemical and Genetic Evidence for the Intermolecular Association of the RNA-Dependent Protein Kinase PKR from Human Cells. Virology, 1996. 215(1): p. 31-39.
66. Wu, Kaufman, and J. R, Double-stranded (ds) RNA binding and not dimerization correlates with the activation of the dsRNA-dependent protein kinase (PKR). The Journal of biological chemistry, 1996. Vol.271(3): p. pp.1756-1763.
67. Tan, S.-L., M.J. Gale, Jr., and M.G. Katze, Double-Stranded RNA-Independent Dimerization of Interferon-Induced Protein Kinase PKR and Inhibition of Dimerization by the Cellular P58IPK Inhibitor. Molecular and Cellular Biology, 1998. 18(5): p. 2431.
68. Dey, M., et al., Mechanistic Link between PKR Dimerization, Autophosphorylation, and eIF2α Substrate Recognition. Cell, 2005. 122(6): p. 901-913.
69. Sadler, A.J. and B.R.G. Williams, Structure and function of the protein kinase R. Current Topics in Microbiology and Immunology, 2007. 316: p. 253-292.
70. Webb, B.L. and C.G. Proud, Eukaryotic initiation factor 2B (eIF2B). Int J Biochem Cell Biol, 1997. 29(10): p. 1127-31.
71. Dever, T.E., Gene-Specific Regulation by General Translation Factors. Cell, 2002. 108(4): p. 545-556.
72. Davies, M.V., et al., The E3L and K3L vaccinia virus gene products stimulate translation through inhibition of the double-stranded RNA-dependent protein kinase by different mechanisms. The Journal of Virology, 1993. 67(3): p. 1688.
73. Jagus, R. and M.M. Gray, Proteins that interact with PKR. Biochimie, 1994. 76(8): p. 779-791.
74. Whitaker-Dowling, P. and J.S. Youngner, Characterization of a specific kinase inhibitory factor produced by vaccinia virus which inhibits the interferon-induced protein kinase. Virology, 1984. 137(1): p. 171-181.
75. Sharp, T.V., et al., The Vaccinia Virus E3L Gene Product Interacts with both the Regulatory and the Substrate Binding Regions of PKR: Implications for PKR Autoregulation. Virology, 1998. 250(2): p. 302-315.
76. George, C.X., et al., Characterization of the Heparin-Mediated Activation of PKR, the Interferon-Inducible RNA-Dependent Protein Kinase. Virology, 1996. 221(1): p. 180-188.
77. Studier, F.W. and B.A. Moffatt, Use of bacteriophage T7 RNA polymerase to direct selective high-level expression of cloned genes. Journal of Molecular Biology, 1986. 189(1): p. 113-130.
78. Huynh, K. and C.L. Partch, Analysis of protein stability and ligand interactions by thermal shift assay. Current protocols in protein science, 2015. 79: p. 28.9.1-28.9.14.
79. Frank, H.N., B. Helena, and V. Masoud, The use of differential scanning fluorimetry to detect ligand interactions that promote protein stability. Nature Protocols, 2007. 2(9): p. 2212.
80. Johnston, R.F., S.C. Pickett, and D.L. Barker, Autoradiography using storage phosphor technology. ELECTROPHORESIS, 1990. 11(5): p. 355-360.
81. Voytas, D. and N. Ke, Detection and quantitation of radiolabeled proteins and DNA in gels and blots. Curr Protoc Immunol, 2002. Appendix 3: p. Appendix 3J.

82. Dupeux, F., et al., A thermal stability assay can help to estimate the crystallization likelihood of biological samples. Acta Crystallographica Section D, 2011. 67(11): p. 915-919.
83. Ericsson, U.B., et al., Thermofluor-based high-throughput stability optimization of proteins for structural studies. Analytical biochemistry, 2006. 357(2): p. 289.
84. Masoud, V., et al., Chemical screening methods to identify ligands that promote protein stability, protein crystallization, and structure determination. Proceedings of the National Academy of Sciences, 2006. 103(43): p. 15835.
85. Romano, P.R., et al., Structural requirements for double-stranded RNA binding, dimerization, and activation of the human eIF-2 alpha kinase DAI in Saccharomyces cerevisiae. Molecular and Cellular Biology, 1995. 15(1): p. 365.
86. Dar, A.C. and F. Sicheri, X-Ray Crystal Structure and Functional Analysis of Vaccinia Virus K3L Reveals Molecular Determinants for PKR Subversion and Substrate Recognition. Molecular Cell, 2002. 10(2): p. 295-305.
87. Zhang, Y., I-TASSER server for protein 3D structure prediction. BMC Bioinformatics, 2008. 9(1): p. 40.
88. Roy, A., A. Kucukural, and Y. Zhang, I-TASSER: a unified platform for automated protein structure and function prediction. Nature protocols, 2010. 5(4): p. 725-738.
89. Yang, J., et al., The I-TASSER Suite: protein structure and function prediction. Nature methods, 2015. 12(1): p. 7-8.
90. Reddy Chichili, V.P., V. Kumar, and J. Sivaraman, Linkers in the structural biology of protein-protein interactions. Protein science : a publication of the Protein Society, 2013. 22(2): p. 153-167.
91. Davies, M.V., et al., The vaccinia virus K3L gene product potentiates translation by inhibiting double-stranded-RNA-activated protein kinase and phosphorylation of the alpha subunit of eukaryotic initiation factor 2. The Journal of Virology, 1992. 66(4): p. 1943.

APPENDICES

Table. A.1. Mass spectrometric analysis of protein bands from SDS-PAGE gels for identification of E3[R131AI110A] protein.

BAQ 1659	Mol. weigh	Fasta headers
4.91E+08	21.504	>sp|P21081.1|E3_VACCC RecName: Full=Protein E3;AltName: Full=p25;>AGJ92033.1 IFN resistance
9.31E+05	24.409	>P00761 SWISS-PROT:P00761|TRYP_PIG Trypsin - Sus scrofa (Pig).
8.99E+05	50.186	>XP_015781692.1 serine/threonine-protein kinase VRK1 [Tetranychus urticae]
2.69E+05	6.2482	>AUL80167.1 hypothetical protein [Vaccinia virus]
1.29E+05	7.4035	>NP_570533.1 ATI fragment [Camelpox virus];>ADE95829.1 A-type inclusion protein fragment [Camelpox virus],
1.27E+05	65.19	>ENSEMBL:ENSBTAP00000037665 (Bos taurus) similar to Pregnancy zone protein, partial
7.37E+04	27.032	>sp|P0ADD7|YJJQ_ECOLI Putative transcription factor YjjQ OS=Escherichia coli (strain K12) GN=yjjQ PE=1 SV=1
4.71E+04	34.401	>sp|P0A9F6|GCVA_ECOLI Glycine cleavage system transcriptional activator OS=Escherichia coli (strain K12) GN=gcvA PE=1 SV=1
4.35E+04	97.24	>CAK11941.1 putative DNA ligase family protein [Rhizobium leguminosarum bv. viciae 3841]
3.16E+04	20.761	>sp|P0AE08|AHPC_ECOLI Alkyl hydroperoxide reductase subunit C OS=Escherichia coli (strain K12) GN=ahpC PE=1 SV=2
2.78E+04	54.895	>KFM73014.1 Serine/threonine-protein kinase VRK1, partial [Stegodyphus mimosarum]
2.58E+04	61.37	>XP_010401306.2 serine/threonine-protein kinase VRK2 isoform X2 [Corvus cornix cornix]s]
2.56E+04	23.64	>sp|P0ACJ8|CRP_ECOLI cAMP-activated global transcriptional regulator CRP OS=Escherichia coli (strain K12) GN=crp PE=1 SV=1
2.25E+04	60.257	>NP_619802.1 CPXV013 protein [Cowpox virus];>AAM13460.1 CPXV013 protein [Cowpox virus]
1.73E+04	45.505	>XP_010345648.1 PREDICTED: LOW QUALITY PROTEIN: serine/threonine-protein kinase VRK1-like [Saimiri boliviensis boliviensis]
1.57E+04	19.923	>sp|P51024|YAIL_ECOLI Uncharacterized protein YaiL OS=Escherichia coli (strain K12) GN=yaiL PE=4 SV=2
1.22E+04	18.166	>AYV61213.1 putative virion protein [Lumpy skin disease virus];>AVR51517.1 putative virion protein [Lumpy skin disease virus]
8.30E+03	44.69	>sp|P75920|OPGC_ECOLI Glucans biosynthesis protein C OS=Escherichia coli (strain K12) GN=mdoC PE=1 SV=1
5.10E+03	84.854	>NP_955320.1 CNPV297 ankyrin repeat protein [Canarypox virus];>AWD84773.1 ankyrin repeat protein [Canarypox virus]
3.93E+03	44.912	>XP_007642066.1 serine/threonine-protein kinase VRK1 isoform X4 [Cricetulus griseus]
3.20E+03	37.06	>sp|P77658|YNAA_ECOLI Putative uncharacterized protein YnaA OS=Escherichia coli (strain K12) GN=ynaA PE=5 SV=1
2.38E+03	67.688	>NP_955337.1 CNPV314 ankyrin repeat protein [Canarypox virus];>AWD84790.1 ankyrin repeat protein [Canarypox virus]
6.99E+02	61.645	>PNF16722.1 hypothetical protein B7P43_G00858 [Cryptotermes secundus]
5.69E+02	139.89	>NP_042747.1 RNA polymerase subunit 2 [African swine fever virus];>AAA65283.1 RNA polymerase subunit 2 [African swine fever virus]
0.00E+00	85.045	>NP_039064.1 hypothetical protein FPV101 [Fowlpox virus];>CAE52642.1 E2L orthologue [Fowlpox virus isolate HP-438/Munich]
0.00E+00	57.742	>XP_003137260.2 CK1/VRK protein kinase [Loa loa];>EFO26803.2 CK1/VRK protein kinase [Loa loa]
0.00E+00	46.536	>KFP75997.1 Serine/threonine-protein kinase VRK1, partial [Acanthisitta chloris]
0.00E+00	56.195	>KRX64467.1 Serine/threonine-protein kinase VRK2 [Trichinella sp. T9] [Trichinella britovi]
0.00E+00	17.033	>sp|P0A6Q6|FABZ_ECOLI 3-hydroxyacyl-[acyl-carrier-protein] dehydratase FabZ OS=Escherichia coli (strain K12) GN=fabZ PE=1 SV=1
0.00E+00	12.141	>sp|P0A8U6|METJ_ECOLI Met repressor OS=Escherichia coli (strain K12) GN=metJ PE=1 SV=2

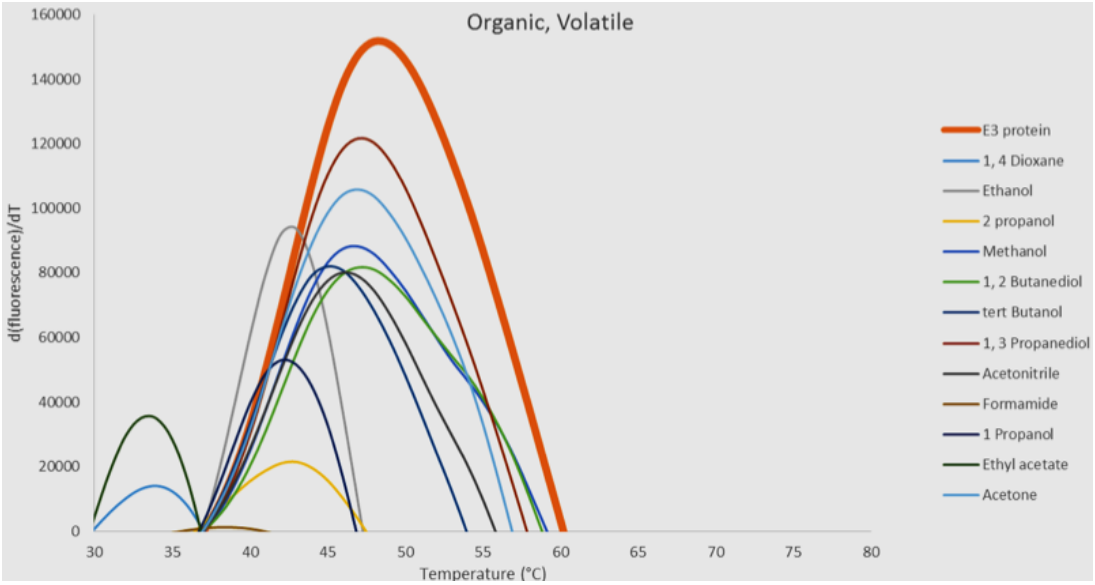

Figure A.1. Thermal shift analysis of E3 protein stability in different volatile organic solutions. The x-axis represents the increasing temperature during thermal shift assays whereas the y-axis corresponds to the first derivative of the fluorescence emission as a function of temperature (d[fluorescence]/dT). The melting temperature (T_m) is represented as the highest part of the curve. The solid red curve represents the T_m of E3[R131A] protein without any additives.

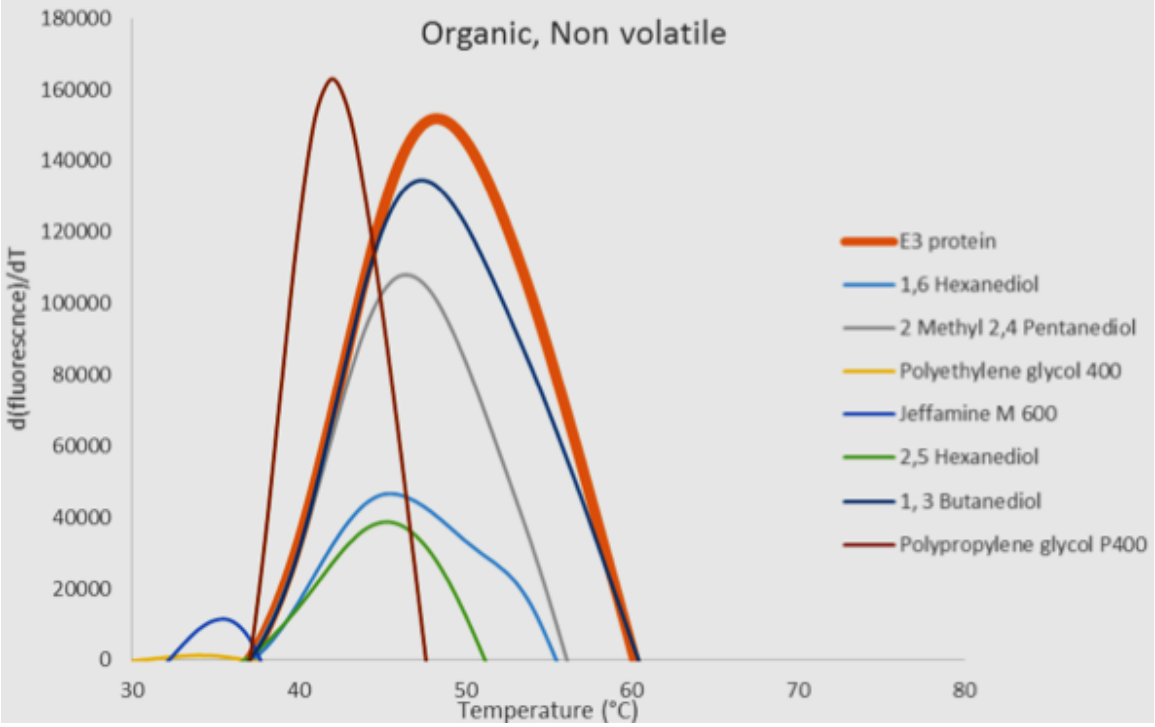

Figure A.2. Thermal shift analysis of E3 protein stability in different non-volatile organic solutions. The x-axis represents the increasing temperature during thermal shift assays whereas the y-axis corresponds to the first derivative of the fluorescence emission as a function of temperature (d[fluorescence]/dT). The melting temperature (T_m) is represented as the highest part of the curve. The solid red curve represents the T_m of E3[R131A] protein without any additives.

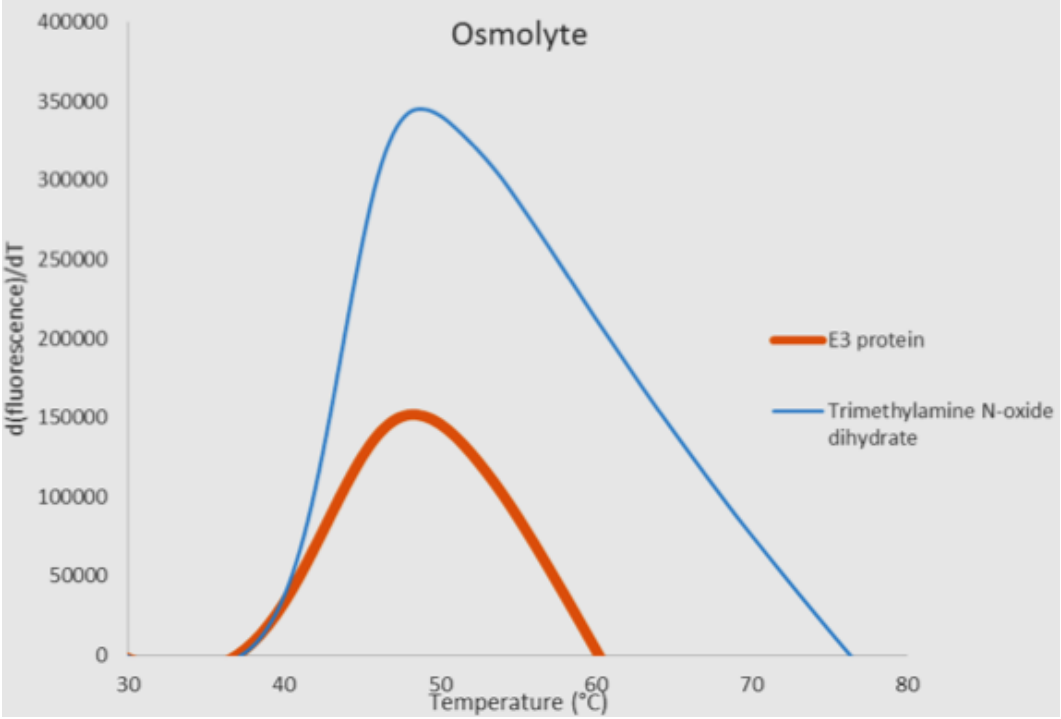

Figure A.3. Thermal shift analysis of E3 protein stability in an osmolyte (Trimethylamine N-oxide dihydrate) solution. The x-axis represents the increasing temperature during thermal shift assays whereas the y-axis corresponds to the first derivative of the fluorescence emission as a function of temperature (d[fluorescence]/dT). The melting temperature (T_m) is represented as the highest part of the curve. The solid red curve represents the T_m of E3[R131A] protein without any additives.

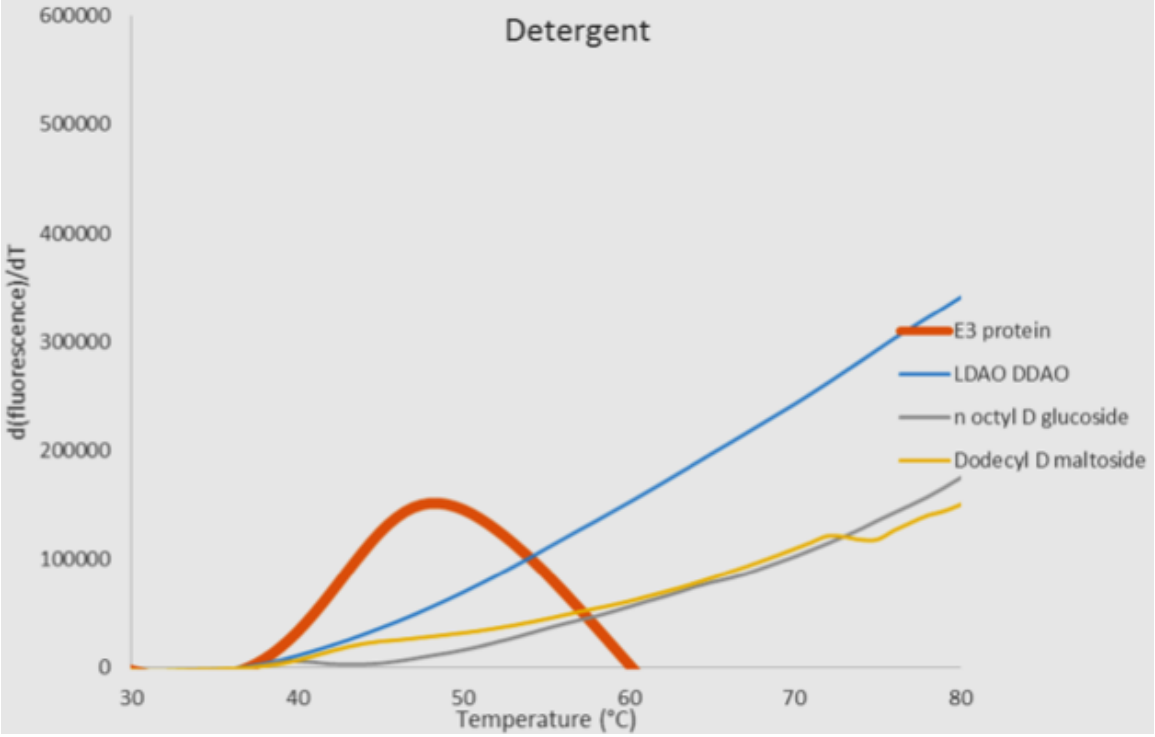

Figure A.4. Thermal shift analysis of E3 protein stability in detergents. The x-axis represents the increasing temperature during thermal shift assays whereas the y-axis corresponds to the first derivative of the fluorescence emission as a function of temperature (d[fluorescence]/dT). The melting temperature (T_m) is represented as the highest part of the curve. The solid red curve represents the T_m of E3[R131A] protein without any additives.

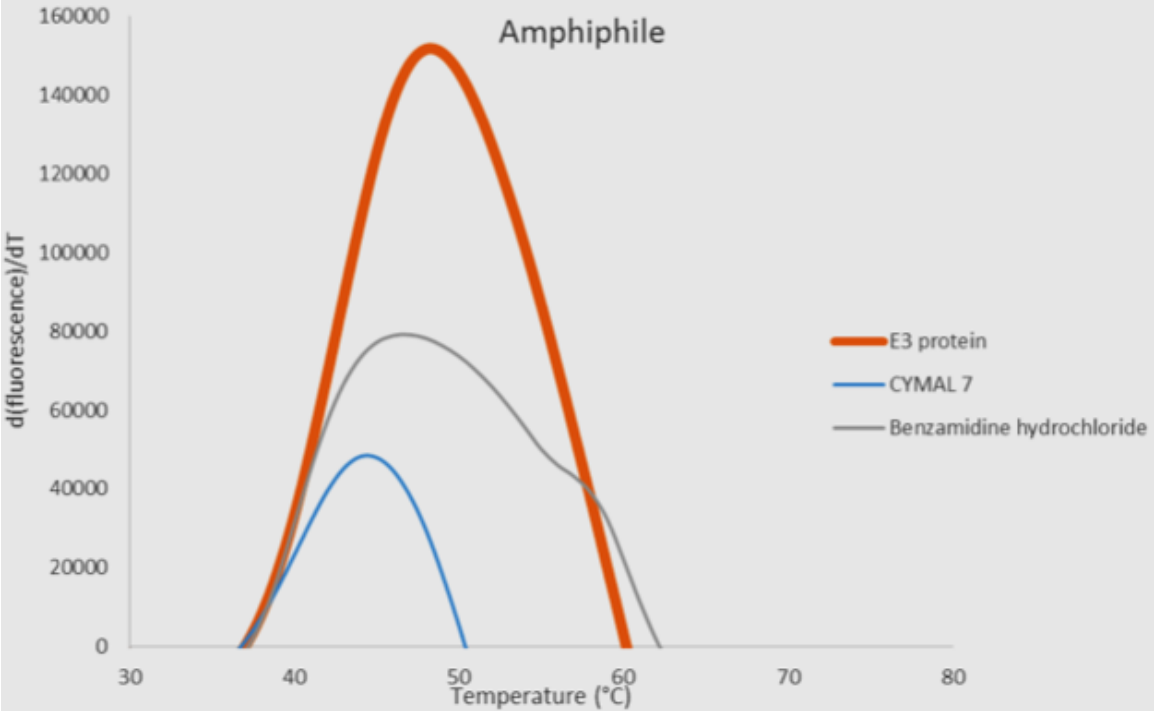

Figure A.5. Thermal shift analysis of E3 protein stability with amphiphiles. The x-axis represents the increasing temperature during thermal shift assays whereas the y-axis corresponds to the first derivative of the fluorescence emission as a function of temperature (d[fluorescence]/dT). The melting temperature (T_m) is represented as the highest part of the curve. The solid red curve represents the T_m of E3[R131A] protein without any additives.

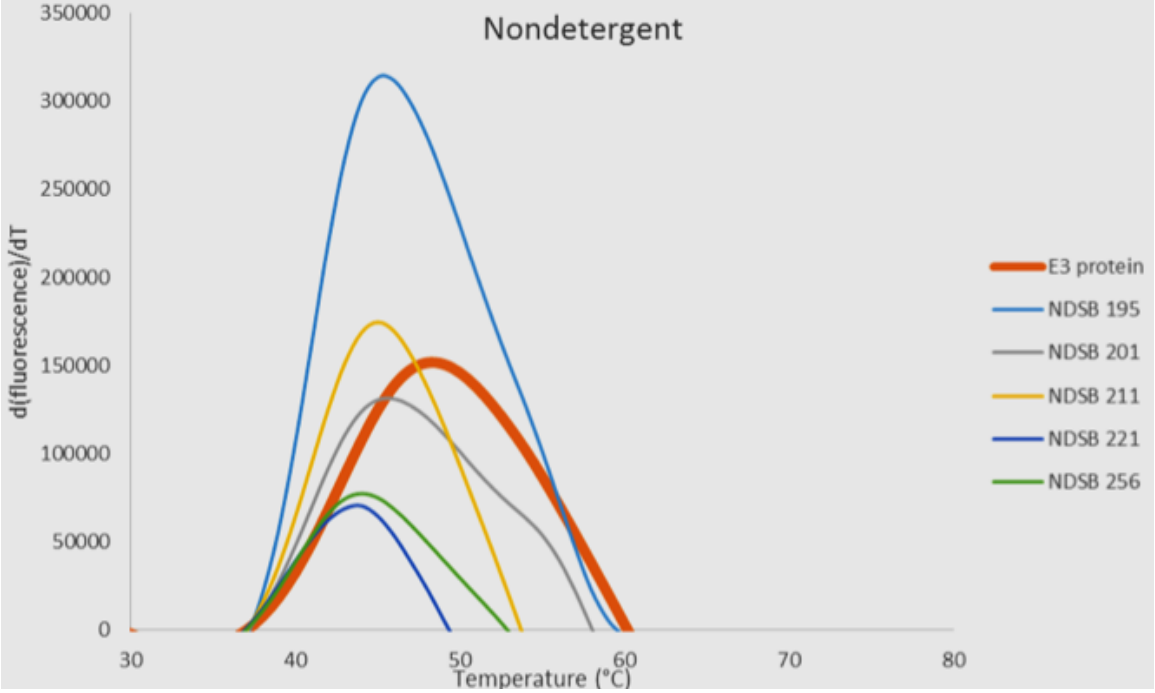

Figure A.6. Thermal shift analysis of E3 protein stability with nondetergent solutions. The x-axis represents the increasing temperature during thermal shift assays whereas the y-axis corresponds to the first derivative of the fluorescence emission as a function of temperature (d[fluorescence]/dT). The melting temperature (T_m) is represented as the highest part of the curve. The solid red curve represents the T_m of E3[R131A] protein without any additives.

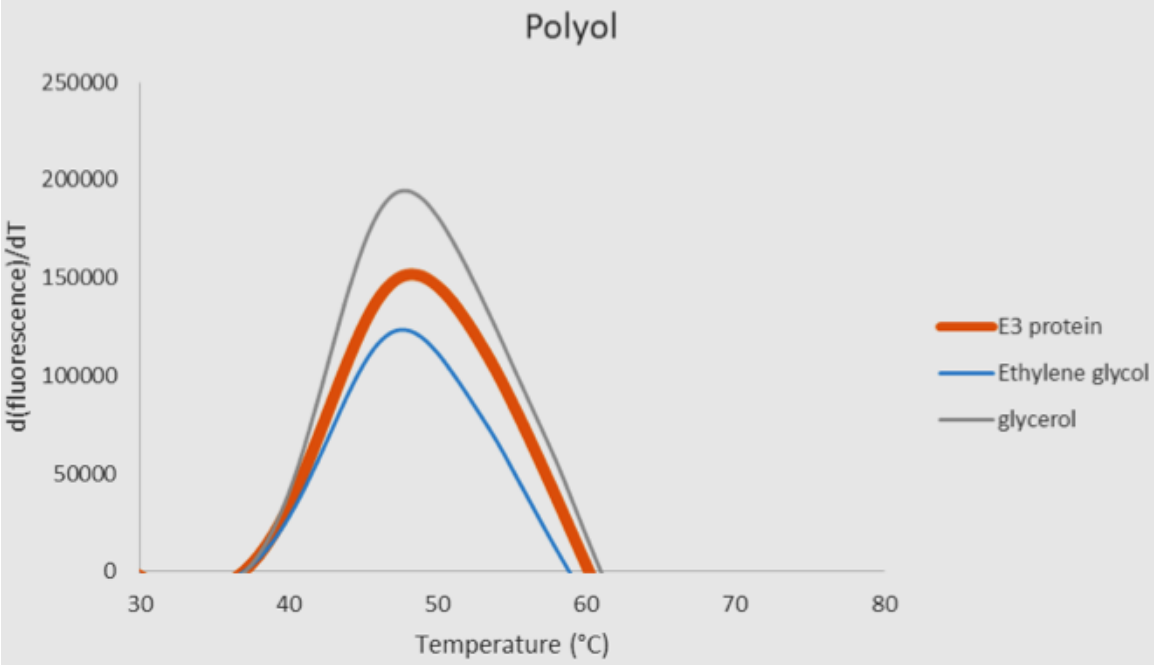

Figure A.7. Thermal shift analysis of E3 protein stability with polyols. The x-axis represents the increasing temperature during thermal shift assays whereas the y-axis corresponds to the first derivative of the fluorescence emission as a function of temperature (d[fluorescence]/dT). The melting temperature (T_m) is represented as the highest part of the curve. The solid red curve represents the T_m of E3[R131A] protein without any additives.

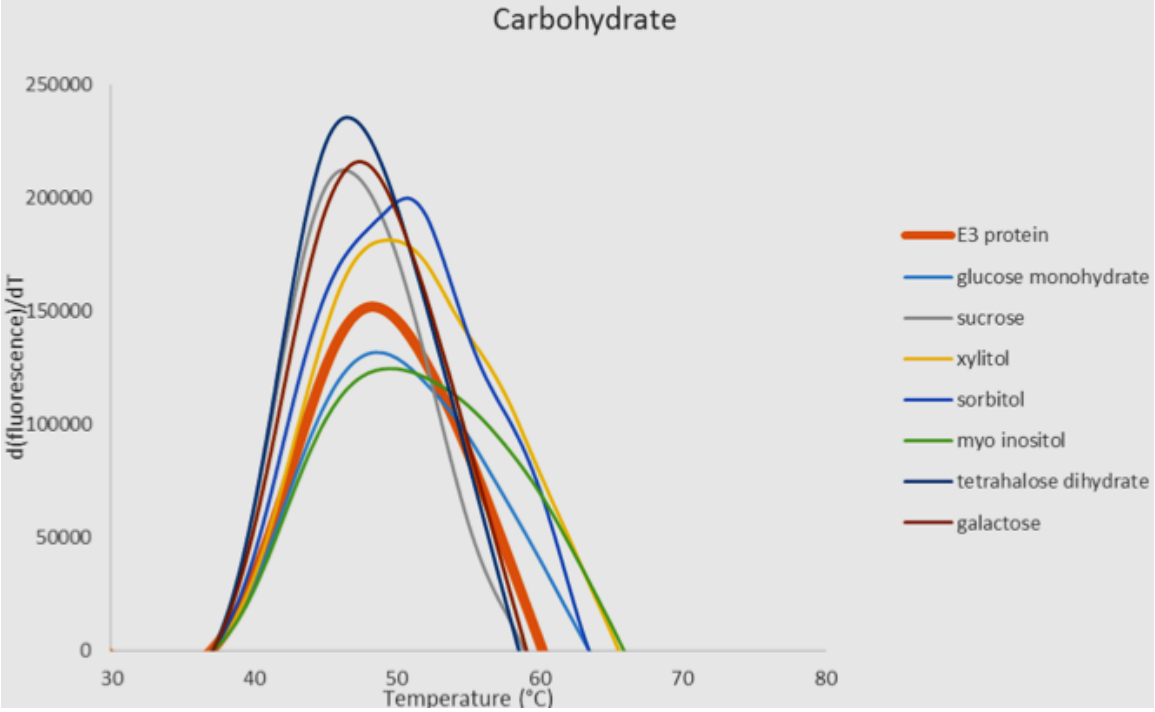

Figure A.8. Thermal shift analysis of E3 protein stability with carbohydrates. The x-axis represents the increasing temperature during thermal shift assays whereas the y-axis corresponds to the first derivative of the fluorescence emission as a function of temperature (d[fluorescence]/dT). The melting temperature (T_m) is represented as the highest part of the curve. The solid red curve represents the T_m of E3[R131A] protein without any additives.

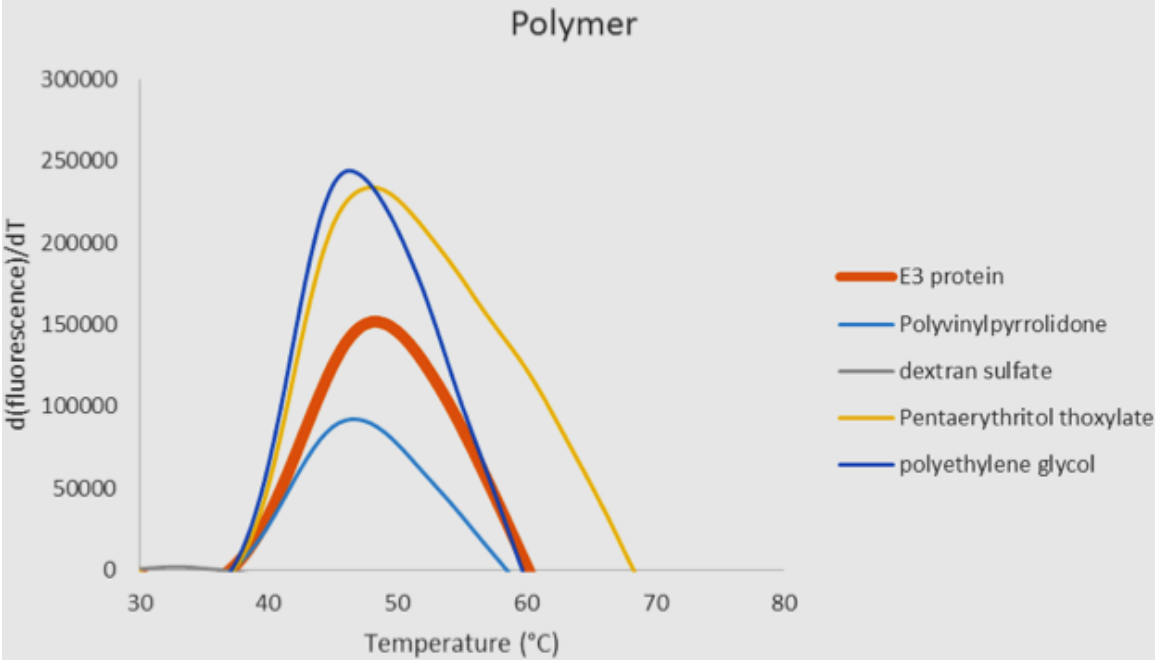

Figure A.9. Thermal shift analysis of E3 protein stability with polymers. The x-axis represents the increasing temperature during thermal shift assays whereas the y-axis corresponds to the first derivative of the fluorescence emission as a function of temperature (d[fluorescence]/dT). The melting temperature (T_m) is represented as the highest part of the curve. The solid red curve represents the T_m of E3[R131A] protein without any additives.

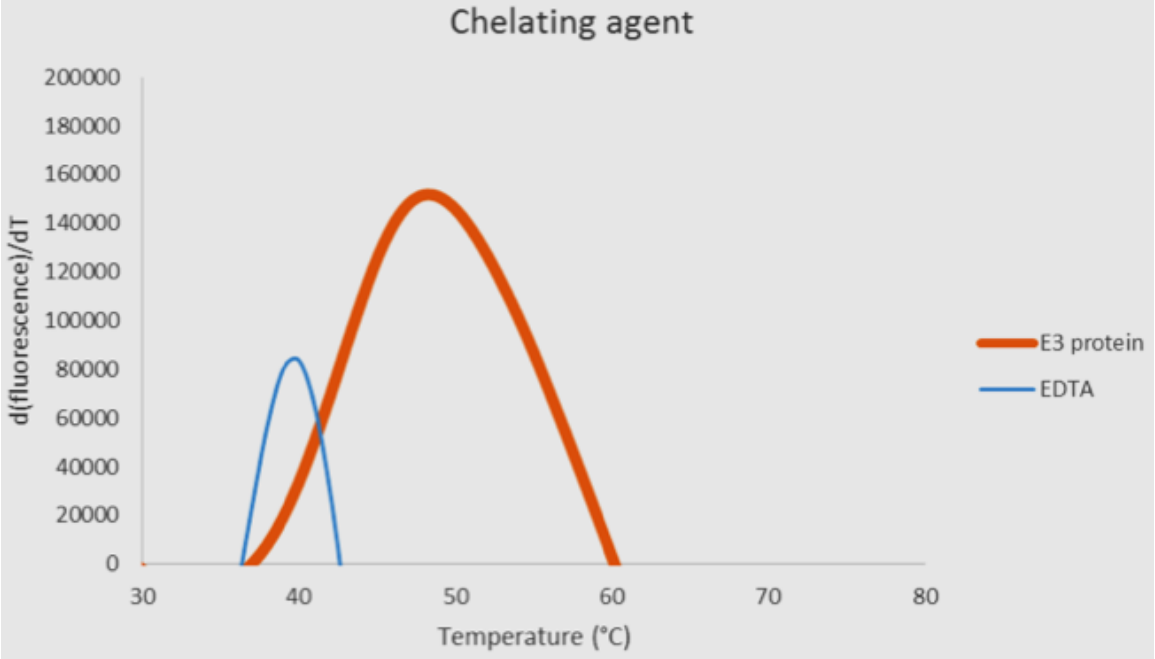

Figure A.10. Thermal shift analysis of E3 protein stability with a chelating agent (EDTA). The x-axis represents the increasing temperature during thermal shift assays whereas the y-axis corresponds to the first derivative of the fluorescence emission as a function of temperature (d[fluorescence]/dT). The melting temperature (T_m) is represented as the highest part of the curve. The solid red curve represents the T_m of E3[R131A] protein without any additives.

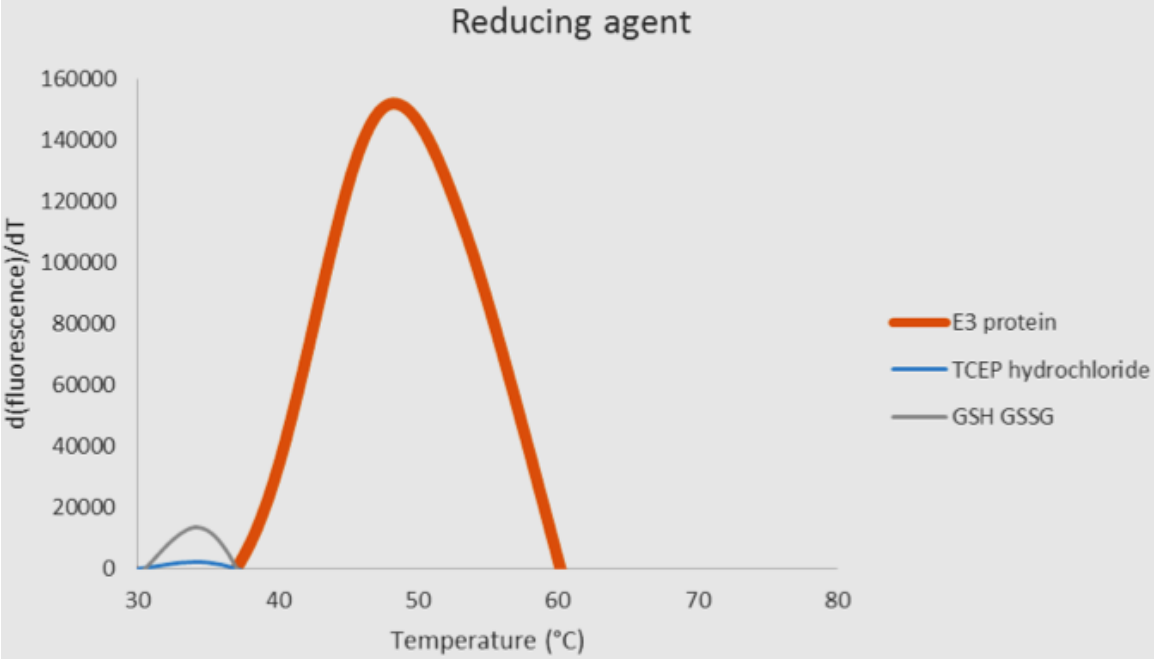

Figure A.11. Thermal shift analysis of E3 protein stability with reducing agents. The x-axis represents the increasing temperature during thermal shift assays whereas the y-axis corresponds to the first derivative of the fluorescence emission as a function of temperature (d[fluorescence]/dT). The melting temperature (T_m) is represented as the highest part of the curve. The solid red curve represents the T_m of E3[R131A] protein without any additives.

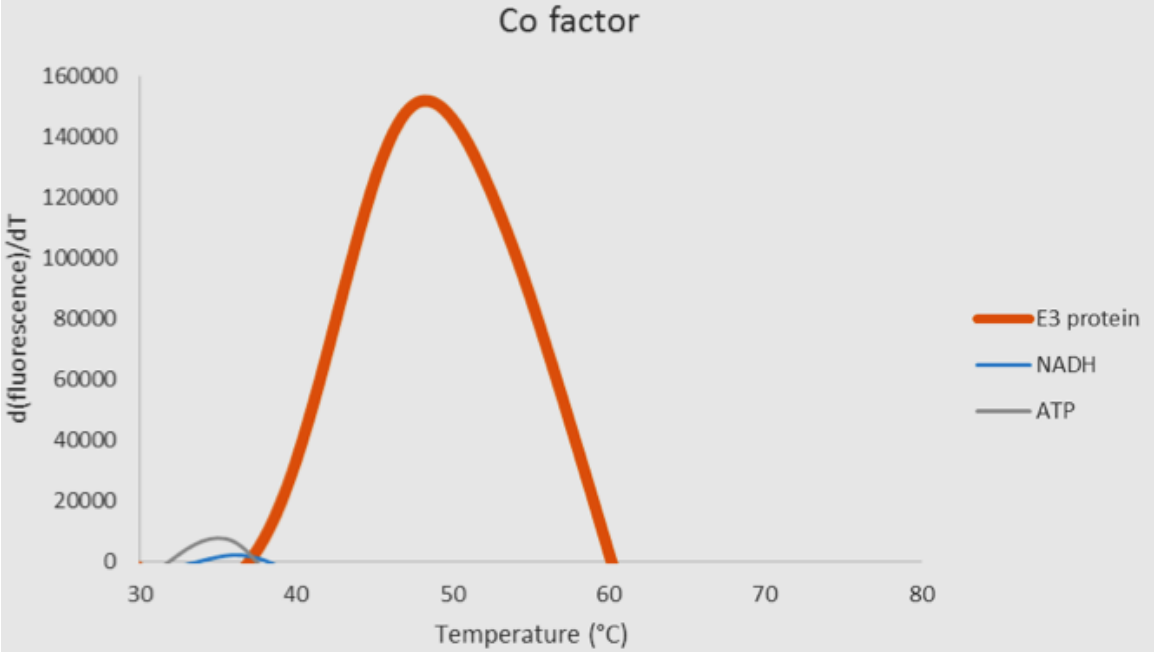

Figure A.12. Thermal shift analysis of E3 protein stability with co-factors (NADH and ATP). The x-axis represents the increasing temperature during thermal shift assays whereas the y-axis corresponds to the first derivative of the fluorescence emission as a function of temperature (d[fluorescence]/dT). The melting temperature (T_m) is represented as the highest part of the curve. The solid red curve represents the T_m of E3[R131A] protein without any additives.

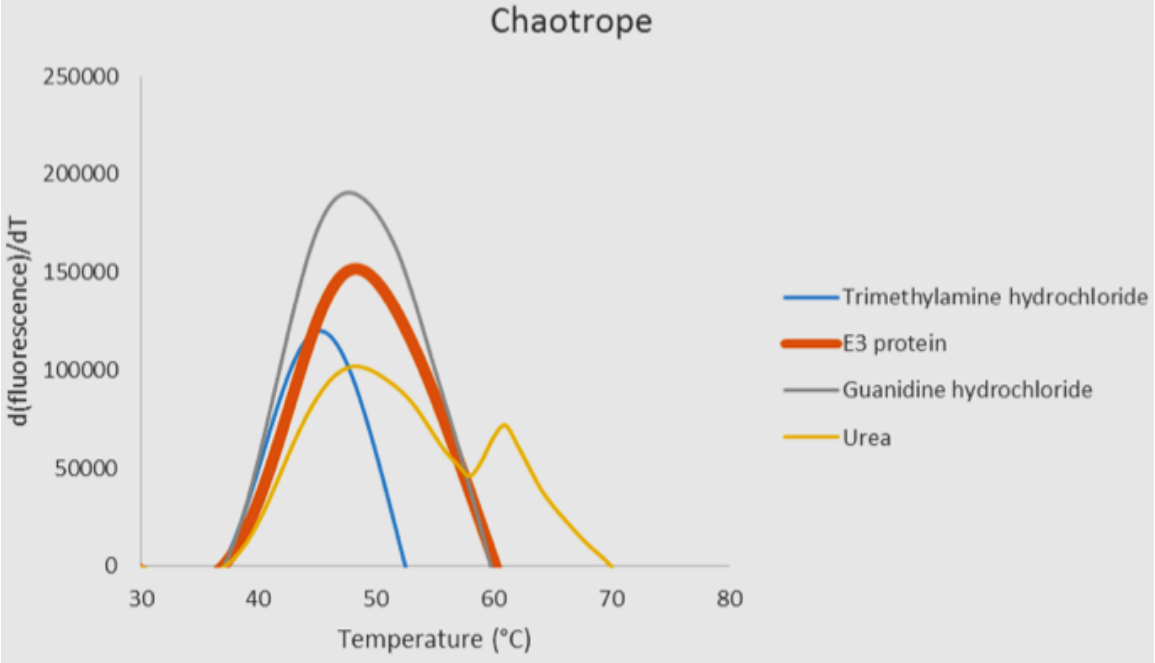

Figure A.13. Thermal shift analysis of E3 protein stability with chaotropes. The x-axis represents the increasing temperature during thermal shift assays whereas the y-axis corresponds to the first derivative of the fluorescence emission as a function of temperature (d[fluorescence]/dT). The melting temperature (T_m) is represented as the highest part of the curve. The solid red curve represents the T_m of E3[R131A] protein without any additives.

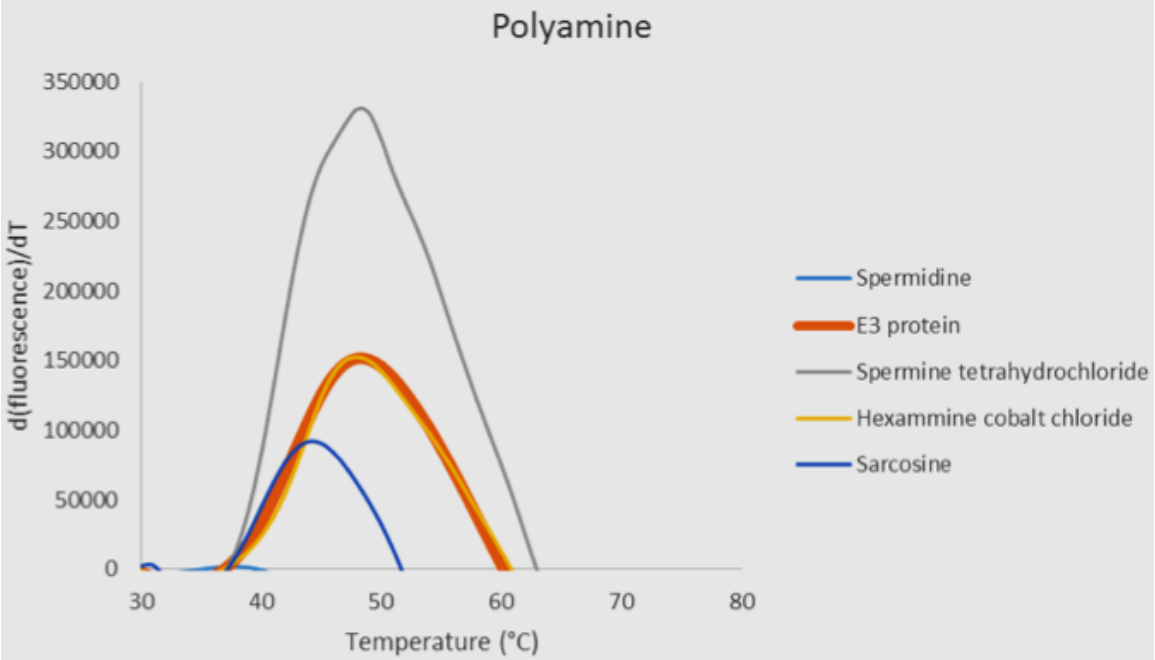

Figure A.14. Thermal shift analysis of E3 protein stability with polyamines. The x-axis represents the increasing temperature during thermal shift assays whereas the y-axis corresponds to the first derivative of the fluorescence emission as a function of temperature (d[fluorescence]/dT). The melting temperature (T_m) is represented as the highest part of the curve. The solid red curve represents the T_m of E3[R131A] protein without any additives.

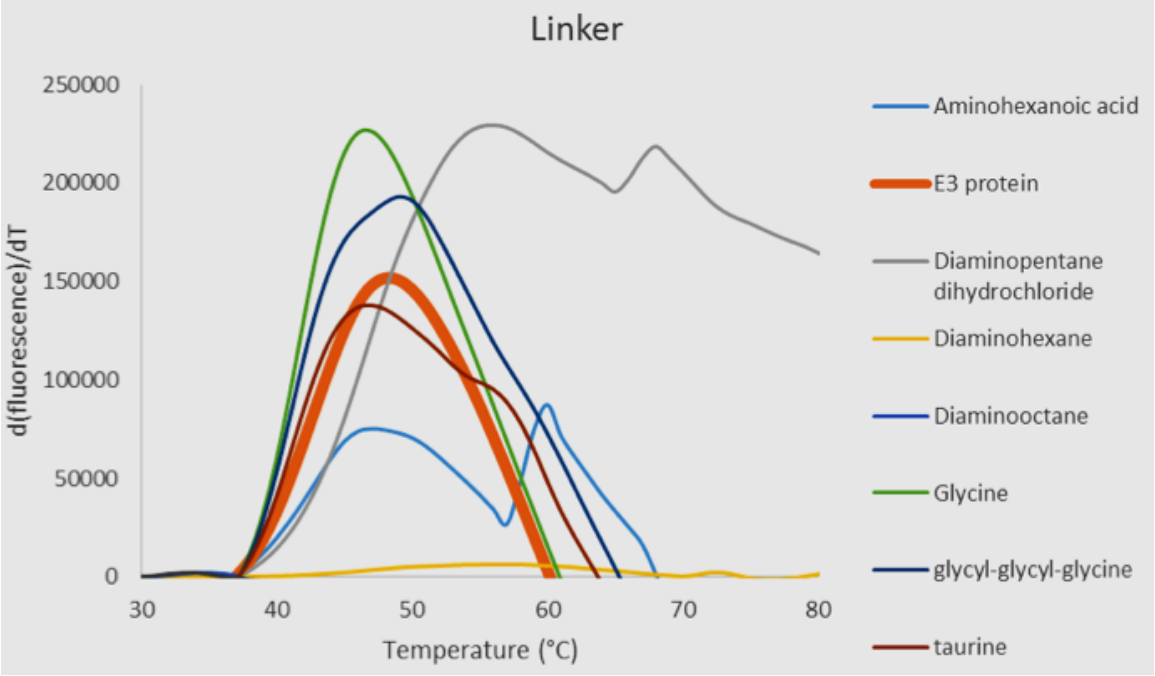

Figure A.15. Thermal shift analysis of E3 protein stability with linkers. The x-axis represents the increasing temperature during thermal shift assays whereas the y-axis corresponds to the first derivative of the fluorescence emission as a function of temperature (d[fluorescence]/dT). The melting temperature (T_m) is represented as the highest part of the curve. The solid red curve represents the T_m of E3[R131A] protein without any additives.

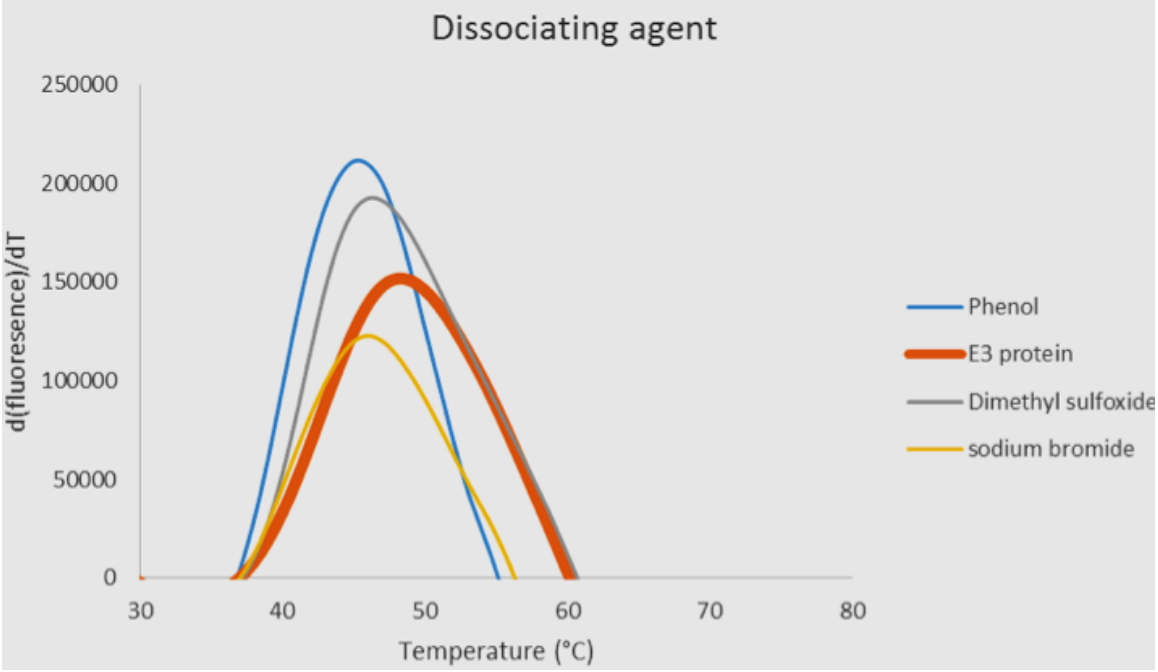

Figure A.16. Thermal shift analysis of E3 protein stability with dissociating agents. The x-axis represents the increasing temperature during thermal shift assays whereas the y-axis corresponds to the first derivative of the fluorescence emission as a function of temperature (d[fluorescence]/dT). The melting temperature (T_m) is represented as the highest part of the curve. The solid red curve represents the T_m of E3[R131A] protein without any additives.

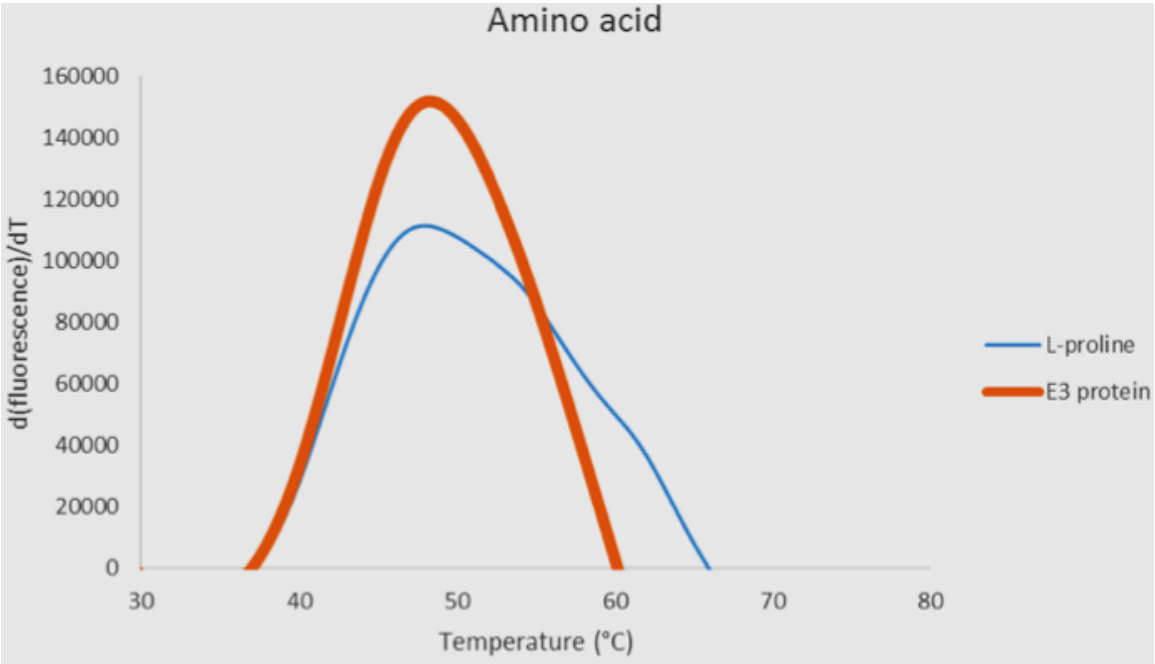

Figure A.17. Thermal shift analysis of E3 protein stability with amino acid (L-proline). The x-axis represents the increasing temperature during thermal shift assays whereas the y-axis corresponds to the first derivative of the fluorescence emission as a function of temperature (d[fluorescence]/dT). The melting temperature (T_m) is represented as the highest part of the curve. The solid red curve represents the T_m of E3[R131A] protein without any additives.

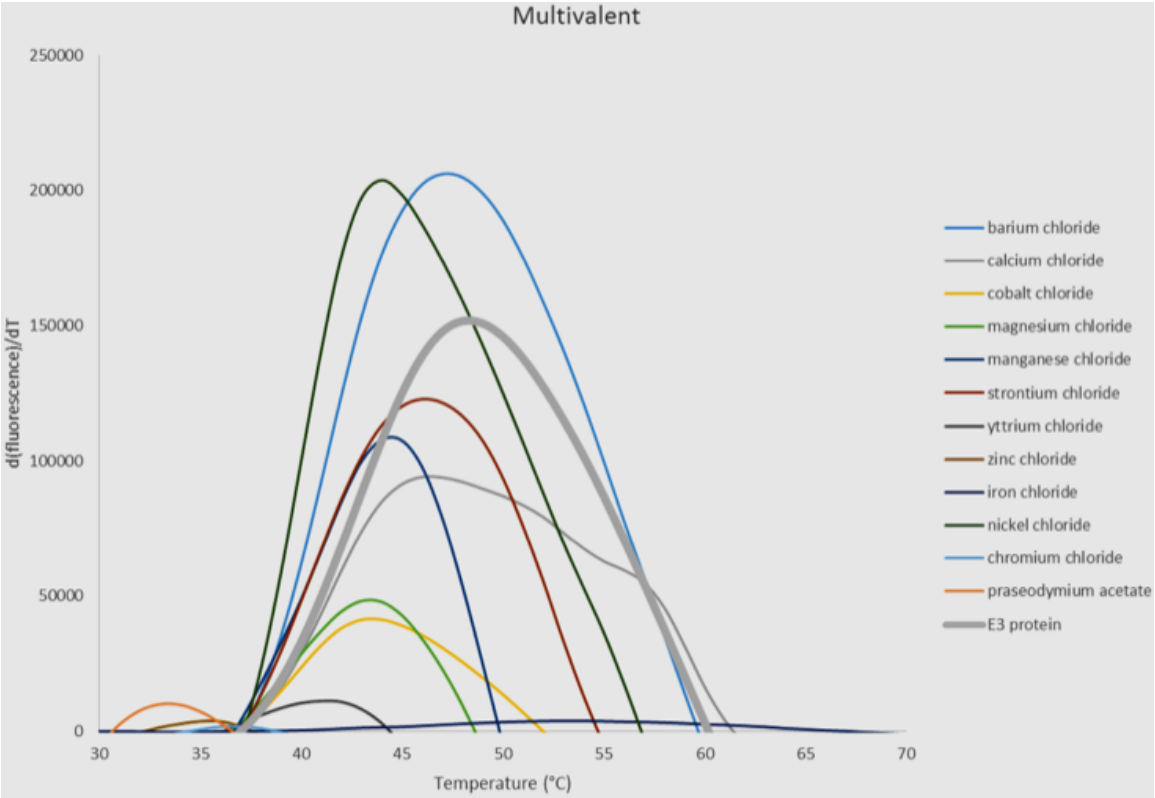

Figure A.18. Thermal shift analysis of E3 protein stability with multivalent solutions. The x-axis represents the increasing temperature during thermal shift assays whereas the y-axis corresponds to the first derivative of the fluorescence emission as a function of temperature (d[fluorescence]/dT). The melting temperature (T_m) is represented as the highest part of the curve. The solid red curve represents the T_m of E3[R131A] protein without any additives.

VITA

Sikta Patnaik

Candidate for the Degree of

Doctor of Philosophy

Dissertation: STRUCTURAL AND FUNCTIONAL STUDIES ON VACCINIA VIRUS E3 PROTEIN

Major Field: Biochemistry and Molecular Biology

Biographical:

Education:

Completed the requirements for the Doctor of Philosophy in Biochemistry and Molecular Biology at Oklahoma State University, Stillwater, Oklahoma in May, 2019.

Completed the requirements for the Master of Science in Biotechnology at Stephen F. Austin State University, Nacogdoches, Texas in 2010.

Completed the requirements for the Bachelor of Science in Agriculture at Acharya N.G. Ranga Agriculture University, Hyderabad, Andhra Pradesh, India in 2007.

Experience:

Research Assistant, Biochemistry and Molecular Biology, Oklahoma State University**,** Jan 2016 –May 2019

Research Assistant, Molecular Biosciences, University of Kansas, Aug 2014 – Dec 2015

Research Technician, Phillips 66, Bartlesville, OK, Mar 2011– Jun 2014

Intern, Medical College of Georgia, Augusta, GA, Jun – Sep 2010

Research Assistant, SFASU, Nacogdoches, TX, Aug 2008 – Dec 2010

Professional Memberships: Phi Kappa Phi honor society, Toastmasters club